الجمهورية الجزائرية الديمقراطية الشعبية
People's Democratic Republic of Algeria
وزارة التعليم العالي والبحث العلمي
Ministry of Higher Education and Scientific Research
جامعة العربي التبسي - تبسة-
University Larbi Tebessi– Tebessa –

Faculty of Science and Technology

Department of Electrical Engineering

Thesis

Submitted for the award of the Academic Master's Degree

Field: Electrical Engineering

Specialization: Industrial Electrical Engineering

By :

BEGGAS Adem
HACINI Mohammed Lamine

Subject

PERFORMANCES ANALYSIS OF A SOLAR PHOTOVOLTAIC WATER PUMPING SYSTEM

Presented and publicly supported, on before the jury composed of:

M/ OUNASS Djamel	**MCA**	**President**
M/ BOUKADOUM Aziz	**Professor**	**supervisor**
M/ DJEBBAR Mohamed Salah	**MCA**	**Examiner**

Promotion : 2024/2025

Acknowledgements

First and foremost, we express our deepest gratitude to Almighty Allah for guiding us to successfully complete this work.

We extend our sincere and heartfelt thanks to our supervisor, ***Professor Boukadoum Aziz****, for his continuous support, valuable guidance, and dedicated mentorship throughout the completion of this work.*

We also express our profound gratitude to all the esteemed professors who contributed to our academic and scientific formation, enriching our educational journey.

We particularly wish to acknowledge the honorable members of the examination committee who graciously accepted to evaluate our work. We are deeply grateful for their time and valuable feedback.

We would also like to express our sincere appreciation to our beloved parents for their unwavering support, patience, and constant encouragement that motivated us throughout our studies.

Finally, we cannot fail to acknowledge everyone who contributed, directly or indirectly, to the completion of this modest work, whether through tangible support or moral encouragement.

Dedication

I dedicate this work to

My beloved ***Parents***
Through their gentle encouragement and tremendous sacrifices, they provided the warm and nurturing family environment that enabled me to continue my studies.
No dedication could ever fully express my respect, appreciation, and deep feelings for you, my dear ***Mother*** *and* ***Father****.*
I pray to Allah to bless them, protect them, and I hope they will always be proud of me.

To my siblings
Soufian*e,* ***Mohammed Taher****, and* ***Aicha****.*

To all my ***family*** *members and* ***friends*** *May they find here an expression of my respect and gratitude for their unwavering support.*

To all my friends in ***Civil Protection***

To my teammate ***Adem***
Who worked with me to complete this project.

To everyone who supported me throughout my journey, thank you for every word of encouragement and every helping hand.

H.Mohammed Lamine

Dedication

I dedicate this work

To the pure souls of ***Gaza****, and to everyone who sacrificed their life for the sake of truth.*

To my ***Mother*** *and* ***Father****, thank you for your constant support and sacrifices.*

To my siblings
Sarra*,* ***Selma*** *and* ***Zineb*** *who have always been my support and strength.*

To my sister's children,
Mayar *and* ***Habib****, who have always been a source of joy in my life.*

To my teammate ***Mohammed Lamine***
Who worked with me to complete this project.

To my friends, colleagues, and teachers.

To everyone who supported me throughout my journey, thank you for every word of encouragement and every helping hand.

B.Adem

Abstract

Since solar energy sources offer clean energy for a variety of systems, their utilization is only increasing. They are also frequently seen in water pumping systems, particularly in places with limited access to energy and water. current (DC) and alternating current (AC) motor-powered solar water pumping systems are becoming more and more popular. pumping device was examined in this study. We evaluate the literature on water pumping systems and solar systems in the first chapter. The modeling and simulation of a photovoltaic system is covered in the second chapter. The third chapter focuses on the modeling and simulation of an induction machine connected to the grid. Finally, the last chapter presents a study of a complete system controlled by the DTC (Direct Torque Control) technique, with analysis and interpretation of the simulation results.

Keywords – PV system, Water Pump, Induction Motor, Control, Performances.

الملخص

تزداد استخدامات مصادر الطاقة الشمسية باستمرار، حيث توفر طاقة نظيفة لمختلف الأنظمة. كما يتم استغلالها على نطاق واسع في أنظمة ضخ المياه، خاصة في المناطق التي يصعب فيها الوصول إلى الماء والكهرباء. وتكتسب أنظمة الضخ الشمسي التي تعتمد على محركات التيار المتردد (AC) والتيار المستمر (DC) تفضيلاً متزايداً. في هذه الدراسة، تم تحليل نظام ضخ مياه يعمل بالطاقة الشمسية.

في الفصل الأول، قدمنا عرضاً لأحدث التطورات في الأنظمة الكهروضوئية وأنظمة الضخ. بينما خُصص الفصل الثاني لنمذجة ومحاكاة النظام الكهروضوئي. أما الفصل الثالث، فيتناول نمذجة ومحاكاة الآلة اللاتزامنية المتصلة بالشبكة. وأخيراً، يعرض الفصل الأخير دراسة لنظام شامل يتم التحكم فيه بتقنية DTC (التحكم المباشر في العزم)، مع تحليل وتفسير نتائج المحاكاة.

الكلمات المفتاحية – نظام كهروضوئي، مضخة مياه، آلة غير متزامنة، تحكم، أداء.

Résumé

Les sources d’énergie solaire fournissent une énergie propre pour divers systèmes, et leur utilisation ne cesse d’augmenter. Elles sont également fréquemment utilisées dans les systèmes de pompage d’eau, en particulier dans les zones où l’accès à l’énergie et à l’eau est limité. Les systèmes de pompage solaire alimentés par des moteurs à courant continu (CC) et à courant alternatif (CA) gagnent en popularité .Dans cette étude, un dispositif de pompage a été examiné. Dans le premier chapitre, nous passons en revue la littérature sur les systèmes de pompage d’eau et les systèmes solaires. Le deuxième chapitre traite de la modélisation et de la simulation d’un système photovoltaïque. Le troisième chapitre se concentre sur la modélisation et la simulation d’une machine asynchrone connectée au réseau. Enfin, le dernier chapitre présente une étude d’un système complet contrôlé par la technique DTC (Direct Torque Control), avec une analyse et une interprétation des résultats de simulation.

Mots-clés – Système photovoltaïque, Pompe à eau, Machine asynchrone, Commande, Performances.

LISTE OF FIGURES

N°	Title	Page
Figure I.1	Solar radiation map of Algeria for a totally clear sky: sum of all daily global solar radiation on horizontal surface	5
Figure I.2	Principle of the Photovoltaic system	6
Figure I.3	Solar cell technologies	8
Figure I.4	Series connection	9
Figure I.5	Parallel connection of photovoltaic cells	9
Figure I.6	Parallel and series connection of photovoltaic cells	10
Figure I.7	Construction of a Photovoltaic Module	10
Figure I.8	Protections of Modules by Reverse-Current and Bypass Diodes	11
Figure I.9	Hybrid Energysystems	12
Figure I.10	Grid-connectedsystems	13
Figure I.11	Principle of operation of sun-following pumping	13
Figure I.12	photovoltaic pumping with energy storage	14
Figure I.13	Components of a photovoltaic module generator	15
Figure I.14	Centrifugal Pump	17
Figure I.15	Volumetric pumps	18
Figure I.16	Varta lithium accumulator	18
Figure I.17	Layout of a surface water pump	19
Figure I.18	Diagram of a submersible water pump	20
Figure I.19	Floating water pump	20
Figure I.20	Main components of the photovoltaic pumping system with batteries	20
Figure II.1	Main components of the photovoltaic system.	25
Figure II.2	Simplified model of the cell	25
Figure II.3	Single-diode model of the PV cell	26
Figure II.4	Two-diode model of the PV cell	28
Figure II.5	Symbolic representation of a DC/DC converter	28
Figure II.6	Basic schematic of the Boost converter	29

Figure II.7	Current and voltage waveforms of a boost converter	30
Figure II.8	Operating principle of the P&O method.	31
Figure II.9	Flowchart of the P&O method.	32
Figure II.10	Flowchart of the INC Method	33
Figure II.11	Simulation of the (I-V) characteristic of the PV module.	34
Figure II.12	Simulation of the (P-V) characteristic of the PV module	35
Figure II.13	SIMULINK model of the PV system	35
Figure II.14	Variation of irradiance at a temperature of T=25°C	36
Figure II.15	Variation of power at the output of the PV system and in Load	36
Figure III.1	Schéma synoptique d'une machine asynchrone triphasée.	39
Figure III.2	Three-phase system to the two-phase system	42
Figure III.3	Three-phase asynchronous motor with respect to the different reference frames.	44
Figure III.4	Principle of PWM technique	48
Figure III.5	Principle of generating duty cycles	49
Figure III.6	Rotor speed	51
Figure III.7	Electromechanical torque	51
Figure III.8	Stator currents	51
Figure III.9	Rotor currents	52
Figure III.10	Rotor speed	52
Figure III.11	Electromechanical torque	53
Figure III.12	Stator currents	53
Figure III.13	Rotor currents	53
Figure IV.1	Sector of Evolution of the Stator Flux Vector	60
Figure IV.2	Selection of the Corresponding Voltage Vectors Vs for the Control of the Amplitude of Φs	61
Figure IV.3	Two-Level Hysteresis Flux Controller	62
Figure IV.4	Block Diagram of the General Structure of Direct Torque Control	63
Figure IV.5	H(Q) Characteristics and pipeline Characteristic	65
Figure IV.6	Simulation block diagram of the PV-powered pump system	66
Figure IV.7	Variable Irradiance	67

Figure IV.8	PV Current	67
Figure IV.9	PV voltage	67
Figure IV.10	PV power	68
Figure IV.11	Voltages source	68
Figure IV.12	Stator currants Ids and Iqs	69
Figure IV.13	Stator currants	69
Figure IV.14	Stator flux	69
Figure IV.15	Rotor speed	70
Figure IV.16	Electromagnetic torque	70
Figure IV.17	Pump Load Torque	71
Figure IV.18	Pump Power	71
Figure IV.19	Pump Startup Characteristics	72
Figure IV.20	Speed Comparison	73
Figure IV.21	Torque Comparison	73

Liste of tables

N°	Title	Page
Table I.1	Solar potential in Algeria	5
Table I.2	Summary of different solar cells technologies and their performances	8
Table II.1	Characteristics of the SST235-60P (China Sunergy (Nanjing)) PV system	34
Table III.1	Asynchronous Machine Parame	50

Abbreviations

Acronym	Meaning
PV	Photovoltaic
GPV	Photovoltaic Generator
MPPT	Maximum Power Point Tracking.
PPM	Maximum Power Point
P&O	Perturbation and Observation (P&O)
INC	The Incremental Conductance
MAS	Induction Motor
PWM	Pulse Width Modulation
DTC	Direct Torque Control

Summary

General introduction……...……1

Chapter I: Overview of photovoltaic pumping systems.

I.1. Introduction……...……4
I.2. Solar energy……...4
I. 2.1. Solar Thermal Energy……..…4
I. 2.2. Photovoltaic (PV) Energy…….……4
I.3. Solar energy in Algeria…….……....4
1.4. Photovoltaic System…….……..…..6
1.4.1. The Photovoltaic Effect…….……6
1.4.2. Principle of Photovoltaic Conversion……...…6
I.5. Different types of photovoltaic cell……..….6
I.5.1. First Generation Solar Cells……....6
I.5.2. Second Generation Solar Cells……..…….7
I.5.3. Third Generation Solar Cell……...…….7
I.6. Cell combination…….…..……8
I.6.1.String connection of photovoltaic cells…….…..……8
I.6.2.Parallel arrangement of photovoltaic cells……...……...9
I.6.3.Parallel and series connection of photovoltaic cells…….……9
I.7. Photovoltaic Modules…….…..……..……..10
I.8. Different types of photovoltaic systems……..…..……..11
I.8.1. Standalone systems……....……..11
I.8.2. Hybrid systems…….……12
I.8.3. Grid-connected systems……...……12
I.9. Photovoltaic Pumping Systems…….…..….13
I.9.1. Sun-following Pumping…….…..13
I.9.2.pumping with Electrochemical Storage (Batteries)……..….14
I.10. Composition of a PV pumping system with energy storage…….….14
I.10.1. Photovoltaic Generator……...…15
I.10.2. Static Converters……15
a) DC/DC Converter (Chopper)……..…15

b) DC/AC converter (Inverter)…….…….15
I.10.3. Drive Motor…….…….16
a) DC Motor…….……..16
b) AC Motor…….…….16
I.10.4. Water pumps…….…….17
I.10.4.1. Centrifugal pumps……..……...…..……17
I.10.4.2.Volumetric Pumps…….…….……..……17
I.10.5. Electrochemical Storage…….…….……...18
I.11.Classification of photovoltaic water pumping systems……..……19
I.11.1. Surface water pumps …….……19
I.11.2.Submersible pumps …….……..19
I.11.3. Floating water pump Floating pumps……...…….20
I.12. Configuration of a photovoltaic pumping system with batteries…….……...…..20
I.13. Operation of a Photovoltaic Generator at Its Maximum Power……..……..21
I.14. Advantages and Disadvantages of a PV system…….…….……..21
I.14.1. Advantages …….…….…..……21
I.14.2. Disadvantages …….…….…..……21
1.15. Conclusion……...…….22

Chapter II: Modeling and simulation of the photovoltaic system.

II.1. Introduction…….……..24
II.2. Photovoltaic generator (PVG)……24
II.2.1. Definition……..……..24
II.2.2. Performances of a PV system…….…...…..24
II.2.3. Structure of a Photovoltaic Generator (PVG)……..……24
II.3. Photovoltaic cell ……..……25
II.3.1. Simplified model……..…….…..25
II.3.2. Single-Diode Model……..……..26
II.3.3. Two-Diode Model……..…….……27
II.4. DC-DC Converter……..……....28
II.4.1. Boost Converter……..29
II.5. Maximum Power Point Tracking (MPPT) Control……...……...…..31
II.5.1. Principle of MPPT……...……...…..31
II.5.2. Perturb and Observe (P&O) Method……...…..……..31

II.5.3.The Incremental Conductance (INC) Method…….33
II.6. Simulation of the Photovoltaic Generator……..……34
II.6.1. Simulation of the PV Module…….……35
II.6.1.1. First case……..…….……..35
II.6.1.2. Second case……..……36
II.6.2. Results and Discussion……..……..……36
II.7. Conclusion……..…….…….…37

Chapter III :Modeling and simulation of induction machine supplied by an inverter.

III.1. Introduction…….…….39
III.2. Modeling of induction machine ……..…..……39
III.3. Simplifying Assumptions ……..……..39
III.3.1. Electrical Equation……..……...…40
III.3.2.Magnetic Equation…….……...…..40
III.4. Park Transformation ……...…….41
III.5. Modeling in two-phase System……..……...……43
III.5.1. Electrical Equation……..……...……43
III.5.2. Mechanical Equation ……..……..……43
III.6. References Frames……...…….43
III.6.1. Reference Frame Fixed with respect to the Stator…….44
III.6.2. Reference Frame Fixed with respect to the rotor…….……..44
III.6.3. Reference Frame Fixed With Respect To The Rotating Field……..….45
III.7. Mechanical Equation …….…….45
III.8. Asynchronous Machine Equations in the Stator-Fixed Reference Frame (α, β) …….46
III.8.1.Voltage Equations…….….46
III.8.2. Flux Equations…….……..46
III.9. Three-phase Inverter…….47
III.9.1. Inverter Modeling……..47
III.10. PWM Control …….……48
III.11. Simulation …….…….……50
III.11.1. Simulation of the Asynchronous Machine.…….……50
III.11.2. Simulation of the Asynchronous Machine powered by an inverter……..……52
III.12.Conclusion…….…….54

CHAPITRE IV :Modeling and simulation of an induction machine pump using the DTC control.

IV.1. Introduction……..……57
IV.2. Direct Torque Control (DTC)……..57
IV.3. Main Features of DTC ……..…..57
IV.3.1. Advantages……..…….…..……58
IV.3.2. Disadvantages…….…….…..……58
IV.4. Structure of Direct Torque Control of the Asynchronous Machine…..…….59
IV.5. Determination of the Sector of Evolution of the Stator Flux Vector.……59
IV.6. Estimators…….……60
IV.6.1. Stator Flux Estimator…….……...……60
IV.6.2. Electromagnetic Torque Estimator……..……..61
IV.7. Elaboration of the Control Vector……..……..61
IV.7.1. Flux Controller……..……61
IV.7.2. Torque Controller……..62
IV.8. General Structure of Direct Torque Control……...…….……..63
IV.9. Modeling of the Centrifugal Pump……..…….63
IV.9.1. Total Manometric Head…….63
IV.9.1.1. Linear Head Losses…….64
IV.9.1.2. Singular (Local) Head Losses……...……..64
IV.9.1.3. Flow Rate-Head Characteristic …….……..……...….64
IV.9.1.4. Pump Torque-Speed Characteristic C(ω)…….…….……..65
IV.9.1.5. Power Calculation……..…….65
IV.10. Simulation Results……..66
IV.10.1.Solar Panel Simulation Results……..……..66
IV.10.2. Simulation Results of the Induction Motor…….68
IV.10.3. Pump Simulation Results……...….……71
IV.10.4 Simulation Results Comparison……..……...……..72
IV.11. Conclusion……...……..74
General conclusion……...….77
Bibliographic references

General Introduction

General Introduction

Energy technologies are now at the forefront of contemporary research and development due to the growing demand for environmentally friendly and sustainable energy sources worldwide. Because of their capacity to capture abundant solar energy and transform it straight into electrical power, solar photovoltaic (PV) systems have become one of the most promising options among these [1]. Water pumping systems are among the most useful uses of PV technology, particularly in isolated and arid areas with little or no access to the electrical grid.[2] These systems provide a low-maintenance, economical, and clean substitute for traditional water pumps that run on diesel or the grid.

The modeling, simulation, and performance assessment of such systems are the main topics of this thesis, "Performance Analysis of a Solar Photovoltaic Water Pumping System". to examine the effects of various control strategies on the performance of the induction motor used in the pumping process, study attempts to give a thorough understanding of various components involved in solar water pumping systems.

The work is organized into four main chapters:

- **Chapter I**explains photovoltaic pumping systems in general. It goes over their fundamental parts, how they work, and the benefits they provide for a range of uses, especially in rural water supply and agriculture.
- **Chapter II** is devoted to photovoltaic system modeling and simulation. This includes using simulation tools to assess system behavior in various environmental settings and mathematically modeling solar panels. [3]
- **Chapter III** focuses on simulating and modeling an induction machine that is powered by an inverter. The electrical and dynamic properties of the motor, as well as how it interacts with the power supply system, are examined in this chapter. [4]
- **Chapter IV** investigates the Direct Torque Control (DTC)-supplied induction machine's modeling and simulation. The effectiveness of this sophisticated control method in improving the dynamic performance and efficiency of the system is assessed. [5]

With a focus on enhancing the functionality of electric drives in these systems, our study seeks to further the continuous development of sustainable and effective water pumping technologies that use solar energy.

CHAPTER I

OVERVIEW OF PHOTOVOLTAIC PUMPING SYSTEMS

I.1. Introduction

According to United Nations projections, the global population could reach between 10 and 12 billion by the end of the 21st century. This raises a critical question: how can the world meet the growing demand for energy in a manner that is environmentally sustainable, safe, and reliable? There is an increasing global consensus that renewable energy sources will play a vital role in addressing this challenge [6]. Solar energy represents the most abundant and readily available form of energy on Earth. It is the fundamental driver of atmospheric dynamics, oceanic circulation, photosynthesis, and various other life-sustaining processes. The Earth continuously receives an estimated 173,000 terawatts of solar energy, approximately 10,000 times greater than the total global energy consumption. In contrast, energy sources not originating from the Sun are relatively limited in both scope and availability [7]. For this context, in this chapter we will first explore some fundamental concepts regarding solar energy. We will then discuss solar resources and prospects, with a particular focus on Algeria, which benefits from exceptional sunlight. Finally, we will examine photovoltaic technology and its applications, particularly in connection with photovoltaic pumping.

I.2. Solar energy

Solar Energy is defined as the energy radiated from the sun, which can be harnessed and converted into useful forms of energy such as heat and electricity by using solar technologies. The two primary types of solar energy systems are:

I. 2.1. Solar Thermal Energy

Solar thermal systems use solar collectors to absorb sunlight and convert it into heat, which can then be used directly or converted into mechanical energy and electricity through steam turbines or other thermal engines.

I. 2.2. Photovoltaic (PV) Energy

Photovoltaic systems directly convert solar radiation into electricity using the photovoltaic effect in semiconductor materials such as silicon [8].

I.3. Solar energy in Algeria

With vast desert areas and over 3,000 hours of sunshine annually, Algeria holds considerable potential for solar energy development. The national strategy targets the installation of 22,000 MW of solar capacity by 2030 as part of its energy transition plan. By 2030, the Algerian government aims to generate 27% of its electricity from renewable energy sources, primarily through the development of solar and wind power. To gain a comprehensive understanding of the programs and initiatives related to solar energy in Algeria, this study begins by outlining the country's potential and capabilities in this energy sector. In response to the post-oil energy

transition, the Algerian government has pursued alternative energy strategies, unveiling an ambitious plan to generate 10% of its electricity from renewable sources by 2020. This direction is supported by Algeria's substantial solar energy potential, owing to its vast landmass and favorable geographic location. A study conducted by the German Space Agency identified the Algerian Sahara as the largest solar energy reservoir in the world, receiving approximately 3,000 hours of solar radiation annually Algeria is regarded as one of the most solar-rich countries globally, with solar irradiance levels in many regions reaching up to 7 kWh/m². According to the Algerian Ministry of Energy and Mines, this immense potential could theoretically supply energy equivalent to 60 times Western Europe's needs, four times global consumption, and nearly 5,000 times Algeria's own electricity demand [9]

Region	Coastal region	Highlands	Sahara
Area (%)	4	10	86
Sunshine average (hour/year)	2650	3000	3500
Solar energy received (KWh/m^2.year)	1700	1900	2650

Table I.1 Solar potential in Algeria [10]

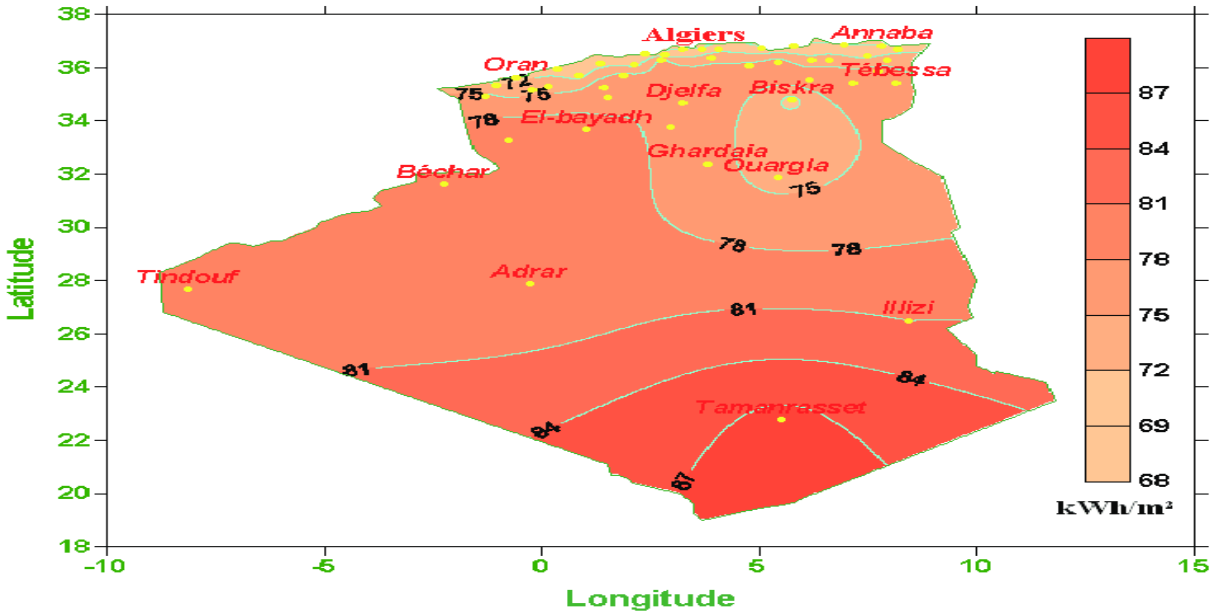


Figure I.1 Solar radiation map of Algeria for a totally clear sky: sum of all daily global solar radiation on horizontal surface [11].

1.4. Photovoltaic System

1.4.1. The Photovoltaic Effect

The photovoltaic effect refers to the physical phenomenon in which incident photons generate electron-hole pairs within a semiconductor material, and these charge carriers are subsequently separated by the internal electric field of a p-n junction, resulting in the direct conversion of light energy into electrical energy within solar cells [12].

1.4.2. Principle of Photovoltaic Conversion

When light strikes a p-n junction, the energy carried by incident photons is absorbed at the junction, resulting in the generation of electron-hole pairs. This process disturbs the thermal equilibrium of the junction. The free electrons generated within the depletion region migrate toward the n-type side, while the corresponding holes move toward the p-type side. As these charge carriers accumulate, the potential barrier at the junction prevents the electrons from crossing into the p-type region and similarly inhibits the holes from moving into the n-type region. This separation of charges leads to a build-up of electrons on the n-type side and holes on the p-type side, creating an electric potential across the junction known as the photo voltage. Consequently, the p-n junction functions like a miniature power source. When an external load is connected, this potential drives an electric current through the circuit. The efficiency and overall performance of the solar cell are primarily influenced by severalfactors, including atmospheric conditions (such as humidity and cloud cover), the intensity of solar irradiation, ambient temperature, air mass, and the specific materials used in the fabrication of the solar cell[13].

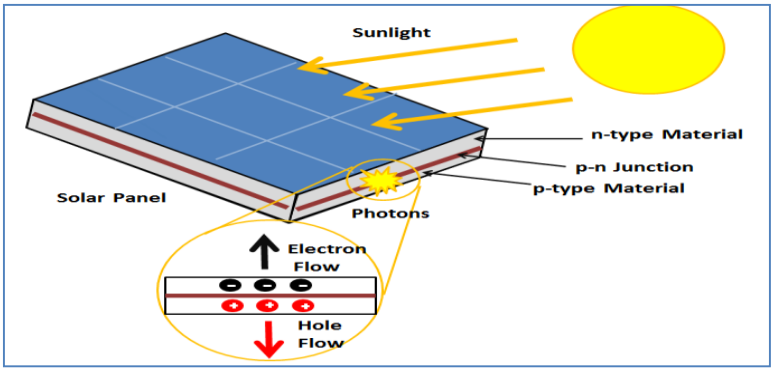


Figure I.2 Principle of the Photovoltaic system [14].

I.5. Different types of photovoltaic cell

I.5.1. First Generation Solar Cells

First-generation solar cells are the most widely used photovoltaic panels and are primarily composed of either mono-crystalline or polycrystalline silicon. Mono-crystalline silicon (Mono-Si) solar panels are manufactured using highly purified silicon, which contributes to their distinctive dark appearance and rounded edges. Due to the high purity of the silicon, these panels achieve superior efficiency levels, typically reaching up to 20%. In contrast, polycrystalline silicon solar panels are characterized by their blue, speckled appearance and square-shaped cells with uncut edges. These panels are produced through a more cost-effective and rapid process, which involves melting raw silicon. However, this manufacturing approach results in lower silicon purity, leading to reduced efficiencytypically around 15%shorter operational lifespan, and decreased space efficiency. Additionally, polycrystalline panels tend to be more susceptible to performance degradation under high-temperature conditions [15].

I.5.2. Second Generation Solar Cells

Second-generation solar cells, also known as thin-film solar cells (TFSC), are primarily utilized in photovoltaic power plants, building-integrated photovoltaic and smaller-scale solar systems. These cells are produced by depositing one or more thin layers of photovoltaic materials such as silicon, cadmium, or copperonto a substrate. Due to the reduced quantity of raw materials required in their manufacturing, thin-film solar cells offer a more cost-effective alternative to traditional solar technologies. They also exhibit better performance at higher temperatures; however, they generally have a shorter operational lifespan and require a larger installation area. Among them, amorphous silicon (a-Si) solar cells are notable for their relatively low efficiency, typically around 7%, which limits their application mainly to low-power devices such as pocket calculators. Nevertheless, their lower production costs remain a significant advantage [18].

I.5.3. Third Generation Solar Cell

Third-generation solar cells represent an emerging class of photovoltaic technologies that are currently under research and development. These advanced solar cells aim to overcome the limitations of earlier generations by utilizing a variety of organic and inorganic materials to convert sunlight into electricity. Examples of these technologies include hybrid solar cells, cadmium telluride (CdTe) solar cells, and concentrated solar cells. While still in the experimental stage, these innovations hold significant potential for improving efficiency and reducing production costs in future solar energy applications [18].

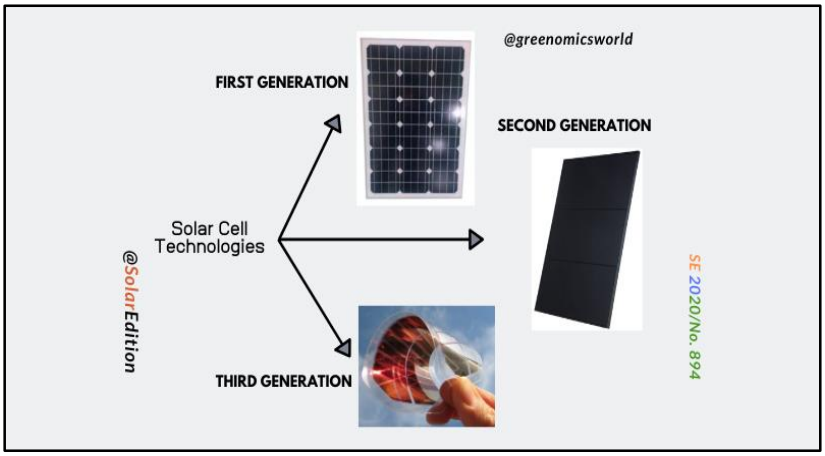


Figure I.3 Solar cell technologies [16].

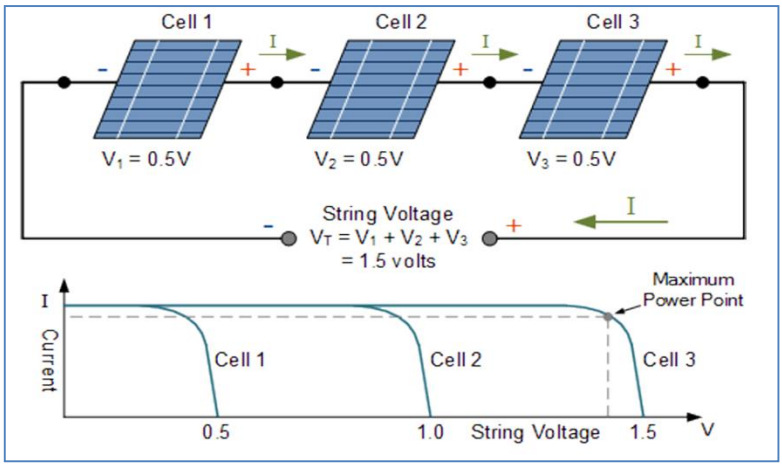
Solar Cell Type	Efficiency Rate	Advantages	Disadvantages
Monocrystalline Solar cells (Mono –Si)	20%	• High Efficiency • High time value • Optimized for commercial use.	• Expensive
Polycrystalline Solar cells (p-Si)	15%	Lower Price	• Sensitive to high temperatures • Lower lifespan • Slightly less efficient
Thin Film Amorphous Silicon Solar panels (A-SI)	5 - 9%	• Relatively low cost • Easy toproduce • Flexible	• Shorter lifespan
Cadmium Telluride	7 - 11%	• Absorbs 90% of the incident photons	• Cadmium is a pollutant and toxic

Table I.2 Summary of different solar cells technologies and their performances [18]

I.6. Cell combination

I.6.1.String connection of photovoltaic cells

Photovoltaic cells are typically connected in series within photovoltaic panels to increase the overall voltage output. This configuration is necessary because the operating voltage of an individual cell is relatively low, typically only a few hundred milli-volts[17], as illustrated in Figure 1.4 below.



FigureI.4 Series connection [18]

Therefore, photovoltaic (PV) cells are connected in series to form strings, enabling the system to achieve a voltage level that satisfies the input specifications of the power processing unit.

I.6.2.Parallel arrangement of photovoltaic cells

The figure I.5 illustrated how the generated current can be increase through parallel connection of photovoltaic cells:

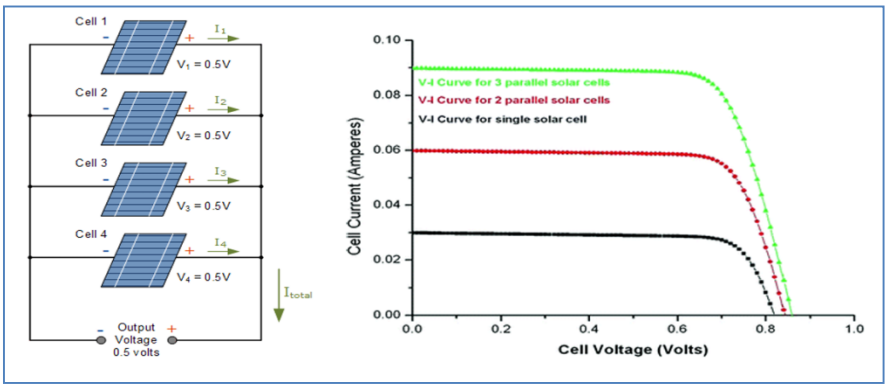


Figure I.5 Parallel connection of photovoltaic cells [18]

Therefore, a parallel configuration of photovoltaic cells is employed to increase the output current, as the potential difference across the terminals remains constant.

I.6.3.Parallel and series connection of photovoltaic cells

The series and parallel configurations of photovoltaic (PV) cells are utilized to enhance both output voltage and current. The total output voltage is determined by multiplying the voltage of a single cell by the number of cells connected in series within each panel. Similarly, the total output current is obtained by multiplying the current of a single cell by the number of parallel-connected strings.

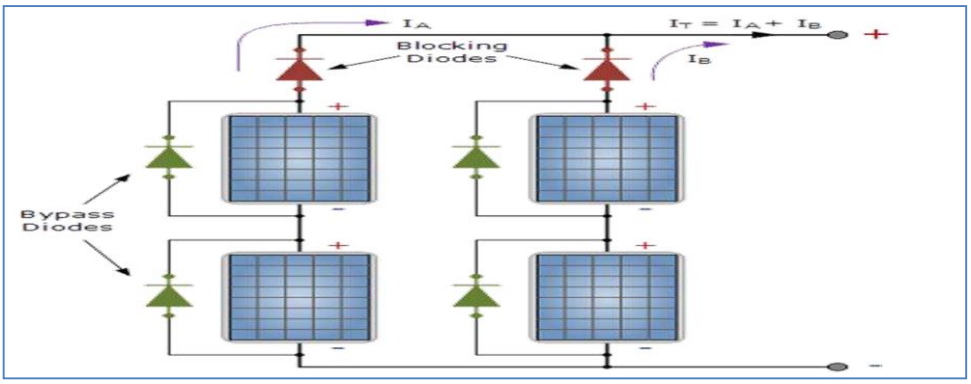


Figure I.6 Parallel and series connection of photovoltaic cells [18]

In the event of an accident where a single photovoltaic (PV) cell is damaged or becomes disconnected, the current flow through the entire series-connected string is interrupted, resulting in the loss of power contribution from the entire string. To mitigate the impact of such occurrences, PV panel manufacturers typically integrate bypass diodes in parallel with the PV cells usually two or three diodes per panel, depending on the panel's power rating.

I.7. Photovoltaic Modules

A module is made up of cells linked in series or parallel. The module's front face ought to be composed of glass that possesses the following qualities:

Good openness, resistance to impact and abrasion blocking off moisture [20], glass (also known as "bifacial" modules) or a combination of Tedlar, alu, and Tedlar (polyethylene) are typically used for the rear face.

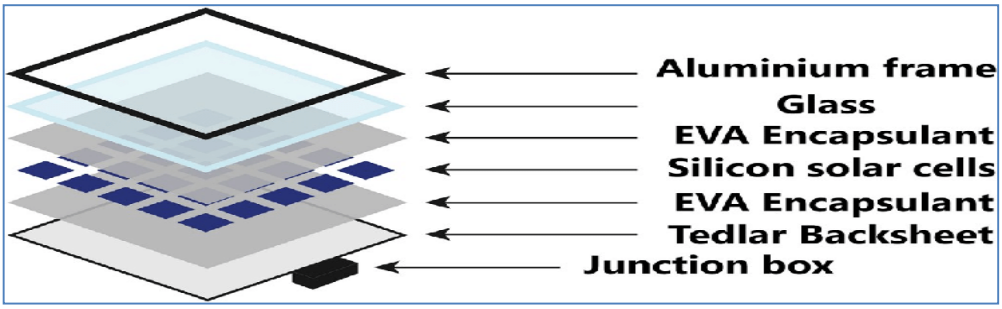


Figure I.7 Construction of a Photovoltaic Module [21]

To enhance the module's lifespan, it must be safeguarded, notably against damaging failures caused by cell connections and operating under shading circumstances. Two forms of protection are commonly required for the effective operation of a solar module [20].

Bypass Diode Protection: When the lighting is uneven, they can separate a sub-network of cells (shading effect), avoiding hot patches and the devastation of cells with inadequate illumination.

A series diode stops negative current in the PV system by being positioned between the module and the battery. This can happen when many modules are linked in parallel or when a load in

direct connection, such a battery, changes from receiving to producing mode at night. It is also known as a reverse-current diode in this context [20]

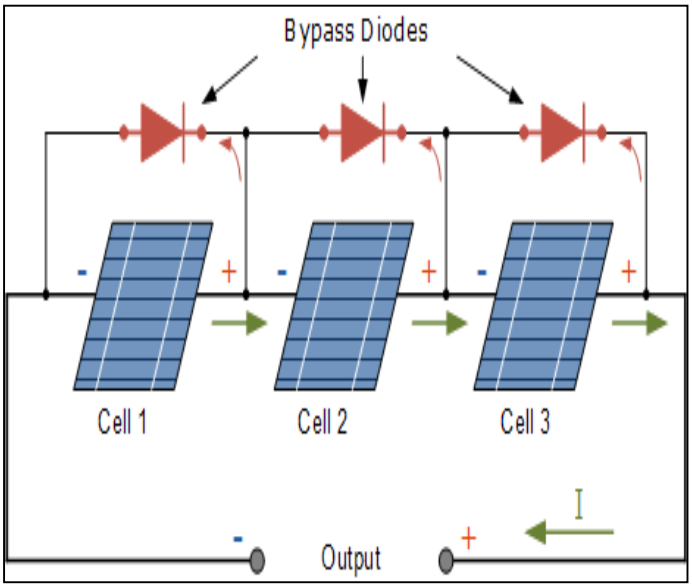


Figure I.8 Protections of Modules by Reverse-Current and Bypass Diodes [18].

Features of a Module Typically, modules are thin, rectangular parallelepipeds that are stiff and just a few millimeters thick. They have the following features:

- **Peak Power (Pc):** The highest amount of electricity the module can produce in typical circumstances (25°C and 1000 W/m² of light).

(I = f (V)) I-V Characteristic: a graph that shows the module's output current (I) as a function of the voltage across it.

Vocor open circuit voltage: the voltage across the module under "full sun" light while there is no current flowing through it.

Short Circuit Current (Isc): The current that the module produces when it is shorted off and exposed to "full sun" light.

Peak power in full sun: is known as the "optimal operating point" (Pm, Vm, Im).

Efficiency: is the ratio of incident radiation power to the ideal electrical power.

Form Factor: The proportion of the cell's maximal power to its ideal power [22].

I.8 Different types of photovoltaic systems

I.8.1 Standalone systems

Neither the electrical grid nor any other energy sources are necessary for a solo solar system to function. This method is typically utilized in isolated areas. Even in the absence of sunshine (during inclement weather or at night), such a system must be able to supply energy. As a result,

batteries are required to store a portion of the solar modules' daily output [23].One or more solar modules, a charge controller, one or more batteries, and maybe an inverter make up this system in most cases.

I.8.2. Hybrid systems

In order to improve the amount of energy available, hybrid systems combine two or more complimentary technologies. Although wind and solar energy don't always supply power, they can eventually be combined to produce electricity more continuously. The way hybrid systems work is that the solar panels charge the batteries during the day and the wind generator charges them during the windy season [24].

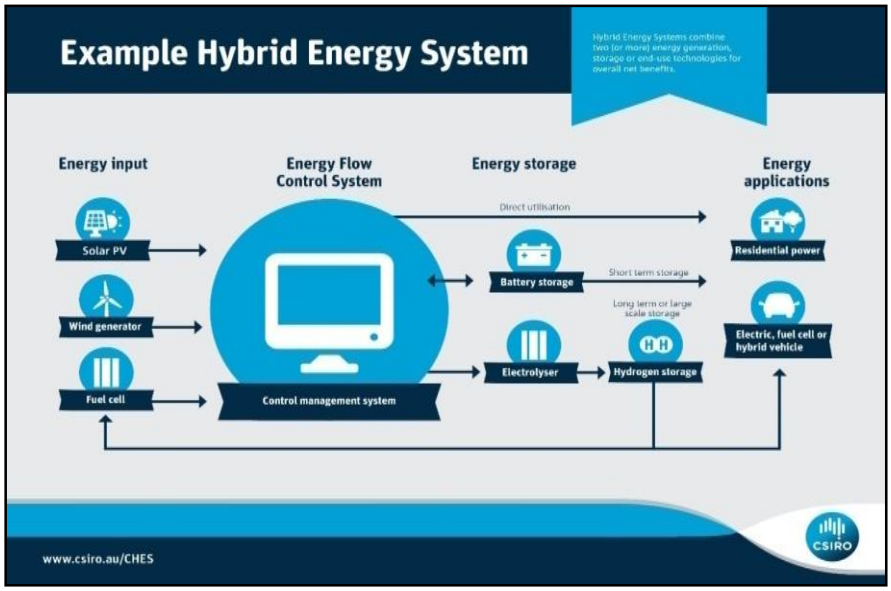


Figure I.9 Hybrid Energy systems [25]

I.8.3. Grid-connected systems

Grid-connected installations (or those linked to a distribution center) generally provide an optimal solution for solar electricity production, both in terms of energy and cost. These systems consist of interconnected photovoltaic modules, one (or more) inverter(s) connected to the electrical grid. The inverter converts the direct current generated by the photovoltaic modules into alternating current compatible with the electrical grid

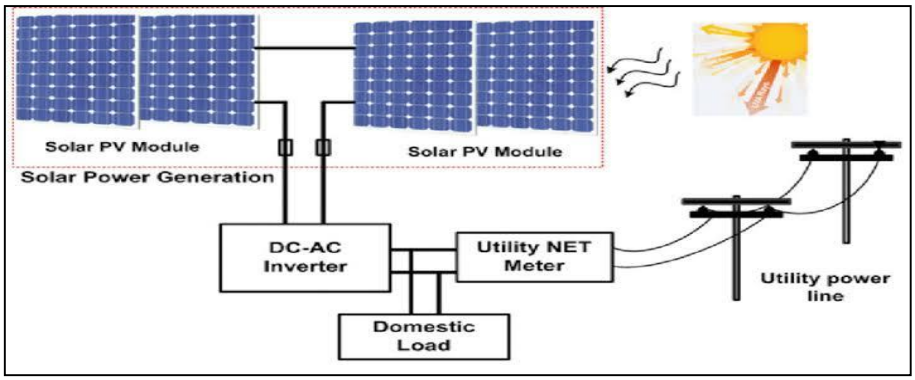


Figure I.10 Grid-connected systems [26].

I.9.Photovoltaic Pumping Systems

There are two types of photovoltaic pumping systems currently in use: those with and without batteries. The main drawback of the battery-less technology is that the water flow depends on the sunlight during the day. We will add batteries to the photovoltaic pumping system in order to conduct a study. Water scarcity is a major problem for many populations in rural areas of developing countries, and it is particularly worse in desert areas. Improving living conditions in these areas is tied to finding appropriate solutions to this problem.

I.9.1. Sun-following Pumping

Hydraulic storage involves pumping water into an aboveground tank when there is enough sunshine. Gravity then distributes it as required. A more straightforward photovoltaic system is made possible by sun-following pumping, as seen in Figure (I.11) [23].

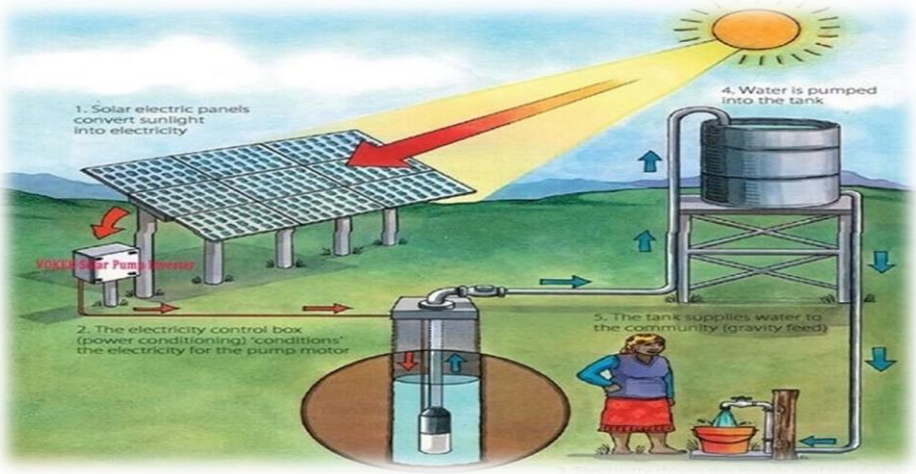


Figure I.11Principle of operation of sun-following pumping [27]

The basic idea behind such a system is still fairly straightforward: when the photovoltaic panels are exposed to sunlight, they power a pump (which can be submerged or surface-mounted) with

the help of a controller regulator, which may be built into the pump depending on the manufacturer. The pump then supplies water. Water is stored in a reservoir by the sun-following pumping system until it is required. Although this option is less expensive, the pumps have a poorer efficiency outside of their nominal working power and do not operate below a particular level of illumination (daily dawn and evening). They also do not have a steady flow rate.

I.9.2.pumping with Electrochemical Storage (Batteries)

Storage is necessary because photovoltaic pumping frequently does not correspond with the hours of sunshine or demands a constant intensity. Energy independence A steady flow rate based on demand are guaranteed by photovoltaic pumping with batteries [28].

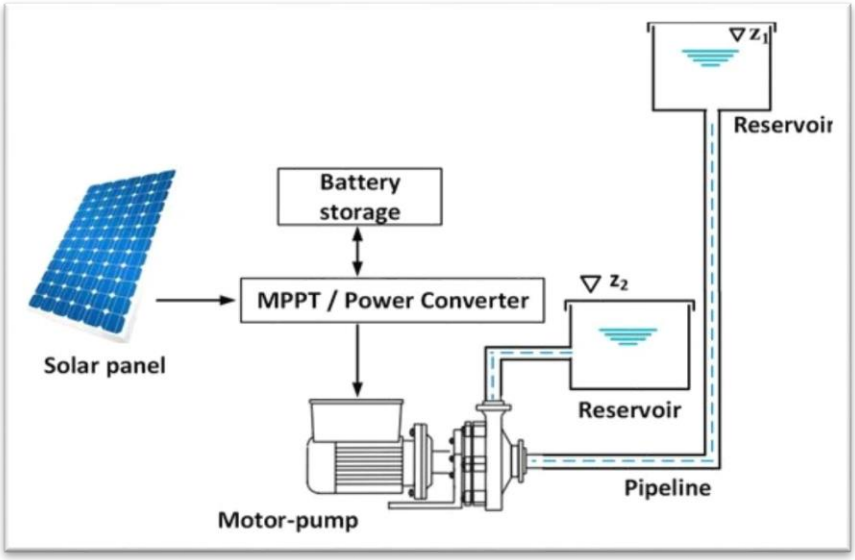


Figure I.12 photovoltaic pumping with energy storage [39].

Electricity may be stored and released when needed thanks to batteries. To prevent severe discharges or overcharging, which might shorten the batteries' lifespan, a regulator is necessary.

I.10. Composition of a PV pumping system with energy storage

The efficiency of the modules, site conditions (sunlight, ambient temperature, geographical obstacles), and other equipment characteristics (inverter, motor, pump, etc.) all affect the performance of water pumping, one of the most popular uses of solar energy for irrigation or drinking water supply. A PV pumping system is a complicated system made up of several interaction components, such as the PV generator, conversion system, drive motor, pump, and storage batteries, all of which have an impact on one another [23]

I.10.1. Photovoltaic Generator

Each of the modules that make up a photovoltaic generator is made up of several solar cells that are coupled in series and parallel to supply the required voltage and current. The generator's performance is contingent upon the diversity of both the cells within the modules and the modules themselves. The number of modules in series determines the photovoltaic generator's output voltage, whereas the number of modules in parallel determines its output current. Figure (I.13) [30] illustrates a photovoltaic array, which is the term used to describe an integrated group of solar modules.

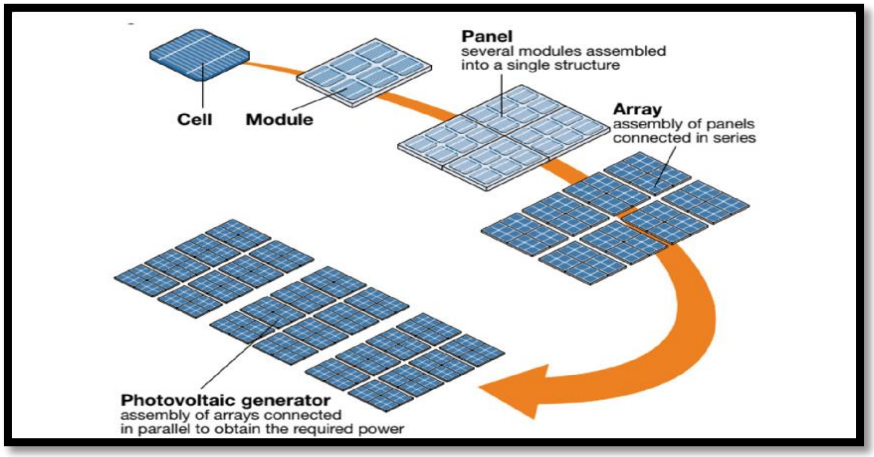


Figure I.13Components of a photovoltaic module generator [31].

I.10.2. Static Converters

Static converters are systems that adapt the electrical energy source to a given load, there are several types of static converters such as:

a) DC/DC Converter (Chopper)

DC/DC converters are used to provide variable DC voltage from a fixed DC voltage. This energy conversion occurs through high frequency "switching," which is characterized by high efficiency [24].

- ❖ Buck Converter (Series Chopper)
- ❖ Boost Converter (Parallel Chopper)

b) DC/AC converter (Inverter)

- ❖ Single-phase Inverter
- ❖ Three-phase inverter

I.10.3. Drive Motor

The drive motor converts electrical energy into mechanical energy. It can be either DC or AC. In the case of AC, an electronic converter or inverter is necessary to convert the DC current from a photovoltaic generator into AC. For this reason, the initial choice of a DC motor might seem more appealing, but we will see that the evolution of efficient electronic converters also makes it possible to choose efficient and, above all, cheaper AC motors [19].

a) DC Motor

These motors are powered by DC voltages. The main advantage of DC machines lies in their simple adaptation to methods for adjusting or varying their speed, torque, and direction of rotation. Its main drawback is the brush/rotary collector assembly, which wears out, is complex to build, and consumes energy [19].

b) AC Motor

For low and medium power applications (up to a few kilowatts), the standard single-phase grid is sufficient. For high-power applications, AC motors are typically powered by a polyphase current source. The most commonly used system is then the three-phase (phases offset by 120°), which is used by electricity distributors. These AC motors come in two types: Synchronous motors and Asynchronous motors [19].

- **Synchronous Motors**

The synchronous machine is often used as a generator and is then called an "alternator." Except for low-power generators, this machine is typically three-phase. Power plants use alternators with powers that can reach up to 1500 MW. As the name suggests, the rotational speed of these machines is always proportional to the frequency of the currents passing through them. There are three types of synchronous machines: wound rotor synchronous machines, reluctance synchronous machines, and permanent magnet synchronous machines [20]

- **Asynchronous Motors**

The asynchronous machine, also known by the Anglo-Saxon term "induction machine," is an alternating current machine without electrical power supplied to the rotor. The term "induction" comes from the currents induced in the rotor by magnetic induction. The term "asynchronous" arises because the speed of these machines is not necessarily proportional to the frequency of the currents passing through them. Using an asynchronous motor (three-phase alternating current) is more economical and practical due to its robustness, lower cost, and lack of maintenance, even if it requires a more complex electronic control circuit for photovoltaic pumping systems. The use of an asynchronous motor thus increases the autonomy and

reliability of the installation. The motor is powered by an inverter (DC/AC converter), which ensures the optimization of the generator.

I.10.4. Water pumps

There are two main types of water pumps used in solar water pumping system which are centrifugal pumps and the positive displacement pumps. The choice of these pumps depend on factors like the head, the desired flow rate, the efficiency and the maintenance of these pumps.

I.10.4.1. Centrifugal pumps

These pumps consist of one or more impellers that spin water by subjecting it to centrifugal force. To attain high lift, a centrifugal pump may have a multitude of stages, each consisting of an impeller at each stage thus increasing the pump's lift capacity. Centrifugal pumps may use over 20 stages to attain high lifts and each stage adds pressure but also imposes friction, resulting in an efficiency loss of about 5% per stage[33]

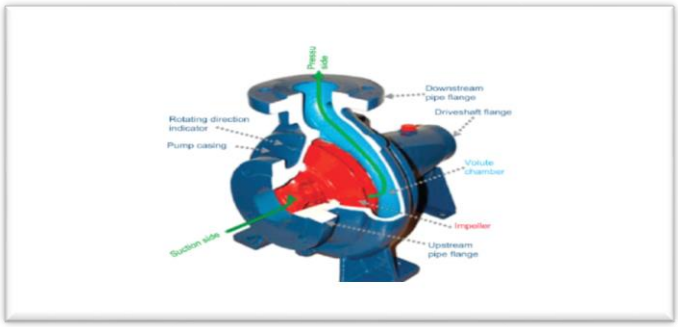


Figure I.14 Centrifugal Pump [31].

I.10.4.2.Volumetric Pumps

In these pumps, the fluid is set in motion by a variation in the volume that contains it.Volumetric pumps come in two types: reciprocating volumetric pumps (e.g., piston pumps, diaphragm pumps, etc.) and rotary volumetric pumps (e.g., screw pumps, etc.).

Their main advantages are as follows:

They are designed for low flow rates (less than 5 m^3/h) and high heads.

They have good efficiencies, and surface pumps are self-priming. The starting torque of a volumetric pump (3 to 5 times the nominal torque) and the $I = f(V)$ characteristic of this type of pump make its direct operation from a photovoltaic panel economically unfeasible. To overcome the problem of over-sizing the generator resulting from this mismatch, an impedance adapter is used to allow the system to achieve the highest possible efficiency [19].

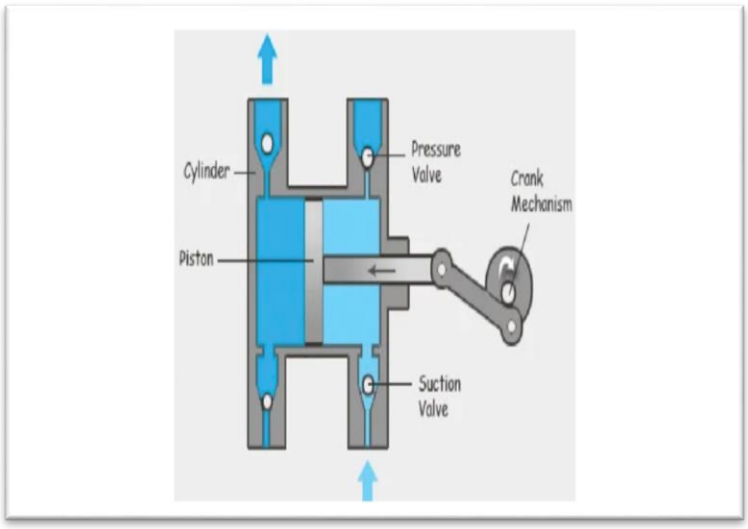


Figure I.15 Volumetric pumps [31].

I.10.5. Electrochemical Storage

Battery assemblies in electrochemical battery storage systems are made to deliver power and capacity according to demand (backup power, grid stabilization). .

In order to store power in off-grid systems, the battery is frequently linked with the solar generator. It releases the electricity that has built up throughout the day at night or on overcast days. There are several kinds of batteries, including [34] Lead-acid battery, Nickel-cadmium battery, Nickel-chloride sodium battery,Lithium-ion battery, Zinc-air battery and Lithium Batteries.



Figure I.16 Varta lithium accumulator [35].

I.11.Classification of photovoltaic water pumping systems

The selection of a water pumping system primarily depends on the total head and the water source. These sources may include deep wells, dams, rivers, or lakes. Consequently, the appropriate system may involve a surface pump, a submersible pump, or a floating pump, depending on the specific application and source characteristics.

I.11.1. Surface water pumps

A surface pump (Figure I.19) is positioned above the water source, which inherently limits the maximum suction lift achievable. The pump must be installed no more than 3 to 6 vertical meters above the water level, exceeding this range may result in air being drawn into the system, ultimately causing pump failure. Surface pumps are suitable for drawing water from sources such as rivers, irrigation ditches, ponds, or storage tanks, but are not appropriate for deep well applications. Compared to submersible pumps, surface pumps are generally more cost-effective and may offer greater efficiency for high-volume water transfer, as illustrated in Figure I.17.

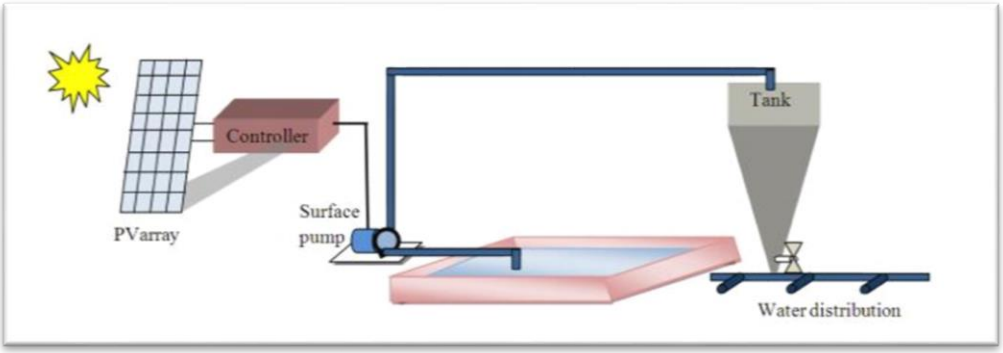


Figure I.17. Layout of a surface water pump.

I.11.2 Submersible pumps

A submersible pump (Figure I.18) is generally easier to install, offers enhanced protection against environmental factors, and is less susceptible to damage caused by dry running due to the integration of water level sensors. Some solar-powered submersible pumps operate using a centrifugal mechanism similar to that of surface pumps, while others employ a positive displacement mechanism. Among these, centrifugal submersible pumps represent the predominant technology for deep well pumping applications

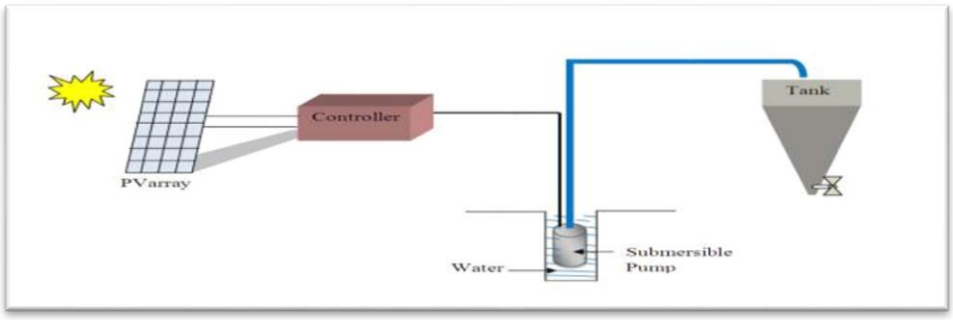


Figure I.18. Diagram of a submersible water pump.

I.11.3Floating water pump Floating pumps

As illustrated in Figure I.19, floating pumps are semi-submersible devices supported and stabilized by a buoyant structure. They are designed for use in situations where inline pumps are unsuitable and are commonly deployed in water bodies such as dams, lakes, and lagoons. These floating or semi-submersible pumps can achieve flow rates of up to 7,000 liters per hour [36]

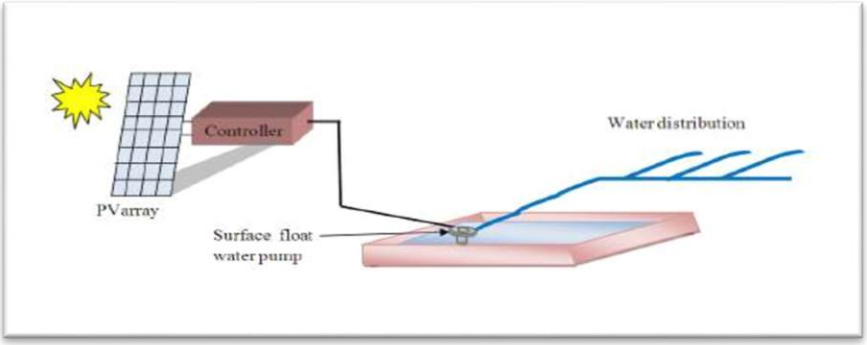


Figure I.19. Floating water pump [37].

I.12 Configuration of a photovoltaic pumping system with batteries

Figure I.20 shows the main components of the photovoltaic pumping system with batteries

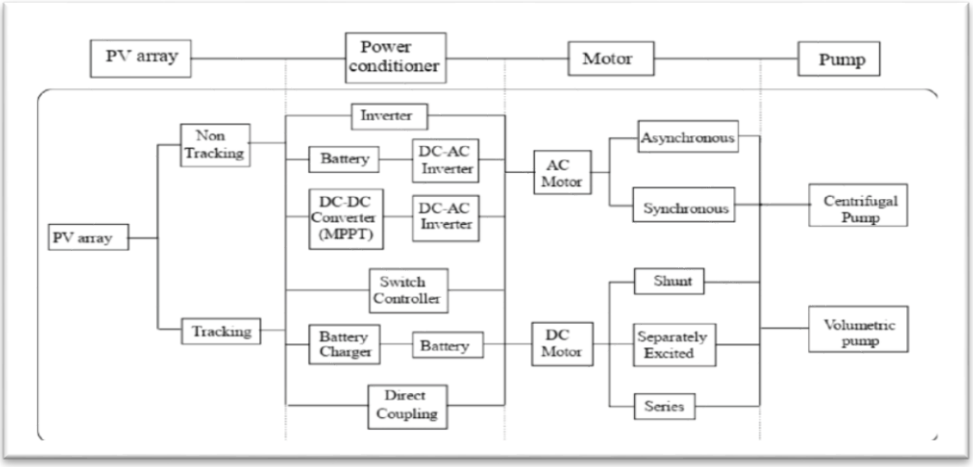


Figure I.20 Main components of the photovoltaic pumping system with batteries [38].

I.13 Operation of a Photovoltaic Generator at Its Maximum Power

An optimal photovoltaic system's overall design is intrinsically complicated. On the source side, a solar generator's power output fluctuates greatly based on temperature, light, and the load's fluctuating behavior based on consumption, all of which are frequently unpredictable. In fact, the extractable power varies in these shifting circumstances. Indeed, this is how the concept of Maximum Power Point Tracking, or MPPT, came to be. Unlike fixed voltage control, the MPPT approach uses a search algorithm to predict the maximum of the power curve without interfering with the solar panel's regular operation. By carefully managing the power and ensuring that the derivative of the power with respect to time is zero, the maximum power is attained. In order to get the highest power on the current/voltage characteristic, MPPT searches for the reference value rather than relying on a preset one. It is vital to note that MPPT is crucial since it minimizes expenses and enhances efficiency. When properly tuned, MPPT may capture over 97% of solar electricity. The conductance increment algorithm, the fuzzy logic technique, the Perturb and Observe (P&O) method, and others are among the MPPT methods that are now accessible [39]

I.14 Advantages and Disadvantages of a PV system

I.14.1 Advantages

- PV systems provide energy independence since sunlight is free and abundant.
- They are environmentally friendly, producing no pollution or noise.
- High reliability and require little maintenance with long operational lifespans.
- Modular design allows easy expansion based on energy needs.
- Enable decentralized energy generation (close to the point of use).
- Energy storage options can reduce the impact of power outages.
- Can be used to power specific devices or to supplement the grid [32]

I.14.2 Disadvantages

- Initial installation costs are high compared to other power sources.
- PV systems have low energy density, needing large areas to install panels.
- Energy output depends on factors like location, sunlight availability, time of year, and panel orientation. [32]

I.15 Conclusion

In preparation for the modeling and analysis of the photovoltaic system, which will be addressed in the following chapter, this chapter has presented fundamental concepts regarding the photovoltaic system. We have also discussed its significant role in modern electricity production, its prospects, particularly in Algeria, its structure, various connection modes, as well as its advantages and disadvantages.

CHAPTER II

MODELING AND SIMULATION OF THE PHOTOVOLTAIC SYSTEM

II.1 Introduction

Modeling is an essential step that must be performed before any system sizing, optimization, or simulation phase .This chapter presents a simulation model of a photovoltaic (PV) system operating under the weather conditions of the installation site. Individual photovoltaic systems are widely deployed in renewable energy applications, and it is crucial to be able to evaluate the performance of the systems in place. The current- voltage and power-voltage characteristics of a photovoltaic generator are influenced by solar irradiation and the operating temperature of the cells. We performed an electrical characterization and modeling of a photovoltaic generator in the context of Matlab.The main objective of this work is to predict the performance of a photovoltaic system .The simulation results obtained attest to the quality of the proposed model.

II.2. Photovoltaic generator (PVG)

II.2.1. Definition

A photovoltaic generator (PVG) is an energy conversion device that converts solar radiation directly into electrical energy through the photovoltaic effect. It is a series of photovoltaic cells interconnected in series and/or parallel to obtain the required voltage and current levels [40].

II.2.2. Performances of a PV system

The performance of a photovoltaic generator (PVG) is influenced by several elements, including solar irradiation, temperature and the electrical characteristics of the photovoltaic cells. This chapter presents presents the basic principles of photovoltaic energy conversion , and then explains the mathematical model of PVG. This is essential for analyzing and simulating the overall operation of the photovoltaic system [41] [42].

II.2.3. Structure of a Photovoltaic Generator (PVG)

A photovoltaic generator (PVG) consists of several photovoltaic cells, which are the basic units responsible for transforming solar energy into electricity.

These cells are usually made from semiconductor materials, such as silicon, and are connected in series and or parallel to form photovoltaic modules. It is possible to assemble several of these modules to form a global photovoltaic system capable of providing the required power. Figure II.1 illustrates the configuration of the photovoltaic connected to the load based on DC-DC converter using MPPT control [43].

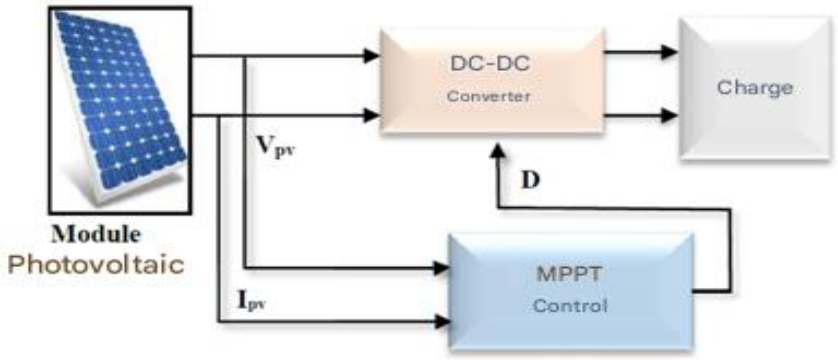


Figure II.1Main components of the photovoltaic system.

II.3. Photovoltaic cell

II.3.1. Simplified model

A photovoltaic cell can be defined as an ideal current source producing a photocurrent (Iph) which is proportional to the power of the incident light. This current source is connected in parallel with a diode which represents the PN junction of the photovoltaic cell. When a resistive load is connected to the terminals of the photovoltaic generator, part of the current (I) is supplied to the load, while the rest of the current (ID) passes through the diode [44]. Figure II.2 represents this relationship, which can be formulated as follows:

$$I = I_{ph} - I_D \quad \text{(II.1)}$$

I: Current delivered by the solar panel.

I_{ph}: The illumination current.

I_D: The current in the diode.

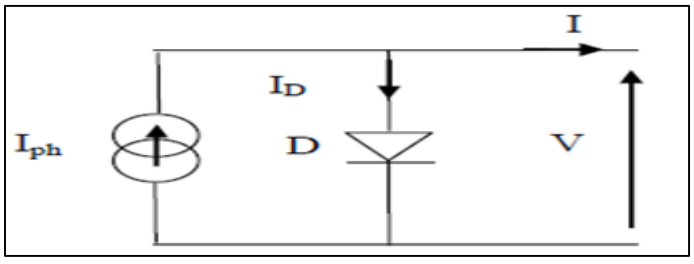


Figure II.2 Simplified model of the cell.

For an ideal photovoltaic generator, the voltage across the load resistor is equal to the voltage across the diode:

$$V = V_D \quad \text{(II.2)}$$

$$I_D = I_0\left(\exp\left(\frac{V_D}{V_t}\right) - 1\right) \quad \text{(II.3)}$$

Where:

I_D : is the current flowing through the diode.

I_0 : is the reverse saturation current.

V_D: is the voltage across the diode.

Vt: is the thermal voltage.

$$I_D = I_0(\exp(\frac{V_D}{V_T}) - 1) \quad \text{(II.4)}$$

Where

V_t : $^{nKT}/_{q}$ is thethermal voltage of a photovoltaic (PV) cell, and it plays a key role in modeling the electrical behavior of the cell (especially in the diode equation).

n: Diode quality factor (1~1.5)

K: Boltzmann constant, $k = 1.38e^{-23}$ [J/K].

q : The charge of the electron$1.6e^{-19}$[eV].

T : Kelvin Temperature at standard test condition [K].

The output current is equivalent to:

$$I_{PH} : I - I_D = I - I_0(\exp(\frac{V_D}{V_t}) - 1) \quad \text{(II.5)}$$

Although this model is purely theoretical and does not take into account the real behavior of a photovoltaic cell, it remains valid under certain conditions, such as the omission of voltage losses and leakage currents. However, some other models, although theoretical, describe the behavior of a photovoltaic cell more precisely.

II.3.2. Single-Diode Model

The old photovoltaic model did not take into account all the phenomena occurring during the conversion of light energy. Under real conditions, output voltage drop and leakage currents are observed, as shown in Figure II.3.

These voltage losses are represented by a series resistance (Rs), while the leakage currents are modeled by a parallel resistance (Rsh) [44].

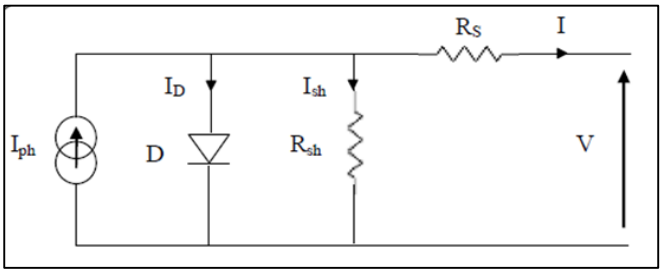


Figure II.3 Single-diode model of the PV cell.

We have:

$$I = I_{Ph} - I_D - I_{sh} \quad \text{(II.6)}$$

$$I_{sh} = \frac{V_D}{Rsh} = \frac{V - Rs * I}{Rsh} \quad \text{(II.7)}$$

$$I_{Pv} = I_{Ph} - I_0 \left(\exp(\frac{V_D}{V_t}) - 1\right) - \frac{V - Rs * I}{Rsh} \quad \text{(II.8)}$$

Where:

R_{sh} : Shunt resistance characterizing the leakage currents of the junction.

R_s: Series resistance representing the various resistances of contacts and connections.

I_{sh}: Current flowing through the shunt resistanceas given as :

$$I_{ph} = I_{Phn} + K_i(T - T_a) \cdot (\frac{G}{G_n})$$

And Vt is thermal voltage of the module for a number as given as :

$$V_t = \frac{Ns \cdot K \cdot T}{q}$$

Where:

q : Electron charge$(1.6 \times 10 - 19\, C)$.

K : Boltzmann constant$(1.3854 \times 10 - 23\, J/K)$.

a: Diode ideality factor.

T: Effective temperature of the cell in Kelvin $[K]$.

Ns: Number of cells in series per module.

T: cell temperature, varying with irradiance and ambient temperature as given as :

$$T - T_a = \frac{G}{800} \cdot (NOCT - 20).$$

With:

Ta: ambient temperature is $20\ °C$ at wind speed greater than 1m/s.

NOCT: Nominal Operating Cell Temperature under the following conditions:

$Gn = 800\ W/m^2$; AM 1.5 .

II.3.3. Two-Diode Model

Currently, the two - diode model, also known as the double exponential model, is considered the most accurate electrical representation of a photovoltaic cell. In this method, the cell is represented as a current source parallel to two diodes, more accurately reflecting the nonlinear behavior of the device. To account for various physical phenomena, such as recombination losses and leakage currents, the model is improved by adding a series resistor (RS) and a shunt (or parallel) resistor (RSh), as demonstrated in the equivalent circuit diagram in Figure II.4 [45].

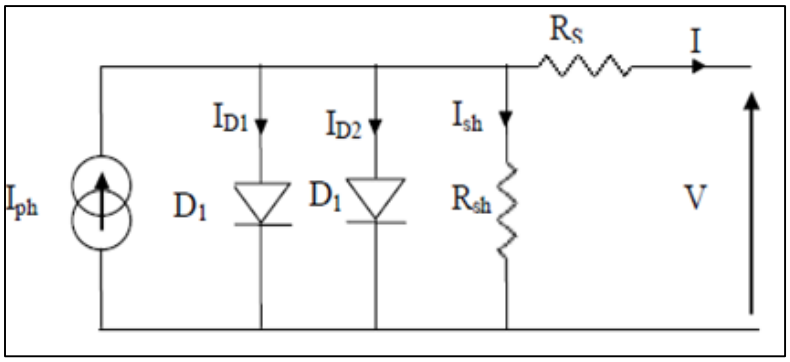


Figure II.4 Two-diode model of the PV cell.

If we apply Kirchhoff's current law (node law) to the circuit in Figure II.4, we obtain:

$$I = I_{Ph} - I_{D1} - I_{D2} - I_P \quad \text{(II.9)}$$

Thus, the relationship becomes:

$$I = I_{Ph} - I_{01}\left(\exp\left(\frac{q(V+Rs\ I)}{a1Vt}\right) - 1\right) - I_{02}\left(\exp\left(\frac{q(V+Rs\ I)}{a2Vt}\right) - 1\right) - \frac{V+Rs*I}{Rsh} \quad \text{(II.10)}$$

Where:

n1 : Ideality factor of diode D1.

n2 : Ideality factor of diode D2.

I_{01}, I_{02}: Reverse saturation currents of diodes D1and D2.

According to the literature, it can be said that the two-diode model of the cell is the closest to reality, as it reproduces the nearly real behavior of the cell.

II.4. DC-DC Converter

DC - DC converters are linear, switching power converters used to change the voltage level of a direct current (DC) power source. They are essential in applications such as storing photovoltaic energy in batteries or supplying a direct current load [46].Linear converters provide a direct current flow from the input to the load, while switching converters regulate the output by fragmenting the input voltage and controlling the average current by adjusting the system duty cycle. The following figure II.5 shows the most commonly used symbolic representation of a DC/DC converter.

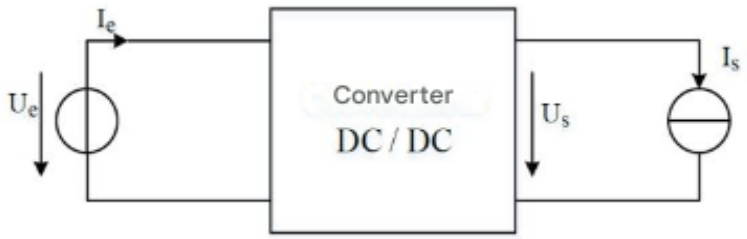


Figure II.5 Symbolic representation of a DC/DC converter.

The most commonly used types of DC-DC converters are:

- Boost converter (voltage increase),
- Buck converter (voltage decrease) ,
- Buck-Boost converter.

In the following section, we briefly review the operating principle of the boost converter.

II.4.1 Boost Converter

Boost converter is a device that steps up the voltage, meaning the output voltage is always higher than the input voltage. It is also commonly referred to as a parallel chopper or step -up regulator in the literature [46]. The basic illustration is shown in figure II.6.

- When the semiconductor switch (K) is conducting, the diode is reverse biased and the power source (usually a series of solar cells) supplies power to the inductor. During this period, the load is supplied by the capacitor.
- When the switch (K) is off, current flows from the power source to the load via the inductor and diode .

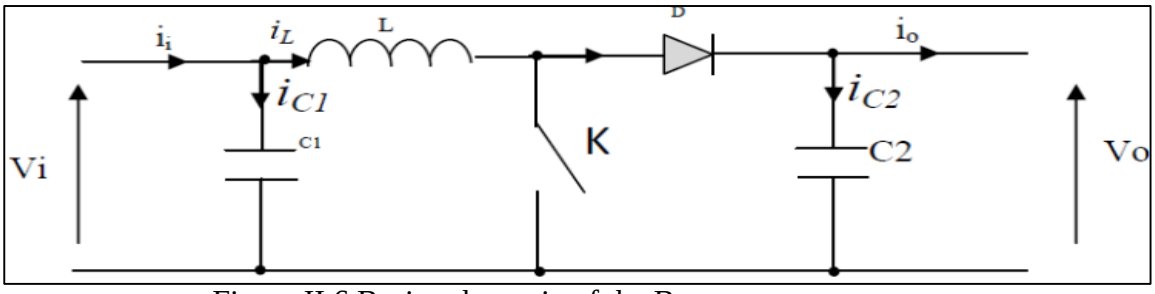


Figure II.6 Basic schematic of the Boost converter.

The operation of a boost converter is divided into two distinct phases, depending on the state of switch K.

When switch K is closed (conducting state), the current through the inductor increases and energy is stored in the form of magnetic energy within the inductor. During this stage, the diode is reverse biased and prevents current from flowing, effectively disconnecting the load from the input source. The expression of the input voltage (Vi) during this phase is therefore:

$$V_i = L\frac{dI_L}{dt} \qquad \text{(II.11)}$$

At the end of the ON-state (conducting phase), the inductor current I_L has increased by an amount ΔI_L, which is expressed as:

$$\Delta I_{LON} = \int_0^{D.T} dI_L = \int_0^{D.T} \frac{V_i.dt}{L} = \frac{V_i.D.T}{L} \qquad \text{(II.12)}$$

D is the duty cycle, which represents the fraction of the switching period T during which the switch S is conducting (ON). It satisfies the condition: $0 < D < 1$.

When the switch K is open (OFF state), the inductor is placed in series with the power source, and its voltage adds to that of the source this is known as the boost effect. The energy previously stored in the inductor is then transferred to the capacitor and the load.

The expression for the input voltage Vi during this phase is:

$$V_i - V_0 = L.\frac{dI_L}{dt} \quad \text{(II.13)}$$

The variation of I_L during the OFF state (when the switch is open) is therefore given by:

$$\Delta I_L = \frac{V_0 - V_i}{L}.(1 - D).T \quad \text{(II.14)}$$

The amount of energy stored in each of the components is the same at the beginning and at the end of one switching cycle. Consequently, the inductor current I_L has the same value at the start and end of each switching period. This allows us to write:

$$\Delta I_{Lon} + \Delta I_{Loff} = \frac{V_i.D.T}{L} + \frac{V_0 - V_i(1-D).T}{L} \quad \text{(II.15)}$$

The ratio between Vi and Vo is therefore

$$\frac{V_0}{V_i} = \frac{1}{1-D} \quad \text{(II.16)}$$

D: is the duty cycle**.**

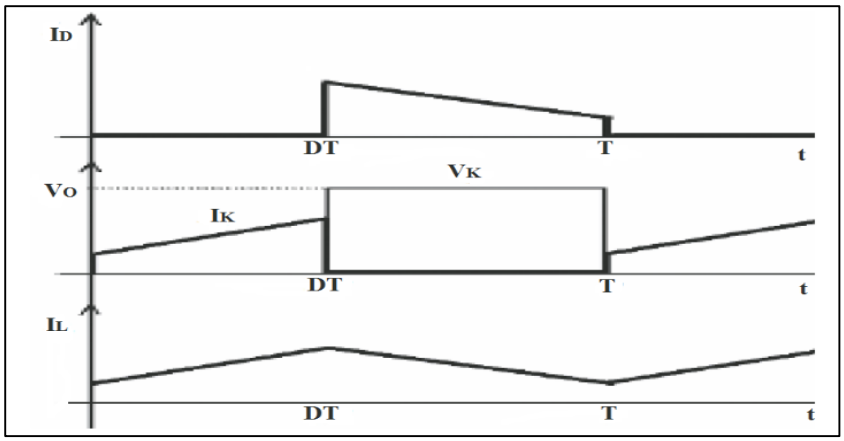


Figure II.7 Current and voltage waveforms of a boost converter.

II.5. Maximum Power Point Tracking (MPPT) Control

Photovoltaic cells are used to provide energy in many electrical applications. To get the best efficiency from the solar panel, Maximum Power Point Tracking (MPPT) is used to manage the converter [47].The PPMR technique, developed since 1968, is essential for the optimal operation of photovoltaic systems.

II.5.1. Principle of MPPT

The principle of Maximum Power Point Tracking (MPP) is based on the use of a control algorithm to extract energy at the maximum power point, based on the measurement of voltage and current from the photovoltaic module. This ensures that the maximum possible energy is delivered to the output.

The Maximum Power Point (MPP) changes depending on conditions, such as irradiance levels and temperature. To continuously extract the maximum power from the photovoltaic panel, it is crucial to constantly operate at the maximum power point (MPP) [47]. Next, we will introduce and study the P&O (Perturb and Observe) method, which is among the most frequently used techniques in publications.

II.5.2. Perturb and Observe (P&O) Method

The Perturb and Observe (P&O) method is the simplest MPPT technique, as it only requires the measurement of a few parameters. This involves disturbing one of the input parameters of the static converter (usually the voltageVpv) and then observing the effect of this change on the output power of the system. This method allows maximum power to be extracted even when irradiance and temperature fluctuate .

The obtained value is then compared with the power $P(k-1)$ calculated during the previous cycle. Depending on the result of the comparison, Vpv is modified either in the same direction as during the previous cycle, or in an opposite direction .Therefore, power increases, reaches a peak, and then decreases .As soon as a decrease in power is identified, the direction of control is reversed, and this cycle continues .Nevertheless, the oscillation of the system around the maximum allows the maximum power point to be tracked [48].Figure II.8 summarizes the operation principle of this method.

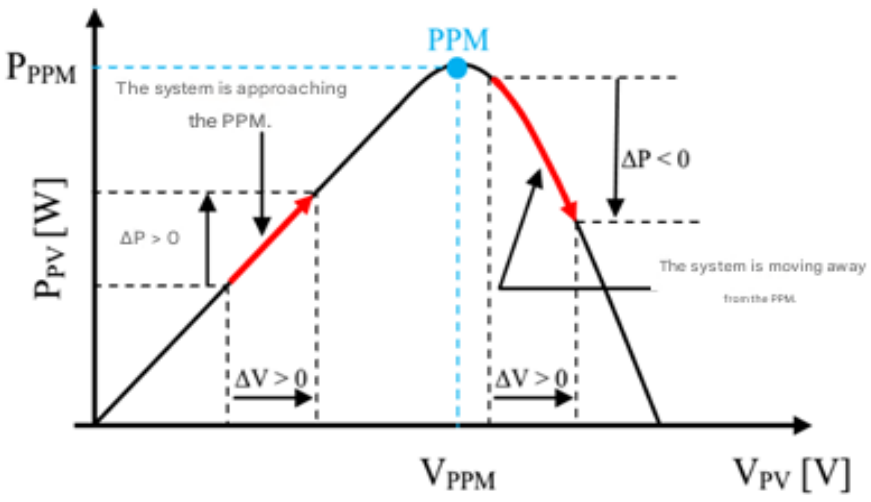


Figure II.8 Operating principle of the P&O method.

Figure II.9 shows the flowchart of the P&O algorithm, as it should be implemented in a control microprocessor [48].

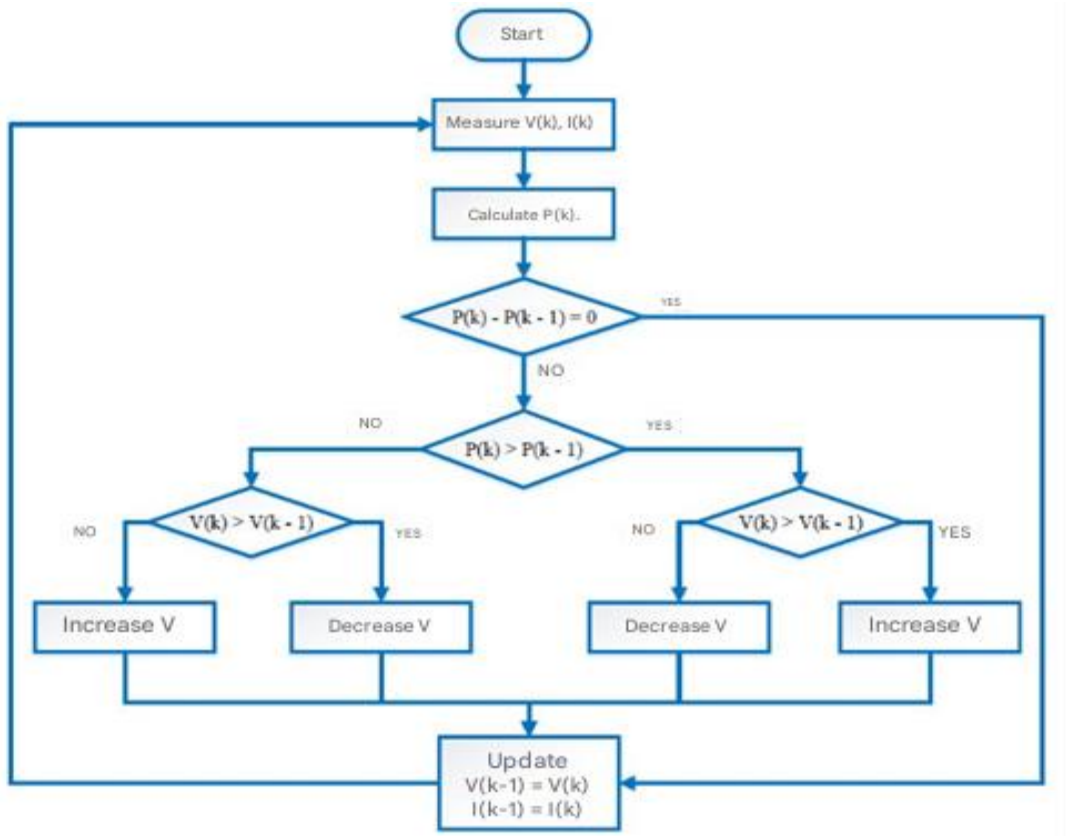


Figure II.9 Flowchart of the P&O method.

II.5.3. The Incremental Conductance (INC) Method

The Incremental Conductance (INC) Maximum Power Point Tracking (MPPT) technique is one of the most widely used MPPT strategies, offering the advantage of rapid tracking of the MPP [49] [50]. Compared to the Perturb & Observe (P&O) MPPT strategy, INC combines and utilizes the unique characteristics of the output P-V curve and the I-V curve of the photovoltaic generator and tracks the MPP more quickly and accurately [51]. This technique is based on the slope of the P-V characteristic curve where the MPP is tracked when$\frac{dp}{dv}$=0, as follows:

$$\frac{dP}{dV} = \frac{d(V.I)}{dV} = I\frac{dV}{dV} + V\frac{dI}{dV} = I + V\frac{dI}{dI}dV \simeq I + \frac{\Delta I}{\Delta V} \quad \text{(II.17)}$$

The slope of the photovoltaic generator's power curve is zero at the MPP, positive to the left, and negative to the right.

Equation II.17indicates that the MPP is reached when$\frac{\mathrm{dI}}{\mathrm{dV}} = -\mathrm{I}/\mathrm{V}$.

- If $\frac{\mathrm{dI}}{\mathrm{dV}} > -I/V$, the operating point is to the left of the MPP on the P-V curve.
- If $\frac{\mathrm{dI}}{\mathrm{dV}} < -I/V$, the operating point is to the right.

The MPP can thus be tracked by comparing the instantaneous conductance (I/V) to the incremental conductance $(\mathrm{dI}/\mathrm{dV})$, as shown in the flowchart in Figure II.9.

The size of the increment determines the tracking speed of the MPP. Fast tracking can be achieved with larger increments, but the system may not operate exactly at the MPP and may oscillate around it.

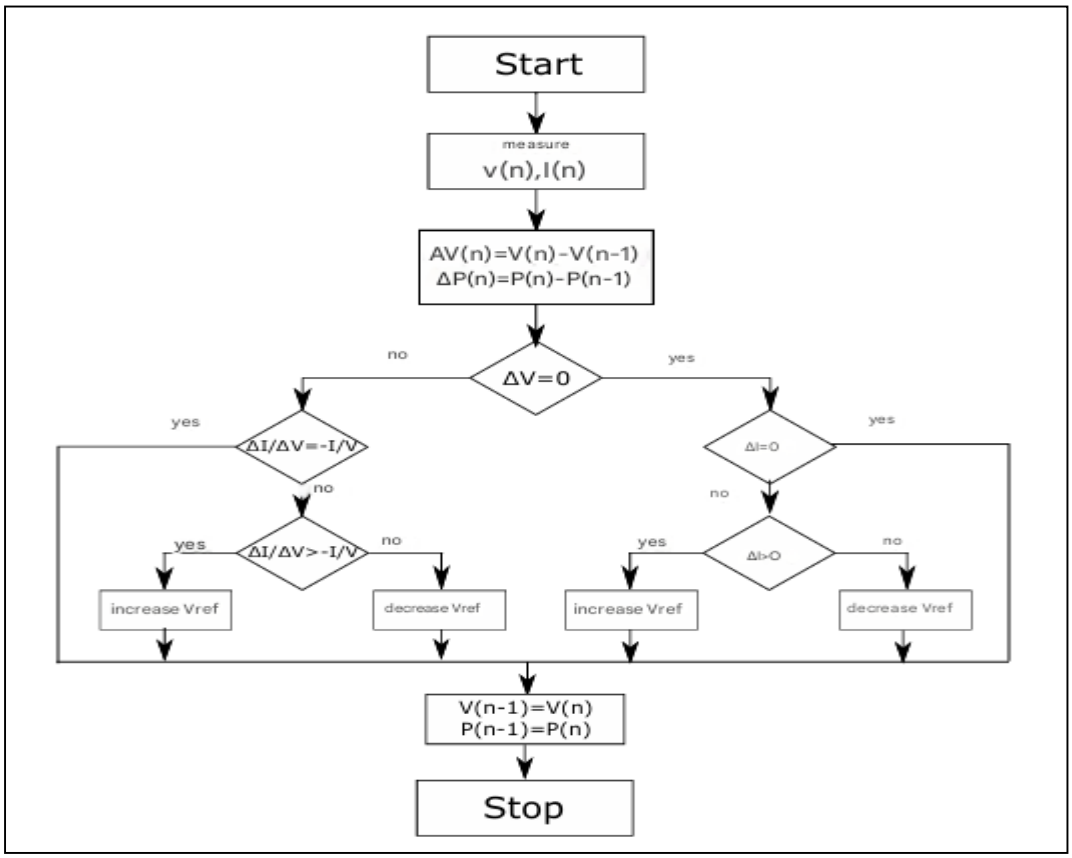


Figure II.10 Flowchart of the INC Method

II.6. Simulation of the Photovoltaic Generator

In this study, we chose to model and simulate our photovoltaic system using a panel composed of a string of 8 modules connected in series, of the SST235-60P type manufactured by China

Sunergy (Nanjing). Each module consists of 60 solar cells. The electrical characteristics of the PV system are presented in Table II.1. [52]

Electrical Characteristics	**The value**
Nominal Power STC P_{MAX} (W)	235.024
Open-circuit Voltage V_{CO}(V)	36.8
Short-circuit Current I_{CC} (A)	8.54
Voltage at Maximum Power V_{PMAX} (V)	29.6
Current at Maximum Power I_{PMAX} (A)	7.94
Temperature Coefficient of I_{SC}(A)	0.06 % / °C
Temperature Coefficient of V_{CO}(V)	-0.37 % / °C

Table II.1 Characteristics of the SST235-60P (China Sunergy (Nanjing)) PV system.

II.6.1 Simulation of the PV Module

II.6.1.1 First case

The PV Module has a maximum power output of 305 W, was first used to model its electrical behavior. As seen in Figures II.11 and II.12, this enabled us to ascertain the PV module's IV (current-voltage) and PV (power-voltage) properties.

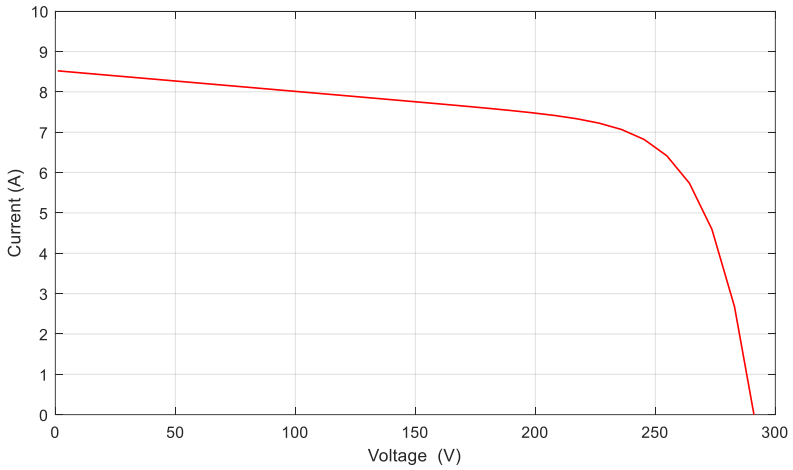


Figure II.11 Simulation of the (I-V) characteristic of the PV module.

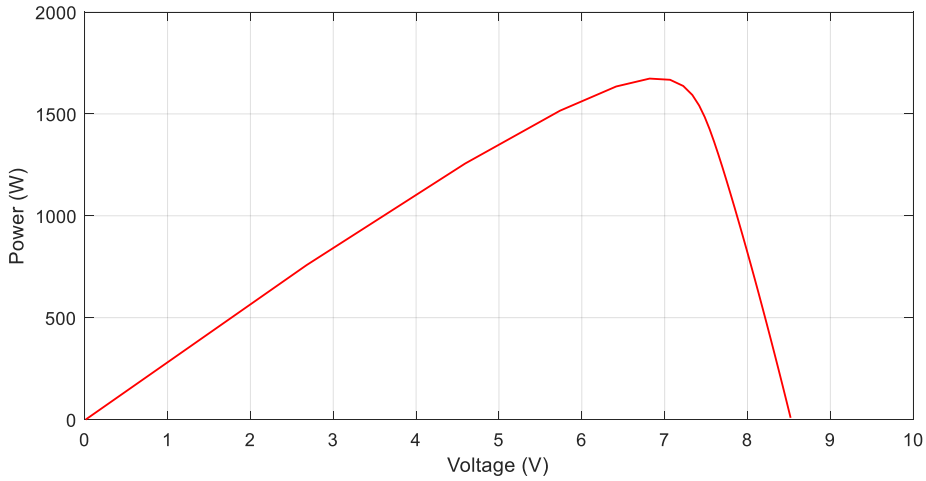


Figure II.12 Simulation of the (P-V) characteristic of the PV module.

These figures illustrate the module current variation at fixed temperature at 25°c and irradiance at 1000 W/m^2 as a function of voltage. Up until about V = 200 V, the current is shown to be almost constant. After that, it drops exponentially until it reaches zero.

We can see that the change in the module power under the same circumstances as a function of voltage. We observe there is a peak in the power curve at about P = 1600W. Up until this moment, the curve rises gradually; after that, it collapses precipitously to zero.

II.6.1.2 Second case

The PV system's overall simulation (GPV, converter, MPPT, load), the photovoltaic (PV) system is connected to a boost DC-DC converter and an MPPT controller employing the INC algorithm, which supplies a DC load. Figure II.16 illustrates the system's SIMULINK schematic

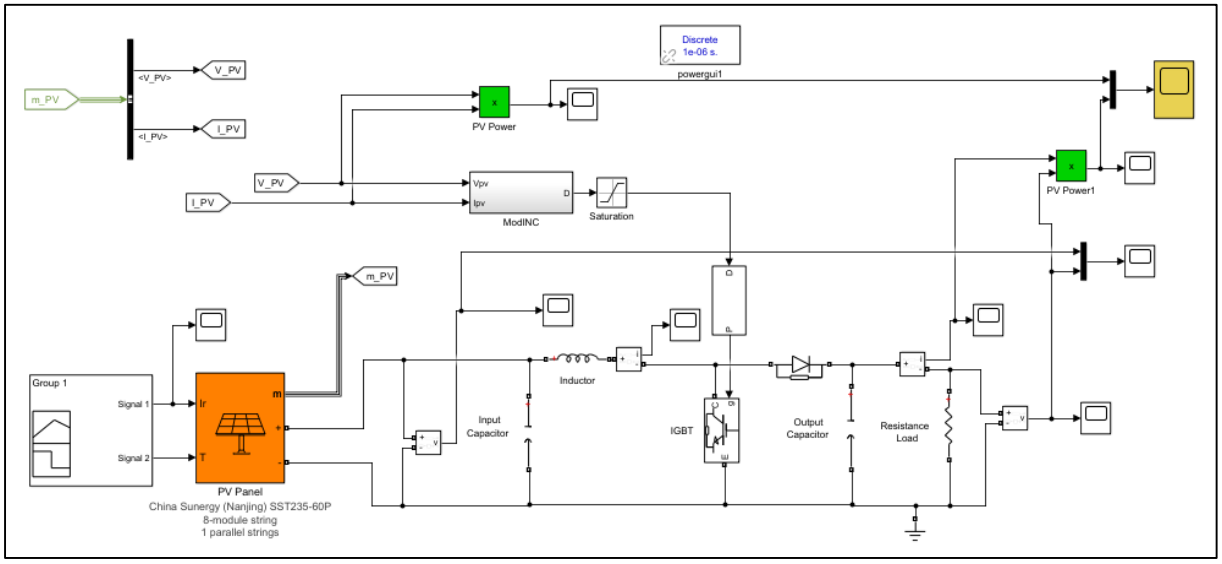


Figure II.13 SIMULINK model of the PV system.

II.6.5 Results and Discussion

The goal of these simulations is to visualize the different power profiles (at the output of the solar panel and the static converter), duty cycles (D), and the voltages delivered by both the photovoltaic panel and the static converter using the Maximum Power Point (MPP) tracking method via INC algorithm (Incremental conductance). In this section, the simulation was carried out using MATLAB-Simulink, with variable irradiance levels (600, 800, 1000 W/m²) and a constant temperature (25°C).

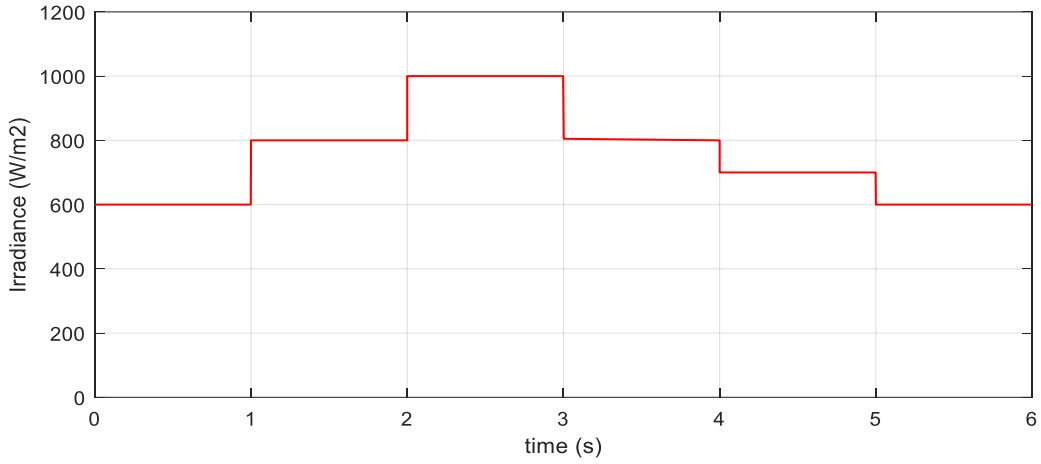


Figure II.14 Variation of irradiance at a temperature of T=25°C.

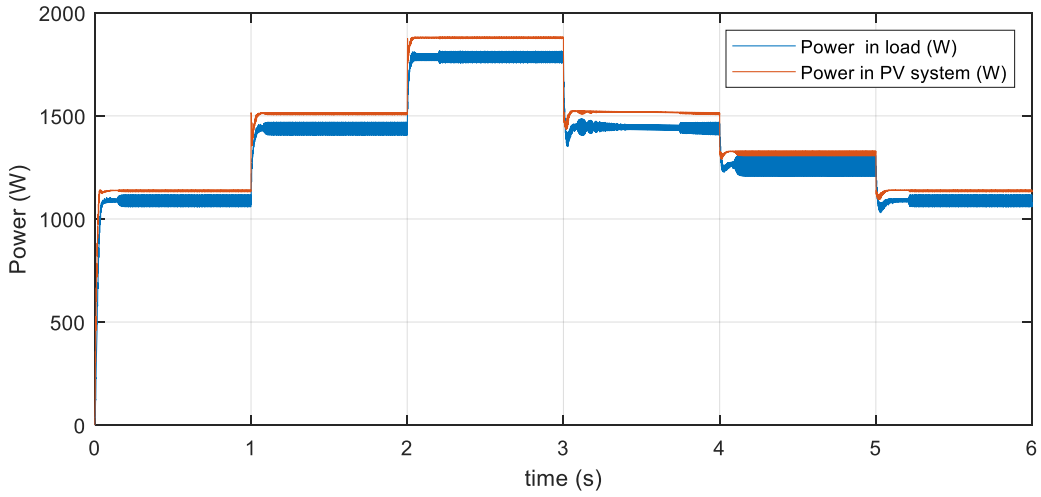


Figure II.15 Variation of power at the output of the PV system and in Load.

The curve shows that the power delivered by the photovoltaic (PV) panel increases with irradiation. At a constant temperature, higher irradiation provides more light energy, which leads to an increase in the current produced by the panel. As a result, the output power increases proportionally with irradiation. It is also observed that the maximum power transferred to the

load closely matches the power generated by the panel, indicating effective tracking of the Maximum Power Point (MPPT). This confirms the system's efficiency in matching the power between the PV generator and the load.

II.7 Conclusion

The modeling and simulation of the photovoltaic system, including the solar generator, boost converter, and MPPT control using the Incremental Conductance (INC) algorithm, have demonstrated the system's effectiveness. Under fixed temperature and varying irradiance conditions, the simulation results confirm that the MPPT control ensures the PV generator consistently operates at its maximum power point. This highlights the efficiency and reliability of the INC-based MPPT algorithm in optimizing the energy output of the photovoltaic system.

CHAPTER III

MODELING AND SIMULATION OF INDUCTION MACHINE SUPPLIED BY AN INVERTER

III.1. Introduction

With the development of power electronics, the squirrel-cage asynchronous machine originally intended for constant-speed applications has emerged as the most popular motor in variable-speed drive systems. Managing torque, speed, or even location is necessary to operate the asynchronous motor. a model that faithfully captures the dynamic behavior of the asynchronous motor control system is required in order to perform simulations of it.

III.2. Modeling of induction machine

The mathematical model is primarily used to analyze the behavior of various electromechanical quantities and to anticipate the control strategies required to address issues related to load and speed variations. In this chapter, the machine is supplied by a two-level voltage inverter. The different equations are expressed in their respective reference frames, as illustrated in the figure III.1.

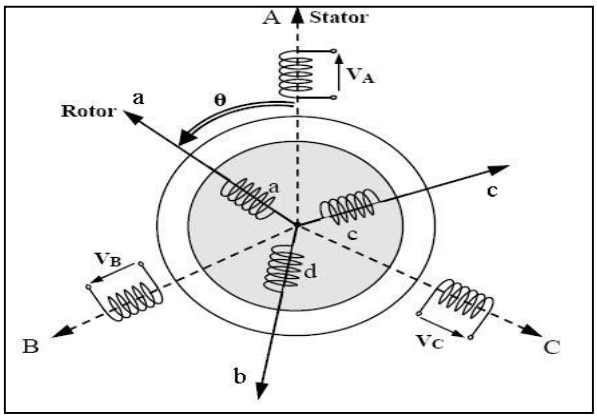


Figure III.1 Schematic Diagram of a Three-Phase Asynchronous Motor.

- sa, sb, sc:Three phases of the stator.
- ra, rb, rc:Three phases of the rotor.
- θ:Is the electrical angle between the axis of the stator phase and the rotor phase.

III.3. Simplifying Assumptions

The study of the modeling of the idealized three-phase asynchronous machine will be carried out within the usual context of simplifying hypotheses [53]

- The air gap is constant.
- The effect of slots is neglected.
- The distribution of the magneto motive forces in the air gap is spatially sinusoidal.
- Ferromagnetic losses are neglected
- The magnetic circuit is unsaturated and has constant permeability.

- The influence of skin effect and heating on the characteristics is not taken into account.

Among the important consequences of these hypotheses, we can mention:

- The additively of fluxes.
- The constancy of self-inductances.
- The sinusoidal variation law of mutual inductances between the stator windings as a function of the electrical angle of their magnetic axes.

III.3.1. Electrical Equation

From Figure III.1, the electrical equations of the three-phase asynchronous machine model are written respectively for the stator with the index "s" and the rotor with the index "r" as follows:

For the stator

$$\begin{bmatrix} Vsa \\ Vsb \\ Vsc \end{bmatrix} = \begin{bmatrix} Rs & 0 & 0 \\ 0 & Rs & 0 \\ 0 & 0 & Rs \end{bmatrix} \cdot \begin{bmatrix} isa \\ isb \\ isc \end{bmatrix} + \frac{d}{dt} \begin{bmatrix} \varphi sa \\ \varphi sb \\ \varphi sc \end{bmatrix} \quad \text{(III.1)}$$

For the rotor

$$\begin{bmatrix} Vra \\ Vrb \\ Vrc \end{bmatrix} = \begin{bmatrix} Rr & 0 & 0 \\ 0 & Rr & 0 \\ 0 & 0 & Rr \end{bmatrix} \cdot \begin{bmatrix} ira \\ irb \\ irc \end{bmatrix} + \frac{d}{dt} \begin{bmatrix} \varphi ra \\ \varphi rb \\ \varphi rc \end{bmatrix} \quad \text{(III.2)}$$

With:

Rs: Resistance of the stator winding.

Rr:Resistance of the rotor winding.

III.3.2.Magnetic Equation

The simplifying hypotheses mentioned earlier lead to linear relationships between the fluxes and currents of the asynchronous machine. These relationships are written in matrix form as follows:

$$[\Phi_s] = [L_{ss}][i_s] + [M_{sr}][i_r] \quad \text{(III.3)}$$

Or

$$[\Phi_r] = [M_{rs}][i_s] + [L_{rr}][i_r] \text{(III.4)}$$

$[L_{ss}]$: stator inductance matrix.

$[L_{rr}]$: Rotor inductance matrix.

$[M_{rs}]$: Mutual inductance matrix.

With:

$$[L_{ss}] = \begin{bmatrix} l_s & m_s & m_s \\ m_s & l_s & m_s \\ m_s & m_s & l_s \end{bmatrix}; [L_{rr}] = \begin{bmatrix} l_r & m_r & m_r \\ m_r & l_r & m_r \\ m_r & m_r & l_r \end{bmatrix}$$

$$[M_{sr}] = M \cdot \begin{bmatrix} \cos(\theta) & \cos\left(\theta - \frac{2\pi}{3}\right) & \cos\left(\theta - \frac{4\pi}{3}\right) \\ \cos\left(\theta - \frac{4\pi}{3}\right) & \cos(\theta) & \cos\left(\theta - \frac{2\pi}{3}\right) \\ \cos\left(\theta - \frac{2\pi}{3}\right) & \cos\left(\theta - \frac{4\pi}{3}\right) & \cos(\theta) \end{bmatrix}$$

l_s,l_r: represent the self-inductances per phase of the stator and rotor, respectively.

m_s : Mutual inductance between two stator phases.

m_r : Mutual inductance between two rotor phases.

M_{sr}: Mutual inductance between a rotor phase and a stator phase.

M : Maximum mutual inductance between a stator phase and a rotor phase.

θ :Angle that defines the instantaneous relative position between the magnetic axes of the "stator" and "rotor" phases taken as reference axes.

The analytical solution of the system of equations faces difficulties due to the fact that the trigonometric terms of the matrix vary with time. This will lead to the use of the Park transformation, which will make these parameters constant [54].

III.4. Park Transformation

The Park Transformation converts a three-phase system into an equivalent two-phase system by mapping real variables to their components. In Figure III.2, the transformation from the three-phase system to the two-phase system consists of expressing the "u, v" components as functions of the original components "X_a ,X_b,X_c"..

The two models are electrically and magnetically equivalent.

- φ: represents the angle between the vector$V_{sp}$and the $X_a$axis of phase a
- θ_a : represents the instantaneous angle between theX_a axis of phase a and the u axis
- $\omega_a = d\theta_a/dt$: angular velocity of the two-phase axis system relative to the three-phase axis system

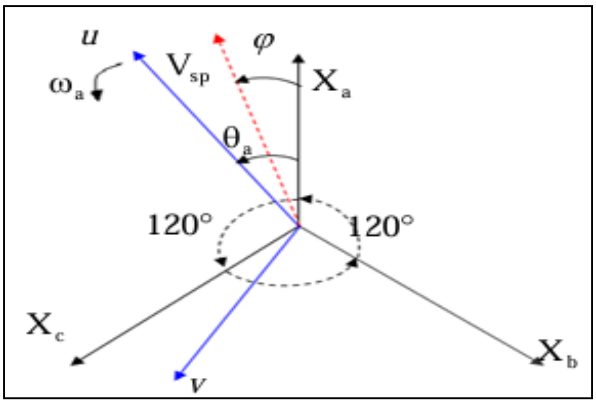


Figure III.2 Three-phase system to the two-phase system.

According to Figure III.2, the projection onto the three-phase axes yields the following equations:

$$\begin{cases} V_{sa} = V_{sp} \cdot \cos(\varphi) \\ V_{sb} = V_{sb} \cdot \cos\left(\varphi - \frac{2\pi}{3}\right) \\ V_{sc} = V_{sc} \cdot \cos\left(\varphi - \frac{4\pi}{3}\right) \end{cases} \quad \text{(III.5)}$$

The projection onto the two-phase axis yields:

$$\begin{cases} V_{su} = k\left[V_{as} \cdot \cos(\theta_a) + V_{sb} \cdot \cos\left(\theta_a - \frac{2\pi}{3}\right) + V_{sc} \cdot \cos\left(\theta_a - \frac{4\pi}{3}\right)\right] \\ V_{sv} = k\left[V_{sa} \cdot \sin(\theta_a) + V_{sb} \cdot \sin\left(\theta_a - \frac{2\pi}{3}\right) + V_{sc} \cdot \sin\left(\theta_a - \frac{4\pi}{3}\right)\right] \end{cases} \quad \text{(III.6)}$$

This transformation depends on an arbitrary normalization coefficient the usual values taken by k are:

- $k = 2/3$: If one wishes to preserve the amplitudes of the quantityX, which, for a motor, will be the currents, voltages, and fluxes.
- $k = \sqrt{2/3}$: If one wants to preserve the power invariant in the transformation.

We add the homopolar component Vso to equation (III.6) to balance the transformation.

$$[P(\theta_a)] = \sqrt{\frac{2}{3}} \cdot \begin{bmatrix} \cos(\theta_a) & \cos\left(\theta_a - \frac{2\pi}{3}\right) & \cos\left(\theta_a - \frac{4\pi}{3}\right) \\ -\sin(\theta_a) & -\sin\left(\theta_a - \frac{2\pi}{3}\right) & -\sin\left(\theta_a - \frac{4\pi}{3}\right) \\ \frac{1}{\sqrt{2}} & \frac{1}{\sqrt{2}} & \frac{1}{\sqrt{2}} \end{bmatrix} \quad \text{(III.7)}$$

The transformation matrix from the two-phase system to the three-phase system is given by:

$$[P(\theta_a)]^{-1} = \sqrt{\frac{2}{3}} \cdot \begin{bmatrix} \cos(\theta_a) & -\sin(\theta_a) & \frac{1}{\sqrt{2}} \\ \cos\left(\theta_a - \frac{2\pi}{3}\right) & -\sin\left(\theta_a - \frac{2\pi}{3}\right) & \frac{1}{\sqrt{2}} \\ \cos\left(\theta_a - \frac{4\pi}{3}\right) & -\sin\left(\theta_a - \frac{4\pi}{3}\right) & \frac{1}{\sqrt{2}} \end{bmatrix} \quad \text{(III.8)}$$

This transformation is valid for currents, voltages, and fluxes. The (u, v)frame rotates at a speed $(\omega_a - \omega_b)$ relative to the rotor.

III.5. Modeling in two-phase System

The Park transformation involves applying a change of variables to the currents, voltages, and fluxes, taking into account the angle between the winding axes and the (u, v) axes.

By multiplying both sides of equations (III.7and III.8) by the Park transformation matrix $[P(\theta a)]$, we obtain

III.5.1. Electrical Equation

By multiplying both sides of equations (III.1and III.2) by the Park transformation matrix $[P(\theta a)]$, we obtain:

$$\begin{bmatrix} V_{su} \\ V_{sv} \end{bmatrix} = \begin{bmatrix} R_s & 0 \\ 0 & R_s \end{bmatrix} \cdot \begin{bmatrix} i_{su} \\ i_{sv} \end{bmatrix} + \frac{d}{dt}\begin{bmatrix} \Phi_{su} \\ \Phi_{sv} \end{bmatrix} + \begin{bmatrix} 0 & -\omega_a \\ \omega_a & 0 \end{bmatrix}\begin{bmatrix} \Phi_{su} \\ \Phi_{sv} \end{bmatrix} \quad \text{(III.9)}$$

$$\begin{bmatrix} V_{ru} \\ V_{rv} \end{bmatrix} = \begin{bmatrix} R_r & 0 \\ 0 & R_r \end{bmatrix} \cdot \begin{bmatrix} i_{ru} \\ i_{rv} \end{bmatrix} + \frac{d}{dt}\begin{bmatrix} \Phi_{ru} \\ \Phi_{rv} \end{bmatrix} + \begin{bmatrix} 0 & -(\omega_a - \omega_r) \\ (\omega_a - \omega_r) & 0 \end{bmatrix} \cdot \begin{bmatrix} \Phi_{ru} \\ \Phi_{rv} \end{bmatrix} \quad \text{(III.10)}$$

III.5.2. Mechanical Equation

By multiplying both sides of equations (III.3and III.4) by the Park transformation matrix $[P(\theta a)]$, we obtain:

$$\begin{bmatrix} \Phi_{su} \\ \Phi_{sv} \end{bmatrix} = \begin{bmatrix} L_s & 0 \\ 0 & L_s \end{bmatrix} \cdot \begin{bmatrix} i_{su} \\ i_{sv} \end{bmatrix} + \begin{bmatrix} L_m & 0 \\ 0 & L_m \end{bmatrix} \cdot \begin{bmatrix} i_{ru} \\ i_{rv} \end{bmatrix} \quad \text{(III.11)}$$

$$\begin{bmatrix} \Phi_{ru} \\ \Phi_{rv} \end{bmatrix} = \begin{bmatrix} L_m & 0 \\ 0 & L_m \end{bmatrix} \cdot \begin{bmatrix} i_{su} \\ i_{sv} \end{bmatrix} + \begin{bmatrix} L_r & 0 \\ 0 & L_r \end{bmatrix} \cdot \begin{bmatrix} i_{ru} \\ i_{rv} \end{bmatrix} \quad \text{(III.12)}$$

With:

$L_s = ls - ms$: cyclic self-inductance of the stator,

$L_r = lr - mr$: cyclic self-inductance of the rotor,

$L_m = \frac{3}{2}M$: cyclic mutual inductance between stator and rotor,

III.6. References Frames

There are different possibilities for choosing the orientation of the "u, v" axis frame, which generally depend on the objectives of the application. One can choose the reference frame best suited to the problems posed. The choice practically boils down to three orthogonal reference frames (Figure III.3).

- (α, β)Axis reference frame: linked to the stator $(\theta a = 0)$for the study of rotor quantities.

- (d, q) axis reference frame: linked to the rotating field $(\theta a = \theta s)$.
- (x, y) axis reference frame: linked to the rotor $(\theta a = \theta r)$.

With:

θa: an arbitrary observation position that can be chosen in three different ways."

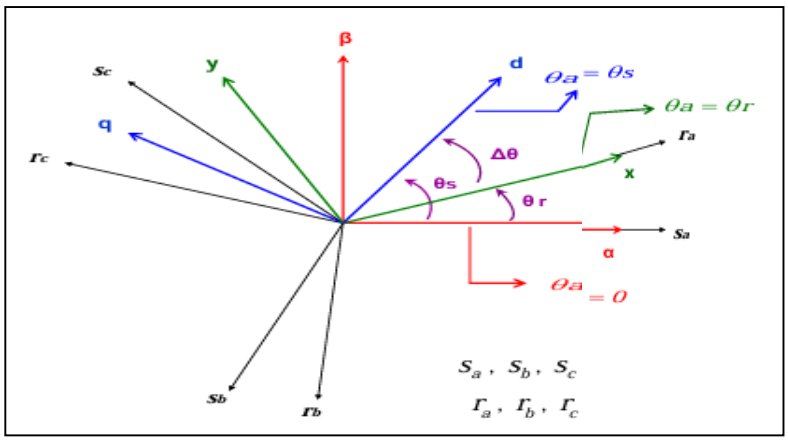


Figure III.3 Three-phase asynchronous motor with respect to the different reference frames.

III.6.1. Reference Frame Fixed with respect to the Stator

This axis system is stationary with respect to the stator; in this case, we have

$$\theta_a = 0 \Rightarrow \begin{Bmatrix} u \to \alpha \\ v \to \beta \end{Bmatrix}, \omega_a = \frac{d\theta_a}{dt} = 0 \quad \text{And} \quad \Delta\omega = -\omega_r$$

The electrical equations given by equations (III.9 and III.10) become:

$$\begin{bmatrix} V_{s\alpha} \\ V_{s\beta} \end{bmatrix} = \begin{bmatrix} R_s & 0 \\ 0 & R_s \end{bmatrix} \cdot \begin{bmatrix} i_{s\alpha} \\ i_{s\beta} \end{bmatrix} + \frac{d}{dt} \begin{bmatrix} \Phi_{s\alpha} \\ \Phi_{s\beta} \end{bmatrix} \tag{III.13}$$

$$\begin{bmatrix} V_{r\alpha} \\ V_{r\beta} \end{bmatrix} = \begin{bmatrix} R_r & 0 \\ 0 & R_r \end{bmatrix} \cdot \begin{bmatrix} i_{r\alpha} \\ i_{r\beta} \end{bmatrix} + \frac{d}{dt} \begin{bmatrix} \Phi_{r\alpha} \\ \Phi_{r\beta} \end{bmatrix} + \begin{bmatrix} 0 & \omega_r \\ -\omega_r & 0 \end{bmatrix} \begin{bmatrix} \Phi_{r\alpha} \\ \Phi_{r\beta} \end{bmatrix} \tag{III.14}$$

The magnetic equations given by equations (III.11and III.12) become:

$$\begin{bmatrix} \Phi_{s\alpha} \\ \Phi_{s\beta} \end{bmatrix} = \begin{bmatrix} L_s & 0 \\ 0 & L_s \end{bmatrix} \cdot \begin{bmatrix} i_{s\alpha} \\ i_{s\beta} \end{bmatrix} + \begin{bmatrix} L_m & 0 \\ 0 & L_m \end{bmatrix} \cdot \begin{bmatrix} i_{r\alpha} \\ i_{r\beta} \end{bmatrix} \tag{III.15}$$

$$\begin{bmatrix} \Phi_{r\alpha} \\ \Phi_{r\beta} \end{bmatrix} = \begin{bmatrix} L_m & 0 \\ 0 & L_m \end{bmatrix} \cdot \begin{bmatrix} i_{s\alpha} \\ i_{s\beta} \end{bmatrix} + \begin{bmatrix} L_r & 0 \\ 0 & L_r \end{bmatrix} \cdot \begin{bmatrix} i_{r\alpha} \\ i_{r\beta} \end{bmatrix} \tag{III.16}$$

III.6.2. Reference Frame Fixed with respect to the rotor

This axis system is stationary with respect to the rotor rotating at a speedωr, in which case:$\theta_a = \theta_r \Rightarrow \begin{Bmatrix} u \to x \\ v \to y \end{Bmatrix}; \frac{d\theta_a}{dt} = \omega_a = \omega_r$

The electrical equations given by equations (III.9 and III.10) become:

$$\begin{bmatrix} V_{sx} \\ V_{sy} \end{bmatrix} = \begin{bmatrix} R_s & 0 \\ 0 & R_s \end{bmatrix} \cdot \begin{bmatrix} i_{sx} \\ i_{sy} \end{bmatrix} + \frac{d}{dt} \begin{bmatrix} \Phi_{sx} \\ \Phi_{sy} \end{bmatrix} + \begin{bmatrix} 0 & -\omega_r \\ \omega_r & 0 \end{bmatrix} \begin{bmatrix} \Phi_{sx} \\ \Phi_{sy} \end{bmatrix} \quad \text{(III.17)}$$

$$\begin{bmatrix} V_{rx} \\ V_{ry} \end{bmatrix} = \begin{bmatrix} R_r & 0 \\ 0 & R_r \end{bmatrix} \cdot \begin{bmatrix} i_{rx} \\ i_{ry} \end{bmatrix} + \frac{d}{dt} \begin{bmatrix} \Phi_{rx} \\ \Phi_{ry} \end{bmatrix} \quad \text{(III.18)}$$

III.6.3. Reference Frame Fixed With Respect To The Rotating Field:

This axis system rotates at the speed of the rotating field ωs created by the stator windings; in this case:

$$\theta_a = \theta_s \Rightarrow \begin{Bmatrix} u \to d \\ v \to q \end{Bmatrix}, \frac{d\theta_s}{dt} = \omega_a = \omega_s \text{ And } \omega_{gl} = \omega_s - \omega_r$$

The electrical equations given by equations (III.9 and III.10) become:

$$\begin{bmatrix} V_{sd} \\ V_{sq} \end{bmatrix} = \begin{bmatrix} R_s & 0 \\ 0 & R_s \end{bmatrix} \begin{bmatrix} i_{sd} \\ i_{sq} \end{bmatrix} + \frac{d}{dt} \begin{bmatrix} \Phi_{sd} \\ \Phi_{sq} \end{bmatrix} + \begin{bmatrix} 0 & -\omega_s \\ \omega_s & 0 \end{bmatrix} \cdot \begin{bmatrix} \Phi_{sd} \\ \Phi_{sq} \end{bmatrix} \quad \text{(III.19)}$$

$$\begin{bmatrix} V_{rd} \\ V_{rq} \end{bmatrix} = \begin{bmatrix} R_r & 0 \\ 0 & R_r \end{bmatrix} \begin{bmatrix} i_{rd} \\ i_{rq} \end{bmatrix} + \frac{d}{dt} \begin{bmatrix} \Phi_{rd} \\ \Phi_{rq} \end{bmatrix} + \begin{bmatrix} 0 & -(\omega_s - \omega_r) \\ (\omega_s - \omega_r) & 0 \end{bmatrix} \begin{bmatrix} \Phi_{rd} \\ \Phi_{rq} \end{bmatrix} \quad \text{(III.20)}$$

The stator reference frame was selected as the reference frame for our investigation, and the machine's mathematical model that was produced as a result of this modeling is as follows:

This reference frame is often used for the study of the power supply of asynchronous motors at variable frequencies, as it is used in particular for the closed-loop control of electrical machines where the quantities to be controlled are necessarily continuous (non-pulsating) [55],[56]."

III.7. Mechanical Equation

The study of the asynchronous machine's behavior in different operating regimes, particularly the transient regime, highlights the equation of motion, which is defined as follows:

$$C_e - C_r = J \cdot \frac{d\Omega}{dt} + f.\Omega \quad \text{(III.21)}$$

With

Ω : rotational speed of the machine,

III.8. Asynchronous Machine Equations in the Stator-Fixed Reference Frame (α, β):

Transient phenomena in asynchronous machines can be studied using the generalized model in a stator-fixed reference frame (α, β). By substituting expressions (III.11 and III.12) into equations (III.13 and III.14) we obtain the following system:

III.8.1.Voltage Equations:

The system of equations (III.13and III.14) allows us to write for this case:

$$\begin{cases} V_{s\alpha} = R_s \cdot i_{s\alpha} + \frac{d\Phi_{s\alpha}}{dt} \\ V_{s\beta} = R_s \cdot i_{s\beta} + \frac{d\Phi_{s\beta}}{dt} \\ V_{r\alpha} = 0 = R_r . i_{r\alpha} + \frac{d\Phi_{r\alpha}}{dt} - \omega_r \cdot \Phi_{r\beta} \\ V_{r\beta} = 0 = R_r . i_{r\beta} + \frac{d\Phi_{r\beta}}{dt} + \omega_r \cdot \Phi_{r\alpha} \end{cases} \quad \text{(III.22)}$$

III.8.2. Flux Equations

The system of equations (III.16 and III.17) can be written in the following matrix form:

$$\begin{cases} \Phi_{s\alpha} = L_s \cdot i_{s\alpha} + L_m \cdot i_{r\alpha} \\ \Phi_{s\beta} = L_s \cdot i_{s\beta} + L_m \cdot i_{r\beta} \\ \Phi_{r\alpha} = L_m \cdot i_{s\alpha} + L_r \cdot i_{r\alpha} \\ \Phi_{r\beta} = L_m \cdot i_{s\beta} + L_r \cdot i_{r\beta} \end{cases} \quad \text{(III.23)}$$

From system (III.23), we obtain:

$$\begin{cases} \Phi_{s\alpha} = L_s \cdot i_{s\alpha} + L_m \cdot i_{r\alpha} \\ \Phi_{s\beta} = L_s \cdot i_{s\beta} + L_m \cdot i_{r\beta} \\ \Phi_{s\alpha} = L_s \cdot i_{s\alpha} + \frac{L_m}{L_r} \cdot [\Phi_{r\alpha} - L_m \cdot i_{s\alpha}] = \left(L_s - \frac{L_m^2}{L_r}\right) \cdot i_{s\alpha} + \frac{L_m}{L_r} \cdot \Phi_{r\alpha} = L_s \cdot \sigma \cdot i_{s\alpha} + \frac{L_m}{L_r} \cdot \Phi_{r\alpha} \\ \Phi_{s\beta} = L_s \cdot i_{s\beta} + \frac{L_m}{L_r} \cdot [\Phi_{r\alpha} - L_m \cdot i_{s\beta}] = \left(L_s - \frac{L_m^2}{L_r}\right) \cdot i_{s\beta} + \frac{L_m}{L_r} \cdot \Phi_{r\beta} = L_s \cdot \sigma \cdot i_{s\beta} + \frac{L_m}{L_r} \cdot \Phi_{r\beta} \end{cases}$$

With:

$\sigma = 1 - \frac{L_m{}^2}{L_s \cdot L_r}$: Blundell's leakage coefficient

The following relation expresses the electromagnetic torque:

$$C_e = P.(\Phi_{s\alpha} i_{s\beta} - \Phi_{s\beta} i_{s\alpha}) \quad \text{(III.24)}$$

The evolution of the rotational speed as a function of the electromagnetic torque and the machine load, characterized by the resistive torque Cr, is described by the following expression (fundamental principle of dynamics) [57]

III.9. Three-phase Inverter

Static converters that convert DC to AC are called inverters. For instance, we may link each load terminal alternately to one input terminal and then to another input terminal if we have a direct current (DC) input voltage. This is made possible by semiconductors. As a result, the voltage between the load terminals alternates between being positive and negative. An alternating voltage with a zero average value may be produced by adequately managing the semiconductor sequence. Depending on whether it is controlled by pulse width modulation (PWM) or alternating modulation, this voltage may comprise one or more slots. If just the semiconductors' control is required for the setup, upkeep, and opening of connections between the inputs and outputs, the inverter is referred to as If the establishment, maintenance, and opening of connections between the inputs and outputs depend solely on the control of the semiconductors, the inverter is said to be autonomous. [58]

III.9.1. Inverter Modeling

To simplify the modeling of the inverter, we will assume that the switches are ideal (zero switching time, negligible losses), and the three-phase load is balanced and star-connected with an isolated neutral [59].

We define the conditions and hypotheses that we will use:

- Simple voltages across each phase of the load:
  V_{an}, V_{bn}, V_{cn}
- Input voltages to the inverter:
  $V_{ao}. V_{bo}. V_{co}$
- Voltage between the neutral point 'n' and the midpoint of the inverter's DC supplyV_{no}
  $V_{an} + V_{bn} + V_{cn} = 0$

Under these conditions, we can write the voltages Vio as a function of the control signals Sa , Sb, Sc and taking into account the midpoint 'o':

$$V_{io} = U_c(S_i - 1/2) \text{ with } (i = a, b, c) \quad \text{(III.25)}$$

The simple voltages across the load terminal are

$$\begin{cases} V_{an} = V_{ao} + V_{on} \\ V_{bn} = V_{bo} + V_{on} \\ V_{cn} = V_{co} + V_{on} \end{cases} \quad \text{(III.26)}$$

The loop equations of the inverter-machine system are

$$V_{an} + V_{bn} + V_{cn} = V_{ao} + V_{bo} + V_{co} + 3V_{ob} = 0 \quad \text{(III.27)}$$

Where:

$$V_{on} = -\frac{1}{3}(V_{ao} + V_{bo} + V_{co}) \quad \text{(III.28)}$$

By substituting equation (III.28) into system (III.26), we obtain:

$$\begin{bmatrix} V_{an} \\ V_{bn} \\ V_{cn} \end{bmatrix} = \frac{1}{3}\begin{bmatrix} 2 & -1 & -1 \\ -1 & 2 & -1 \\ -1 & -1 & 2 \end{bmatrix}\begin{bmatrix} V_{ao} \\ V_{bo} \\ V_{co} \end{bmatrix} \quad \text{(III.29)}$$

From equation (III.25), we can write:

$$\begin{bmatrix} V_{an} \\ V_{bn} \\ V_{cn} \end{bmatrix} = \frac{U_c}{3}\begin{bmatrix} 2 & -1 & -1 \\ -1 & 2 & -1 \\ -1 & -1 & 2 \end{bmatrix}\begin{bmatrix} S_a \\ S_b \\ S_c \end{bmatrix} \quad \text{(III.30)}$$

III.10. PWM Control

The basic idea behind intersective pulse width modulation (PWM) is simple. It involves comparing a sinusoidal reference signal provided by the control system, sometimes referred to as the modulating signal, with a high-frequency carrier signal F_{dec}, which is frequently a symmetrical triangular wave. This comparison determines the state of the switches at the switching frequency F_{dec}. When the reference signal exceeds the triangle signal, the control signal ci is set to 1. Otherwise, it is set to 0. Consequently, the average driving signal value (sometimes referred to as the duty cycle) throughout a single carrier period equals the instantaneous value of the modulating signal. [60]

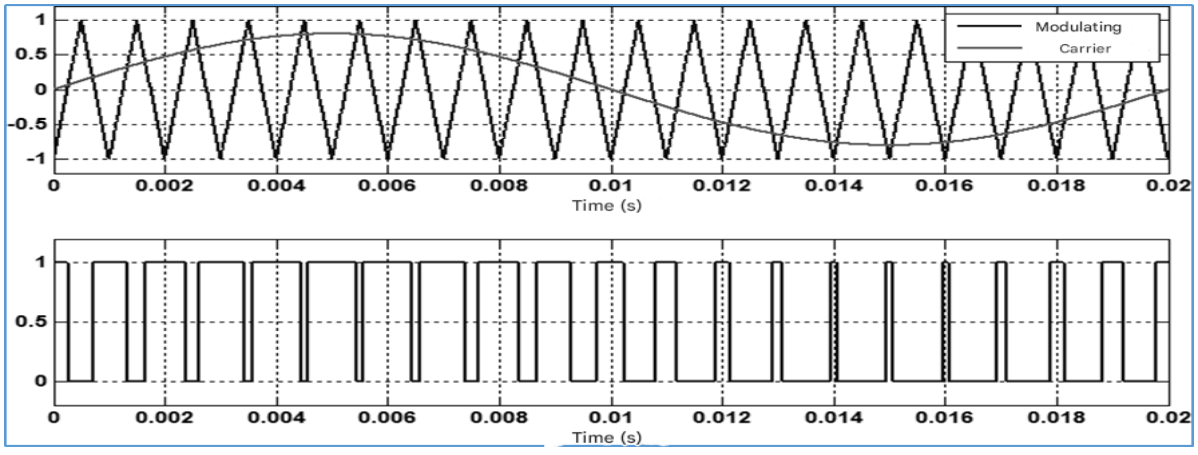


Figure III.4 Principle of PWM technique

To create the control signals for the six switches in the application of interest to us (three-phase inverter-machine association), a single carrier is compared to the three stator voltage references.

$$\begin{bmatrix} V_{AN} \\ V_{bN} \\ V_{cN} \end{bmatrix} = \frac{V_{ds}}{3} \begin{bmatrix} 2 & -1 & -1 \\ -1 & 2 & -1 \\ -1 & -1 & 2 \end{bmatrix} \begin{bmatrix} C1 \\ C2 \\ C3 \end{bmatrix} \quad \text{(III.31)}$$

We calculate the mean of both components in this equation (operator $\langle . \rangle$) during a sampling time Tdec. In terms of the duty cycles $\alpha 1, \alpha 2$, and $\alpha 3$, this results in the following equation.

$$\begin{bmatrix} < V_{AN} > \\ < V_{bN} > \\ < V_{cN} > \end{bmatrix} = \frac{V_{ds}}{3} \begin{bmatrix} 2 & -1 & -1 \\ -1 & 2 & -1 \\ -1 & -1 & 2 \end{bmatrix} \begin{bmatrix} \alpha 1 \\ \alpha 2 \\ \alpha 3 \end{bmatrix} \quad \text{(III.32)}$$

If we want to have reference voltages ($Van*$, $Vbn*$, $Vcn*$) across each stator phase of the motor and the common neutral point, it will be necessary to determine the duty cycles to generate.

Thus the following equation must be solved:

$[V_{AN} * B_{BN} * C_{CN}]^T = A[\alpha 1\ \alpha 2\ \alpha 3]^T$ Or

$$A = \begin{bmatrix} 2 & -1 & -1 \\ -1 & 2 & -1 \\ -1 & -1 & 2 \end{bmatrix} \quad \text{(III.33)}$$

The answer to the above equation is not unique, though, because matrix A is single. Consequently, the duty cycle calculation and, by extension, the switch control signal computation are not unique [61]. The matrix equation cannot be solved without an extra restriction. Therefore, the duty cycles may be generated from the desired stator reference voltages in an endless number of ways. For this reason, a variety of PWM approaches have been created. But they all have one thing in common: they use the neutral point voltage VNO fluctuation to accomplish their different goals [62]. Figure III.05 provides an illustration of this concept.

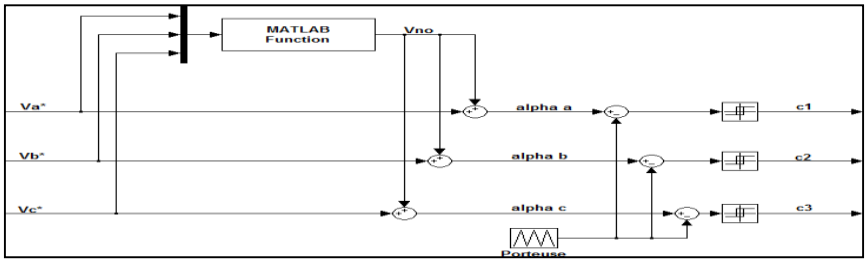


Figure III.5 Principle of generating duty cycles.

Among the variants of intersective PWM, the most popular is three-phase PWM. In this case, we set [9]: $VNO = {}^{V(med)}/_{2}$

Where: V_{med} is the median voltage of the three stator reference voltages, defined as follows:

If $V_{AN}<V_{BN}<V_{CN}$ then $V_{med} = V_{BN}$

Thus, we will have [11]:

$$\alpha i = {}^{1}/_{Vdc}\left(Vin* + {}^{Vmed}/_{2}\right) + 0.5 \quad \text{(III.34)}$$

This relation will be used in the closed-loop control of our inverter

III.11. Simulation

This simulation's goals are to verify the chosen model of the asynchronous machine and examine how it behaves when powered by the grid directly at first, then by a voltage inverter that is controlled by pulse width modulation (PWM).

Symbol	parameters	Value
J	Moment of inertia	0.05 Kgm^2
f	Viscous friction coefficient	0.001SI
P	Number of pole pairs	2
Lr	Total rotor cyclic inductance	0.1568 H
Ls	Total stator cyclic inductance	0.1568 H
Msr	Mutual inductance between stator and rotor	0.15 H
Rr	Rotor resistance	1.2 Ω
Rs	Stator resistance	1.8 Ω
Vs	Stator voltage	220 / 380V
Φref	The Flux	0.85 Wb

Table III.1. Asynchronous Machine Parame

III.11.1. Simulation of the Asynchronous Machine

The simulation of cage asynchronous machine (directly powered by the network) was performed using MATLAB/SIMULINK software using the machine parameters mentioned in the following table.

The machine parameters used in the simulation are as follows:

The simulation results obtained are shown in the figures below and illustrate the evolution of the following quantities: speed, electromagnetic torque, rotor fluxes, direct and quadrature rotor

currents, and the stator current in one phase. The results presented correspond to the loaded condition

- **Machine directly connected to the grid with: (Cr = 30 N·m at t = 3 s)**

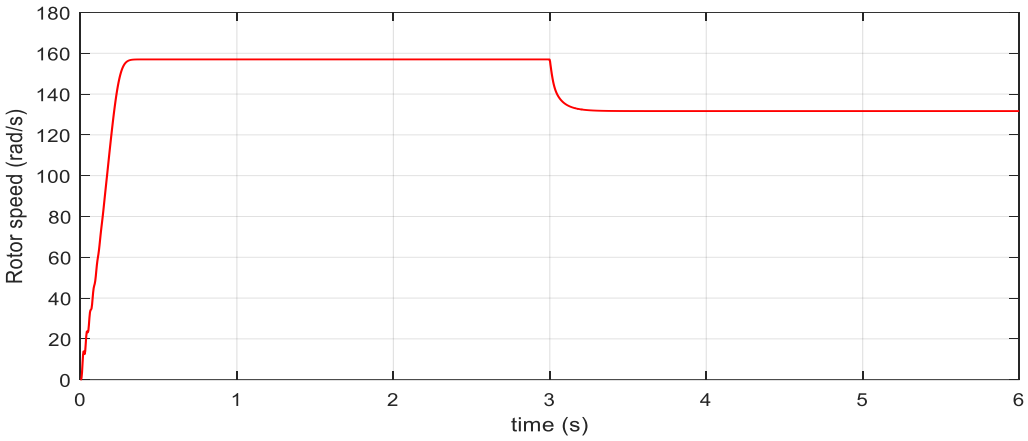


Figure III.6 Rotor speed.

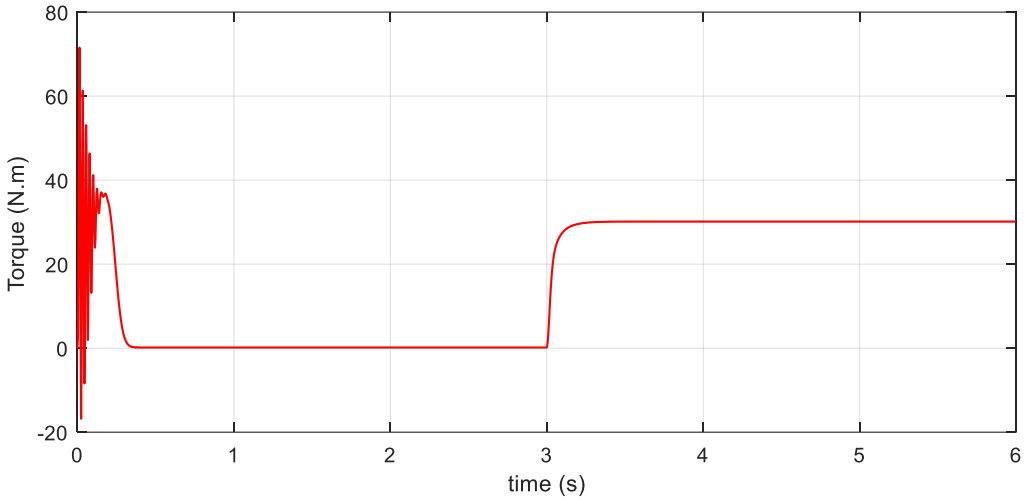


Figure III.7 Electromechanical torque .

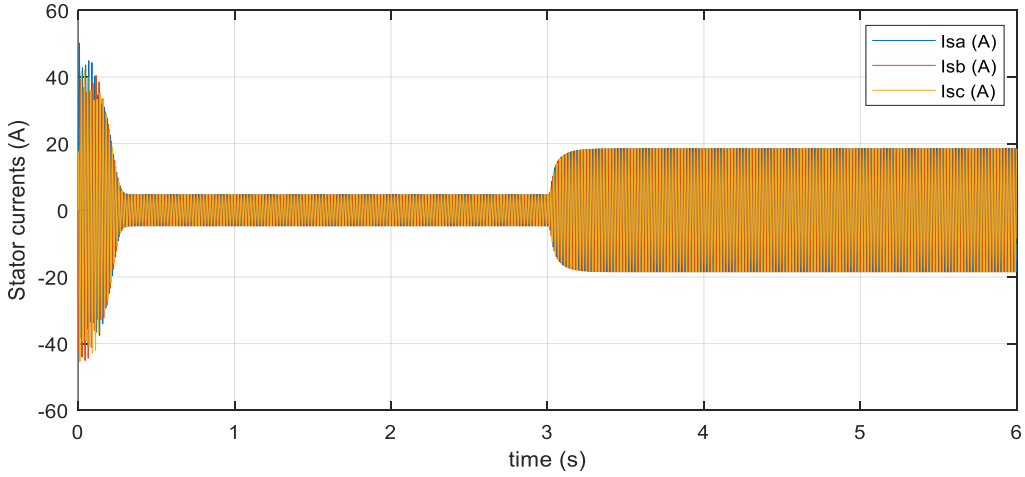


Figure III.8 Stator currents .

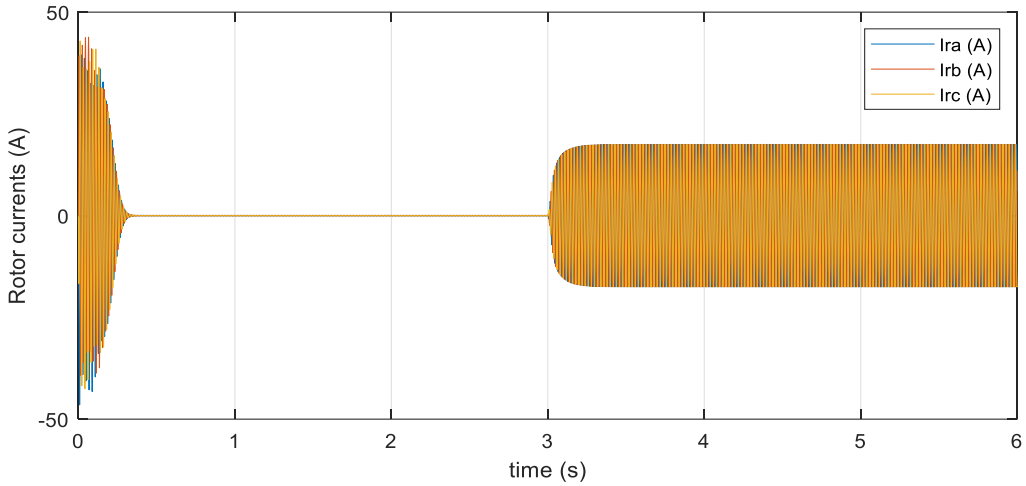


Figure III.9 Rotor currents.

III.11.2. Simulation of the Asynchronous Machine powered by an inverter

The figures below illustrate the simulation of a cage asynchronous machine powered by an inverter:

- **Machine connected directly to the network by an inverter with:(Cr = 30 N.m à 3 s)**

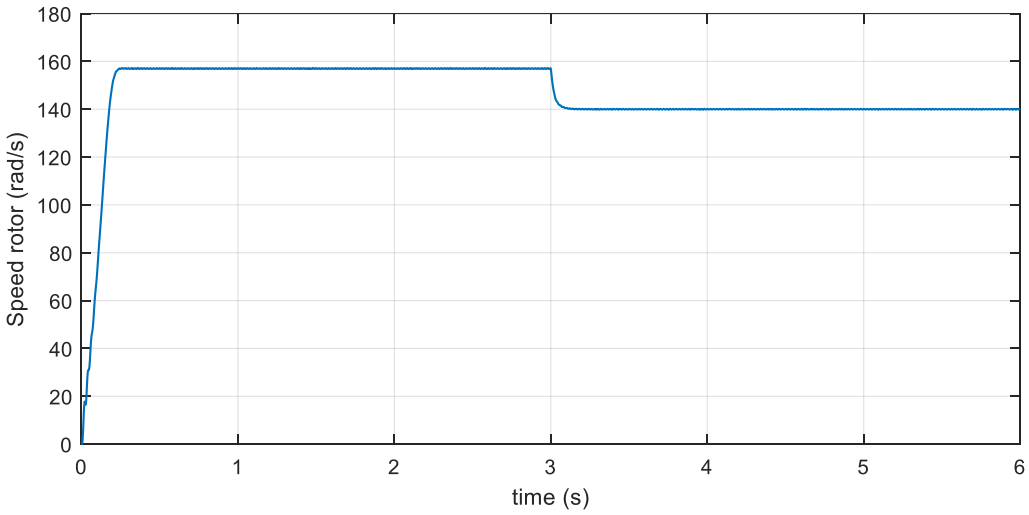


Figure III.10 Rotor speed.

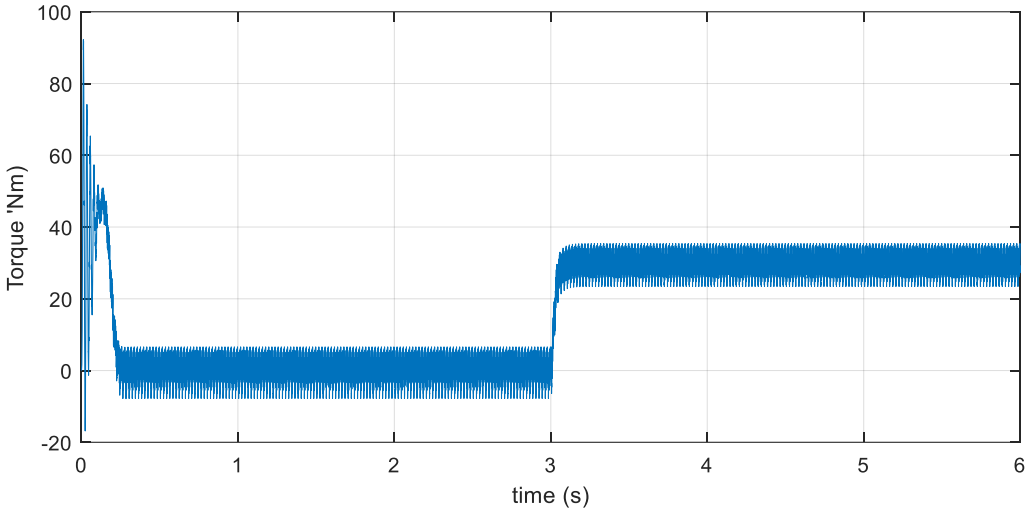


Figure III.11 Electromechanical torque.

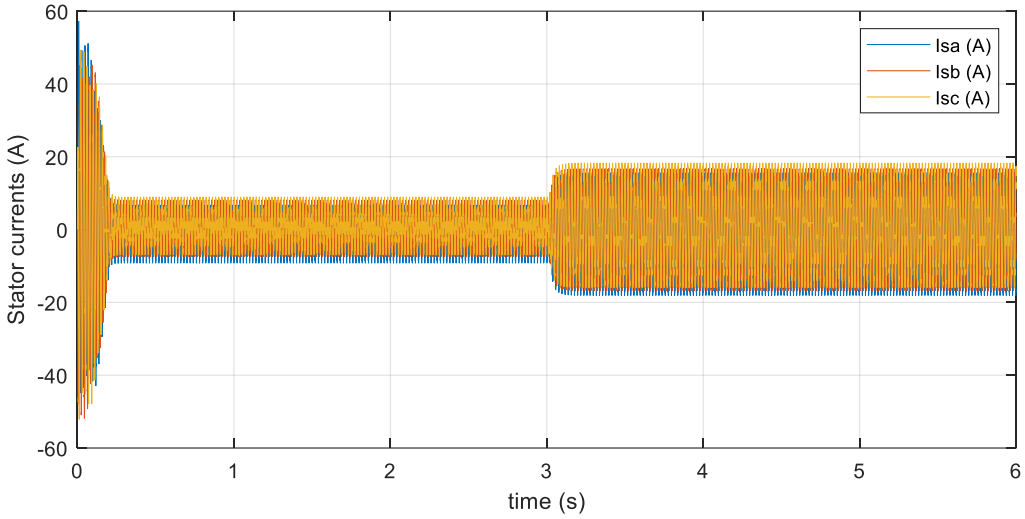


Figure III.12 Stator currents.

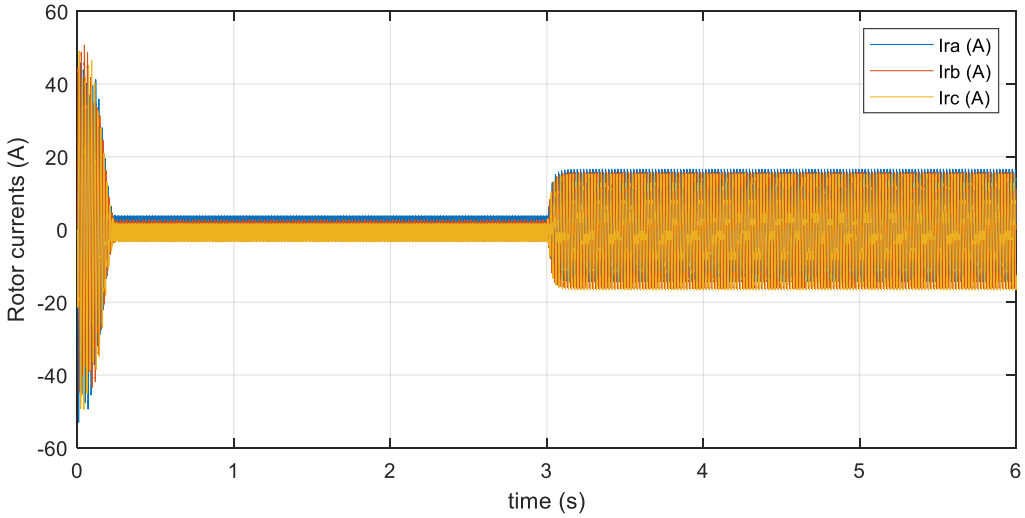


Figure III.13 Rotor currents.

The curves below allow us to make the following observations:

- The rotational speed reaches its nominal value of $(157\frac{rad}{s})$ after (0.2) seconds.
- At $(t = 2s)$, the speed decreases to a value below its nominal speed $(140\ rad/s)$ due to the application of a load $(Cr = 30\ N.m)$, which results in slip.

After transient regime behavior, the electromagnetic torque drops to $0\ N \cdot m$, then increases to match the applied load torque of $30\ N \cdot m$.

The stator current amplitude (in three-phase reference frame) increases at $(t = 2s)$ in response to the mechanical load applied to the motor shaft.

The waveforms of electrical and electromechanical quantities in the inverter-fed machine, we observe that:

- The speed profile remains identical to that obtained with three-phase source supply.
- The electromagnetic torque and rotor currents (in the two-phase reference frame) maintain their previous profiles (identical values) but exhibit ripple due to harmonic pollution - a direct consequence of PWM-controlled inverter leg switching.

III.12. Conclusion

We thoroughly examined the induction machine and its control in this chapter. We started by creating a mathematical model of the machine in the three-phase reference frame, which was made simpler by using the two-phase transformation. We also went into detail about the PWM-controlled inverter's modeling. To guarantee its power supply, this inverter will be connected to the induction motor. Second, we used MATLAB/Simulink to simulate the induction motor operating both directly from a three-phase source supply and from an inverter. The implemented models were validated by these simulations.

CHAPTER IV

MODELING AND SIMULATION OF AN INDUCTION MACHIINE PUMP USING THE DIRECT TORQUE CONTROL TECHNIQUE

IV.1. Introduction

Induction motors are widely used in industrial and domestic applications due to their robustness, simplicity, and cost-effectiveness. Among their many applications, induction motors are commonly employed in hydraulic pumping systems. The performance of these pumps driven by such types of motors has a significant impact on the overall efficiency, energy consumption, and reliability of these systems.

Volts-per-Hertz (V/f) and other scalar control techniques have been used to induction motors. These techniques are less efficient under changing load circumstances and only provide a limited amount of dynamic performance. Advanced vector control methods have been created to get around these restrictions, and Direct Torque Control (DTC) has become well-known among them. good option for high-performance applications as it offers quick torque and flux control without requiring intricate conversions or current regulators. rate are all directly impacted by accurate and effective motor torque control in pumping systems. to improving dynamic responsiveness, DTC implementation in these systems lowers mechanical stress and energy losses, both of which are essential for long-term operational sustainability.

The modeling and simulation of an induction motor pump under the Direct Torque Control method are the main topics of this chapter. The motor's dynamic performance under various operating situations is examined and contrasted using MATLAB/Simulink. primary goal is to assess how well DTC works in pumping applications to enhance reaction time, torque control, and overall system efficiency.

IV.2. Direct Torque Control (DTC)

Direct Torque Control (DTC) was created in the late 1980s as an alternative to traditional methods that employed PWM and magnetic flux direction in order to separate flux and torque. easy to use and effectively decouples these aspects. Its advantages over conventional systems include direct control over torque and stator flux ripple amplitudes, improved resilience to rotor parameter changes, faster torque response, and the removal of the requirement for Park conversions. also effective when mechanical position or speed sensors are not needed. Much effort has been made to enhance this fundamental tactic that Takahashi suggested. [63]

IV.3. Main Features of DTC

To lessen torque oscillations brought on by the hysteresis controllers, a high calculation frequency is advised in Direct Torque Control (DTC) systems. This condition suggests that in

order to satisfy the demands of real-time processing, high-performance computers are required. Direct torque control'sgeneralattributes include [64]:

- Direct control of torque and flux is achieved through the selection of optimal switching vectors of the inverter.
- Obtaining stator fluxes and currents close to sinusoidal waveforms.
- Very fast dynamic response of the machine.
- The existence of torque oscillations that depend on the width of the hysteresis controller bands.
- The switching frequency of the inverter depends on the amplitude of the hysteresis bands.

The following is a list of the benefits and drawbacks of this control system in the context of motor operating speed regulation.

IV.3.1.Advantages

- Since currents and voltages are taken into account in a stator-fixed reference frame, coordinate transformations are not required. A simplified model of the induction motor is used.
- For voltage modulation, a Pulse Width Modulation (PWM) block is not necessary.
- It is not required to decouple currents from control voltages, as is required in vector control.
- It requires two hysteresis comparators and a PI speed controller, whereas vector control typically needs two PI controllers and a PWM modulator [65].
- In contrast to vector control, which normally requires two PI controllers and a PWM modulator, it requires two hysteresis comparators and a PI speed controller [65].
- torque has a very quick dynamic response.
- It is resilient to changes in the parameters.

IV.3.2. Disadvantages

- Issues at low speeds are present.
- need for torque and stator flux estimates.
- The existence of torque oscillations.

- Because hysteresis controllers are used, the switching frequency fluctuates. Rich harmonic content, rising losses, acoustic noise, and torque oscillations that might trigger mechanical resonances are the results of this.

IV.4. Structure of Direct Torque Control of the Asynchronous Machine

The following algorithm served as the foundation for TAKHHASHI's torque and flux control strategy:

- There are distinct time periods inside the temporal domain.
- The asynchronous machine's phase voltages and line currents are monitored for every period.
- The stator flux vector's constituent parts are rebuilt.
- The estimation of the electromagnetic torque of the asynchronous machine is then possible thanks to the estimation of the flux components and the measurements of the line currents.
- The error between the reference flux and the estimated flux is fed into a hysteresis controller, which generates a binary output variable K_{Φ}.
- The error between the reference torque and the estimated torque is fed into a hysteresis controller, which generates a three-level logic output variable K_c.

Since the dynamics of the torque are often quicker than those of the flux, it was suggested to employ three states to control the torque in an effort to reduce the average switching frequency. In a look-up table, the inverter states V0 and V7 are selected based on the angular sector θi, which contains the stator flow vector, and the logic variables Kc and KΦ.

In fact, it is possible to ascertain the control sequence of the inverter switches for a particular sector by splitting the complex plane into six angular sectors (see Figure IV.1) [66].

IV.5 Determination of the Sector of Evolution of the Stator Flux Vector

location of the flux in its evolving space, which is broken down into six symmetrical sectors.

$$-\frac{\pi}{6}+(i-1)\frac{\pi}{3}\leq\theta_i\leq\frac{\pi}{6}+(i-1)\frac{\pi}{3} \qquad \text{(IV.1)}$$

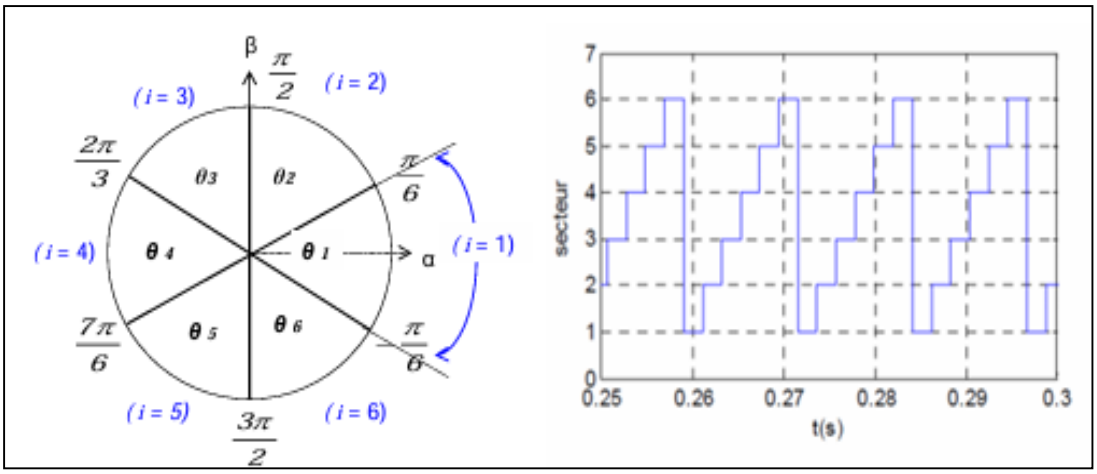


Figure IV.1 Sector of Evolution of the Stator Flux Vector.

IV.6. Estimators

The stator voltage and current vectors are used to estimate the stator flux and electromagnetic torque.

IV.6.1. Stator Flux Estimator

Measurements of the machine's stator quantities (voltage and current) are used to build the flux estimator..

From the control signals (Sa, Sb, Sc) and the DC voltage Vdc, the values of the voltages $Vs\alpha$ and $Vs\beta$ are determined by applying the Concordia transformation [67]:

$$\begin{cases} V_{sa} = \sqrt{\frac{2}{3}} V_{dc} \cdot \left[S_a - \frac{1}{2}(S_b + S_c) \right] \\ V_{s\beta} = \frac{1}{\sqrt{2}} V_{dc} \cdot [S_b - S_c] \end{cases} \quad \text{(IV.2)}$$

Similarly, the currents isα andisβ are obtained by applying the Concordia transformation to the measured currents (i_{sa}, i_{sb}, i_{sc}):

$$\begin{cases} i_{s\alpha} = \sqrt{\frac{2}{3}} \cdot i_{s\alpha} \\ i_{s\beta} = 2 \cdot (i_{sb} - i_{sc}) \end{cases} \quad \text{(IV.3)}$$

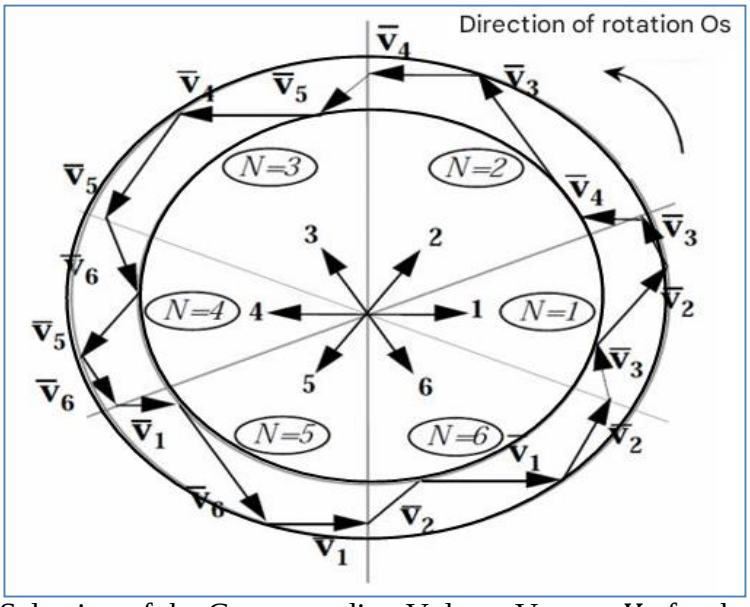


Figure IV.2 Selection of the Corresponding Voltage Vectors Vs for the Control of the Amplitude ofΦs.

It is then possible to directly determine the (α, β) components of the stator flux vector Φ_s:

$$\begin{cases} \Phi_{s\alpha} = \int_0^1 (V_{s\alpha} - R, \cdot i_{s\alpha})dt \\ \Phi_{s\beta} = \int_0^1 (V_{s\beta} - R_s \cdot i_{s\beta})dt \end{cases} \quad \text{(IV.4)}$$

Whose magnitude is written as:

$$\Phi_s = \sqrt{(\Phi_{s\alpha})^2 + (\Phi_{s\beta})^2} \quad \text{(IV.5)}$$

The sector θ_i in which the vector Φ_s is located is determined from the components $\Phi_{sa}$and$\Phi_{s\beta}$

$$\theta_i = \text{arct}(\frac{\Phi_{s\beta}}{\Phi_{s\alpha}}) \quad \text{(IV.6)}$$

IV.6.2 Electromagnetic Torque Estimator

The torque is estimated directly from the estimated flux quantities (Φ_{sa} and$\Phi_{s\beta}$) and the calculated current quantities ($Is\alpha$ and $Is\beta$):

$$C_e = P(\Phi_{s\alpha}. I_{s\beta} - \Phi_{S\beta}. I_{s\alpha}) \quad \text{(IV.7)}$$

IV.7. Elaboration of the Control Vector

IV.7.1 Flux Controller

The hysteresis controller controls the stator flux vector's rotational speed. in Figure IV.2, its goal is to keep the stator flux vector's point inside a circular band. .

In the zone where the flux is N=1, V_{i+1}or $V_{i-1}$are chosen to increase the flux amplitude,

And V_{i+2}orV_{i-2} are chosen to decrease the flux amplitude [68].

That the voltage vector selection is contingent upon the flux error's sign rather than its amount. Therefore, the output of the flux controller can be a Boolean variable:

- 1: when the flux error is positive
- 0: when the flux error is negative

Because the two-level controller makes it easy to manage and maintain the flux vector Φs tip within a circular band, it appears to be the most straightforward and appropriate solution for the control under study.

The output of the controller, represented by a Boolean variable, directly indicates whether the flux amplitude should be increased (K_Φ=1) or decreased (K_Φ=0) in order to maintain it (see FigureIV.3)

$$|\Phi_s^* - \Phi_s| \leq \Delta\Phi_s \quad \text{(IV.8)}$$

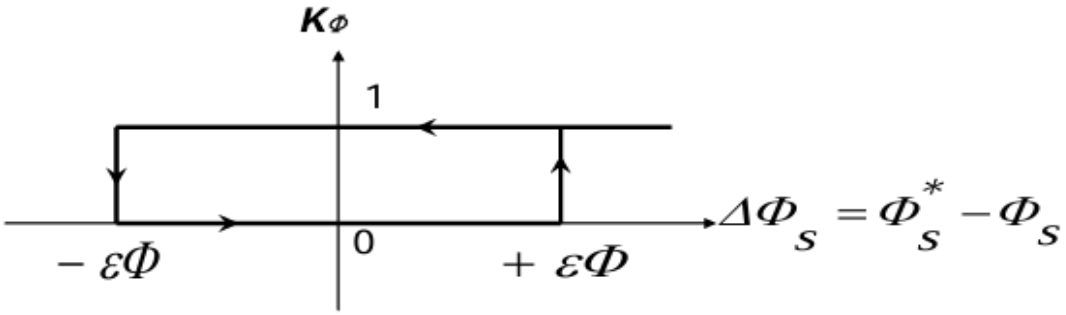


Figure IV.3 Two-Level Hysteresis Flux Controller

With:

Φ_s^*: is the reference flux

Φ_s: is the estimated flux

$\Delta\Phi_s$: is the width of the hysteresis band of the controller

If $\Delta\Phi_s \leq -\varepsilon_\phi$ or $\Delta\Phi_s > \varepsilon_\phi$, It indicates the departure of the stator flux from the hysteresis band. To reduce the stator flux's magnitude in the first scenario, a voltage vector has to be applied. second scenario, the stator flow is increased by applying a voltage vector [69].

IV.7.2 Torque Controller:

The purpose of this controller is to keep the torque within the following acceptable bounds:

$$|C_e^* - C_e| \leq \Delta C_e \quad \text{(IV.9)}$$

With:

C_e^* : is the reference torque

C_e : is the estimated torque

ΔC_e : is the width of the hysteresis band of the controller

IV.8 General Structure of Direct Torque Control:

The fundamental components of a DTC-ASM (Direct Torque Control-Asynchronous Machine) system are depicted in Figure III4. In comparison to the machine's time constants, the sampling period Te of this sampled control system is extremely tiny[70].

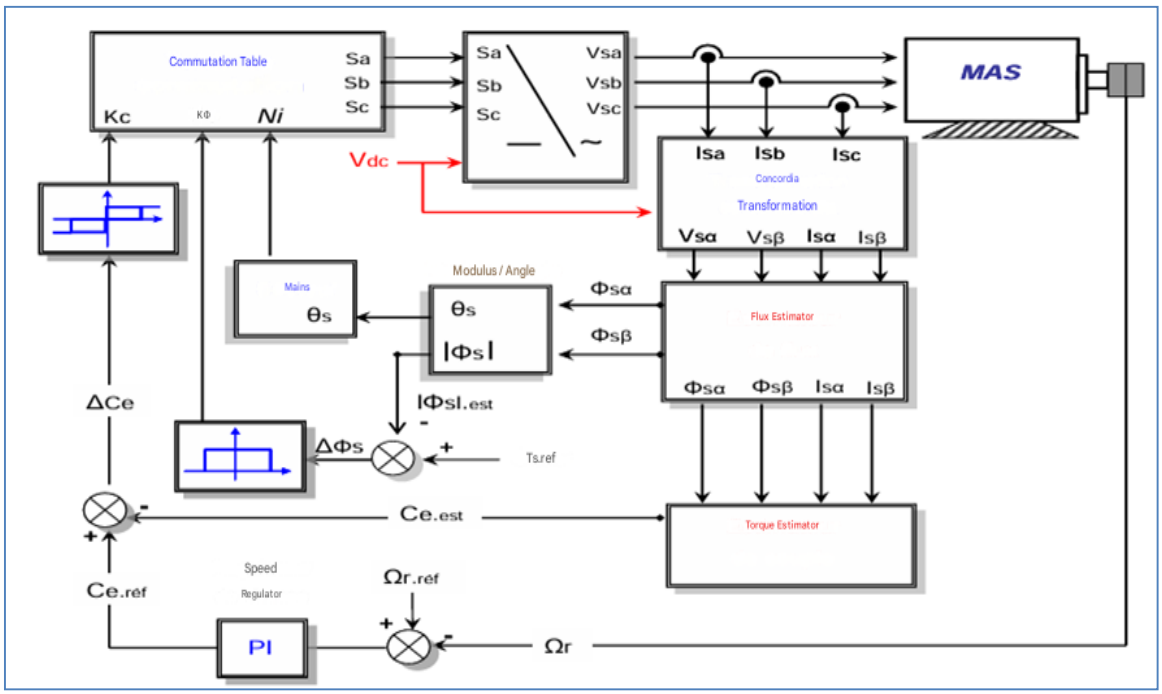


Figure IV.4 Block Diagram of the General Structure of Direct Torque Control.

The switching table, one of the key components of this construction, enables the selection of the voltage vector Vs without requiring the rotor location, which often calls for a speed sensor.

IV.9. Modeling of the Centrifugal Pump

Three factors are taken into consideration while sizing a centrifugal pump: head, speed, and flow rate. Head losses and the pipe's discharge pressure both raise the head.

IV.9.1. Total Manometric Head

The geodetic head, or the net height of water conveyance, has a significant influence on the overall manometric head. Apart from the geodetic head, the pipes' linear head losses ($\Delta H1$) and singular head losses ($\Delta H2$) also affect the overall manometric head. The following formula may be used to represent this head [71] [72]:

IV.9.1.1. Linear Head Losses

These are the water losses in the piping given by the formula

With:

$$\Delta H_1 = \lambda \frac{L}{D} \frac{v^2}{2g} \quad \text{(IV.10)}$$

λ : Coefficient of linear head losses.

D : Diameter of the piping (m).

L : Length of the piping (m).

g : Acceleration due to gravity (m/s²).

v : Average fluid velocity (m/s) which is given by: $v = \frac{4Q}{\pi D^2}$

$$\Delta H_1 = \lambda \frac{L}{D} \left(\frac{8 \cdot Q^2}{\pi^2 D^4 g} \right)$$

The pipeline's length determines the linear head losses. These losses reduce with increasing pipeline diameter, and they drop significantly with increasing pipe diameter.

IV.9.1.2. Singular (Local) Head Losses

The primary cause of these losses is a variety of cross-sectional changes that correlate to hydraulic network flow disruptions. [73] [74]

Can be used to express them:

$$\Delta H = \left(\lambda \frac{L}{D} + \varepsilon \right) \left(\frac{BQ^2}{\pi^2 D^4 g} \right) = K_{fr} Q^2 \quad \text{(IV.11)}$$

$$\Delta H = \Delta H_1 + \Delta H_2 \quad \text{(IV.12)}$$

Where:

$$\Delta H = \left(\lambda \frac{L}{D} + \varepsilon \right) \left(\frac{BQ^2}{\pi^2 D^4 g} \right) = K_{fr} Q^2$$

And :K_{fr} : pipeline constant.

The total pumping head is:

$$H = H_g + K_{fr} Q^2 \text{(IV.13)}$$

IV.9.1.3. Flow Rate-Head Characteristic

The head-flow rate characteristic of a pump is often expressed as H(Q), where (H) is the total manometric head and (Q) is the flow rate of the pump. The 'Pleider-Peterman' model may be used to estimate this attribute [75], and the formula (II.94) indicates it:

$$H = a_0 \omega_m^2 - a_1 \omega_m Q - a_2 Q^2 \quad \text{(IV.14)}$$

With:

a_0, a_1, a_2Coefficients given by the manufacturers.

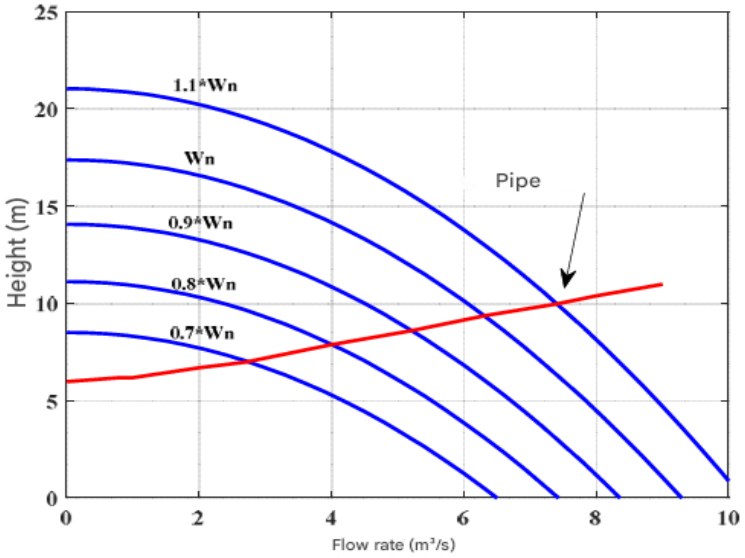


Figure IV.5 H(Q) Characteristics and pipeline Characteristic

IV.9.1.4 Pump Torque-Speed Characteristic C(ω)

[The phrase appears to be missing or unfinished at the beginning. Presuming it alludes to manufacturer-provided coefficients…] .

The primary characteristic of a centrifugal pump is a load torque that is proportional to the square of the motor speed and has the following form:

$$T_{\mathrm{L}} = k_{\mathrm{r}}\omega_{\mathrm{m}}^2 \qquad \text{(IV.15)}$$

With:

$$K_r = \frac{P_m}{\omega_m^3}$$

II.9.1.5 Power Calculation

Because of the different frictions between the spinning elements, the mechanical energy needed by a pump is always more than the energy transferred to the fluid. The following is the typical phrase for hydraulic power:

$$P_H = \frac{\rho g Q H}{\eta_p} \qquad \text{(IV.16)}$$

With: $\eta_p$being the efficiency of the pump, which is in the order of 0.4 to 0.8 for centrifugal pumps.

IV.10. Simulation Results

The Direct Torque Control (DTC) simulation results for an induction motor (MAS) powered by a centrifugal hydraulic pump are shown in this section. A three-phase voltage inverter coupled to a solar panel powers the device. We were able to precisely replicate the behavior of several electrical and mechanical parameters of the system under study by using a simulation software created in the Matlab environment. The simulation block of the entire system is depicted in the following diagram.

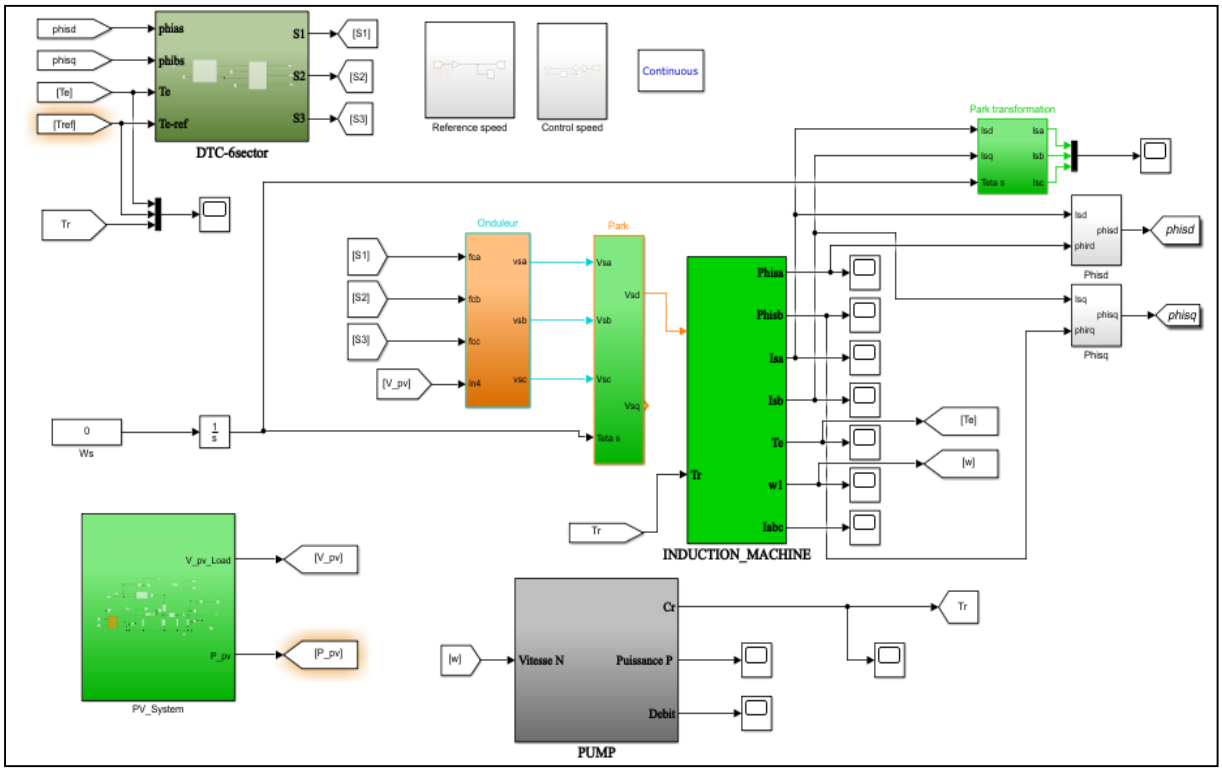


Figure IV.6 Simulation block diagram of the PV-powered pump system.

IV.10.1.Solar Panel Simulation Results

A solar panel coupled to a boost converter under varied irradiance levels (between 1000 W/m² and 600 W/m²) and a fixed temperature of 25°C are the parameters of the PV system that are shown in the figures below.

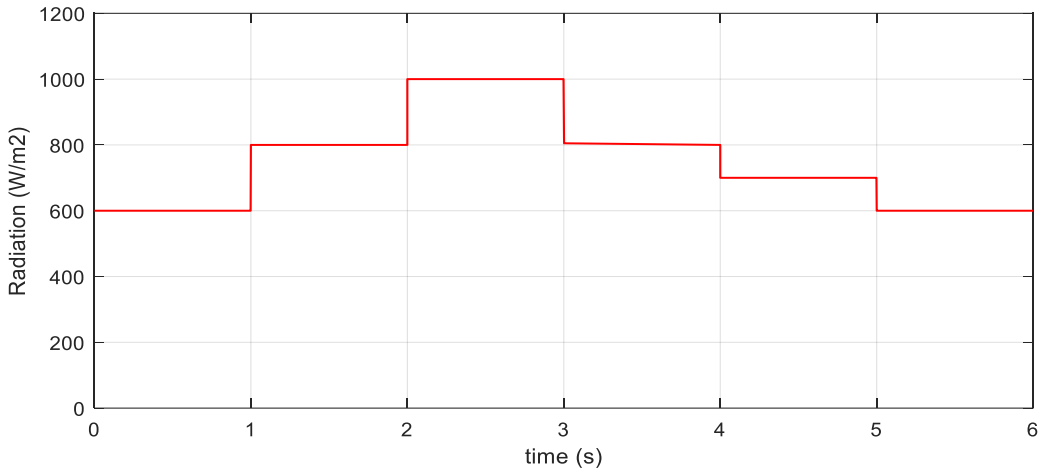


Figure IV.7 Variable Irradiance.

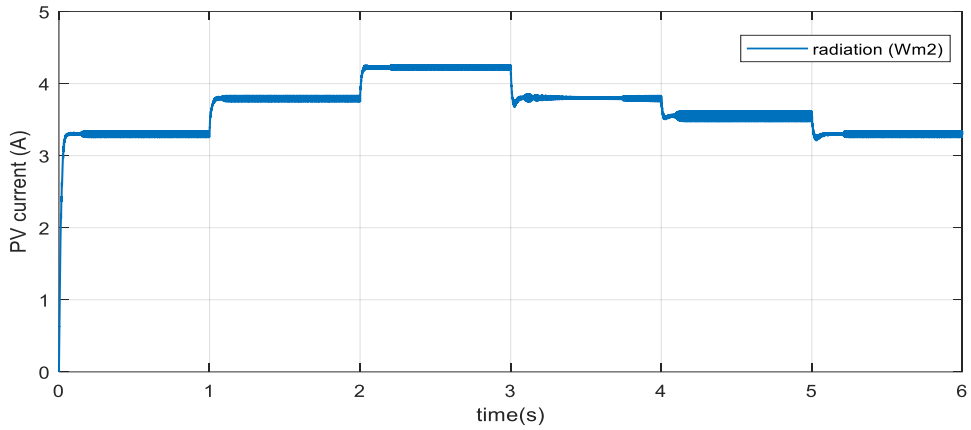


Figure IV.8 PV Current.

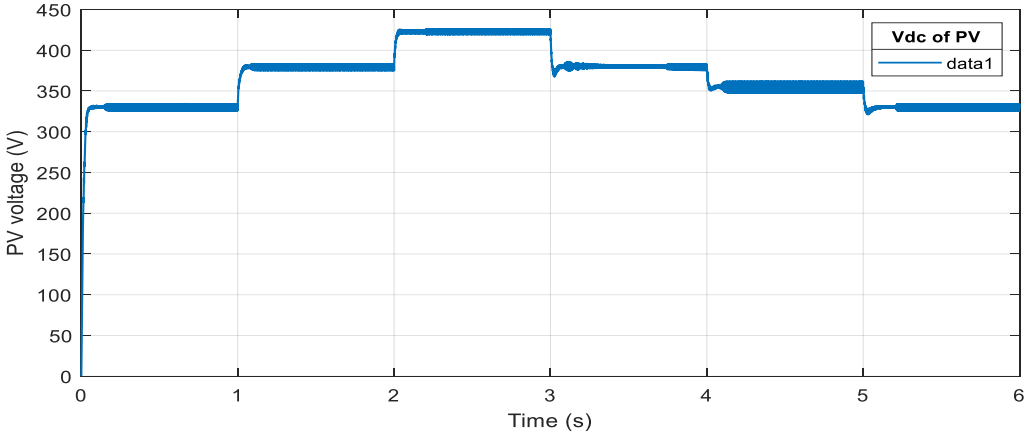


Figure IV.9 PV voltage.

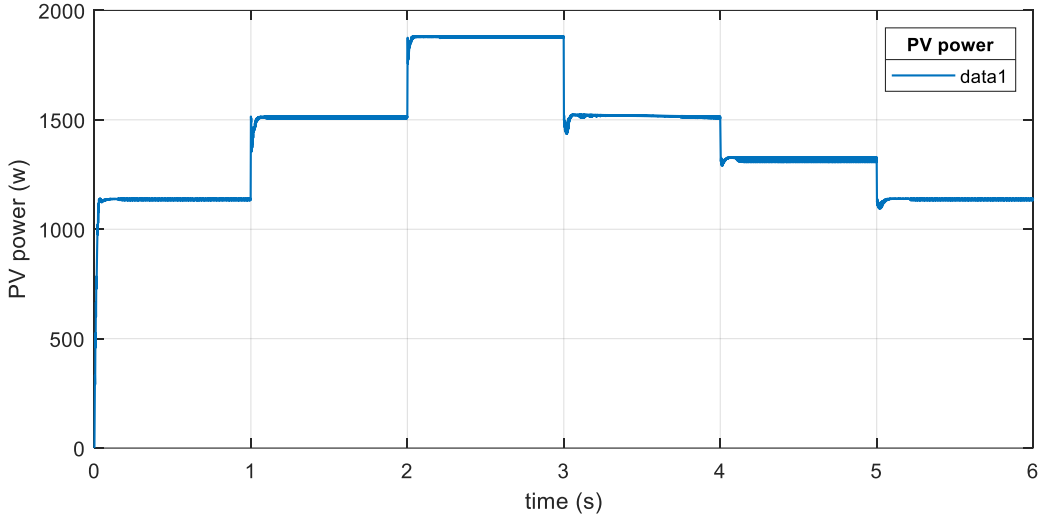


Figure IV.10 PV power.

It can be observed that with variations in solar irradiance, the power output of the PV system will fluctuate. With a fixed temperature of 25°C and irradiance levels varying between 600 W/m², 800 W/m², 1000 W/m², 700 W/m², and then returning to 600 W/m², the power will decrease and increase according to the irradiance value.

IV.10.2. Simulation Results of the Induction Motor

This section presents the simulation results of the induction motor (asynchronous machine) powered by a two-level voltage inverter with Direct Torque Control (DTC). The inverter is supplied by the solar panel, whose simulation results were illustrated in the previous figures.

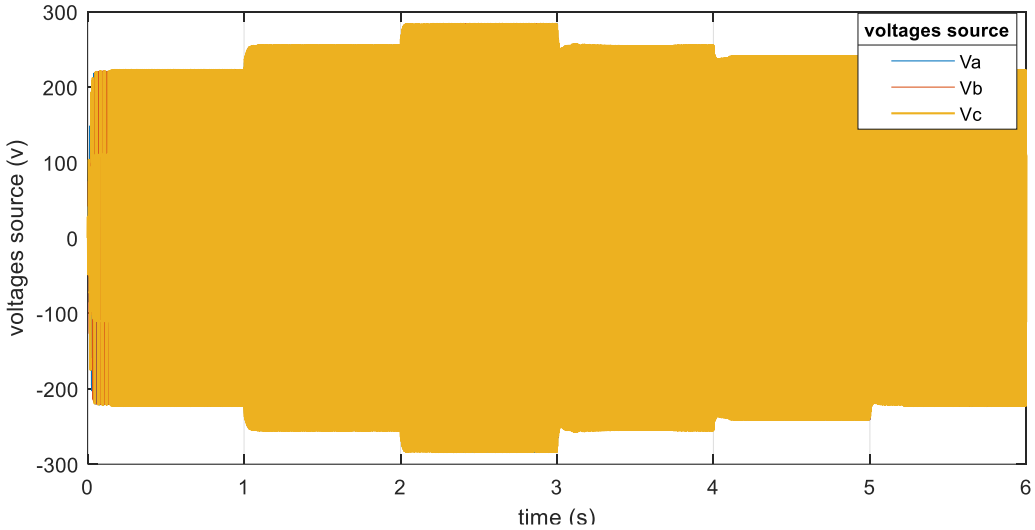


Figure IV.11 Voltages source.

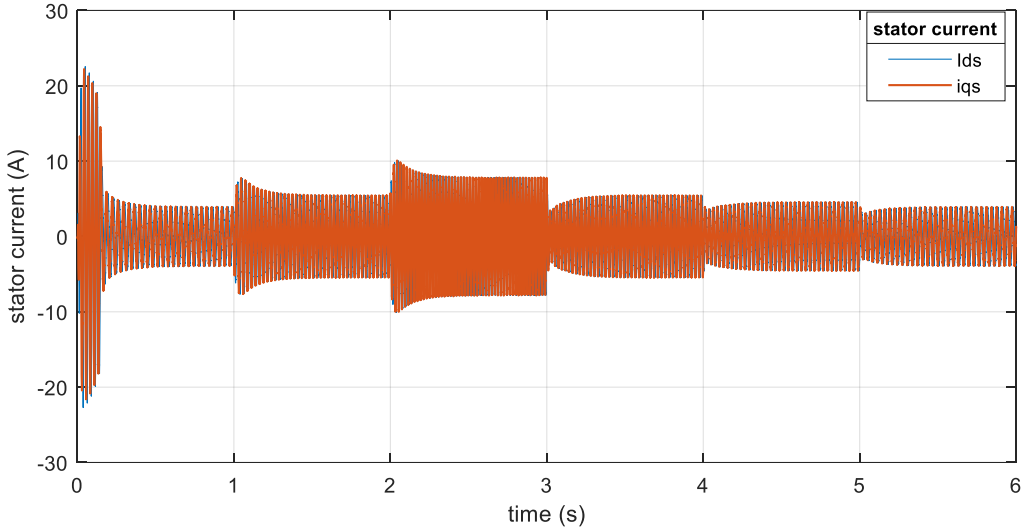


Figure IV.12 Stator currants Ids and Iqs.

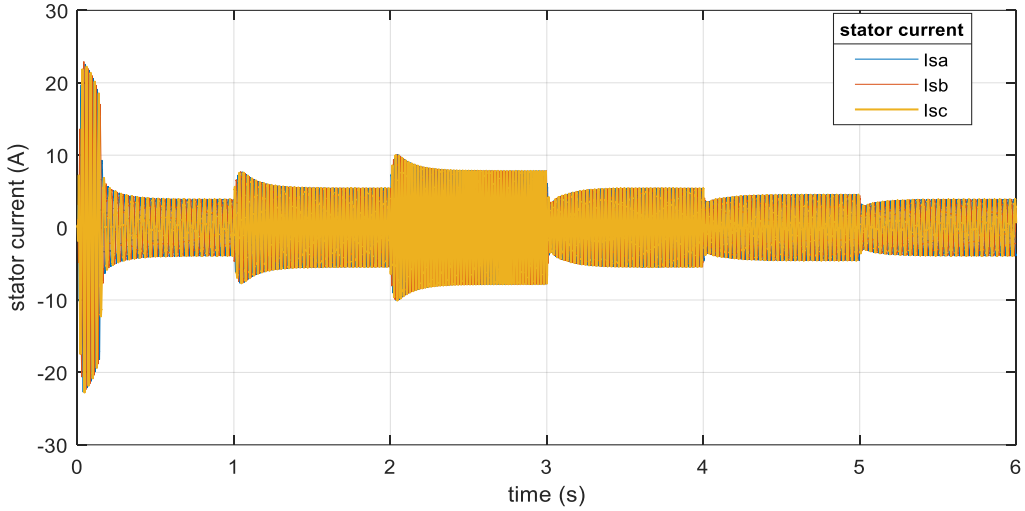


Figure IV.13 Stator currants.

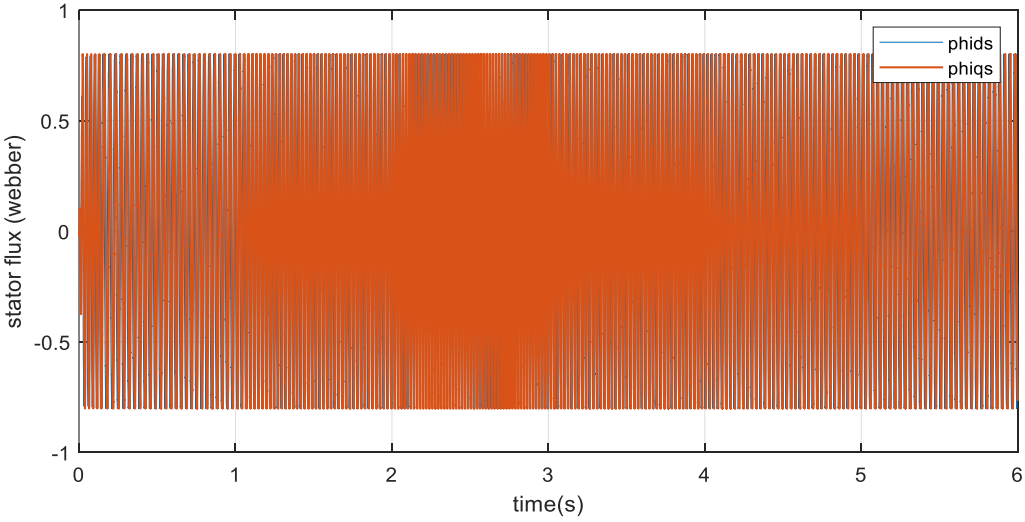


Figure IV.14 Stator flux.

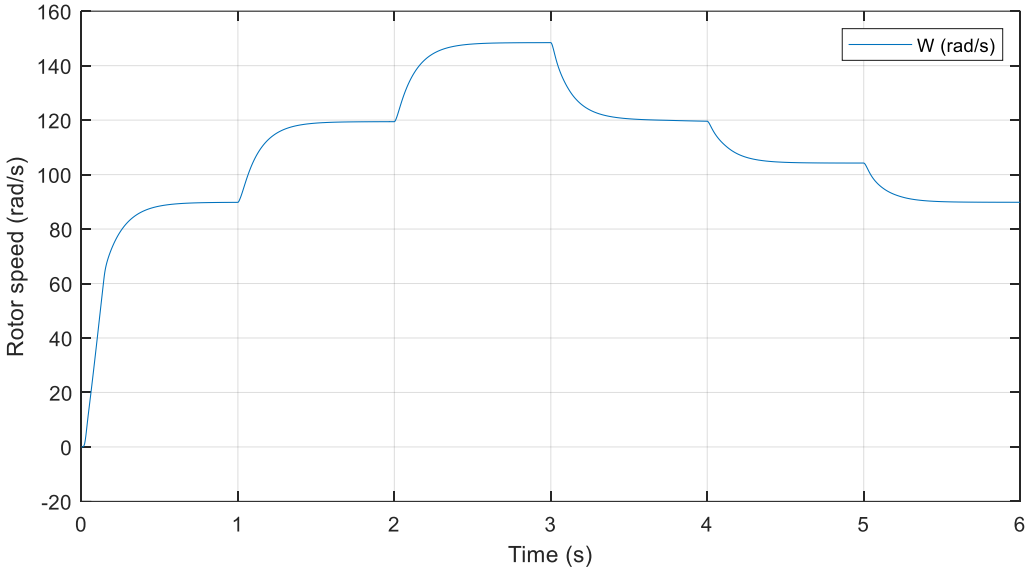


Figure IV.15 Rotor speed.

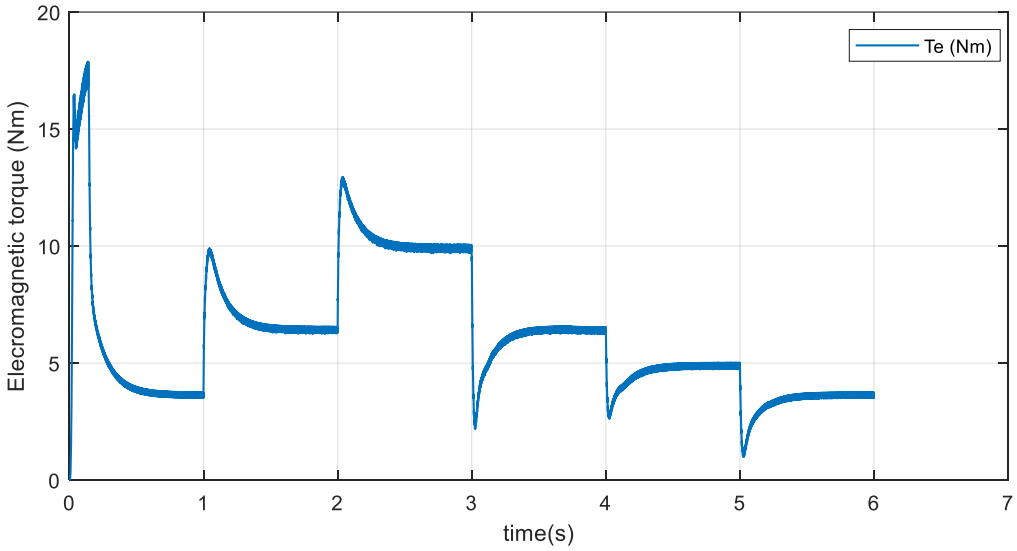


Figure IV.16 Electromagnetic torque.

Based on the obtained results, it is observed that the stator currents of the machine are purely sinusoidal, particularly in steady-state operation. Their amplitudes increase and decrease according to the solar irradiance level. Similar observations were recorded for the torque and speed quantities.

The flux values in both axes (Id and Iq) remain sinusoidal with a fixed amplitude of 0.8 Weber (as imposed by the DTC control) and a 90° phase shift between them.

IV.10.3. Pump Simulation Results

In this study, we used a centrifugal hydraulic pump coupled with an induction motor. The simulation results of the pump are illustrated in the figures below.

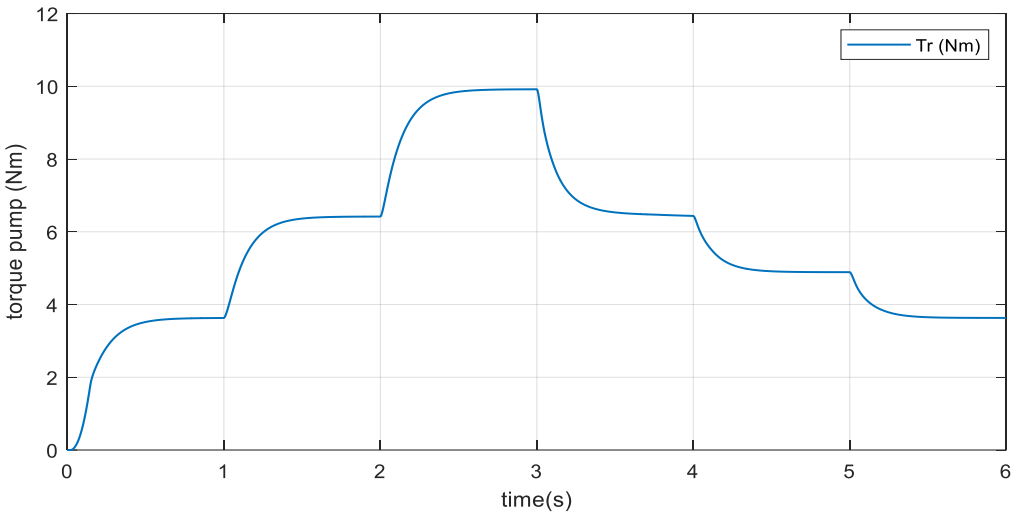


Figure IV.17 Pump Load Torque.

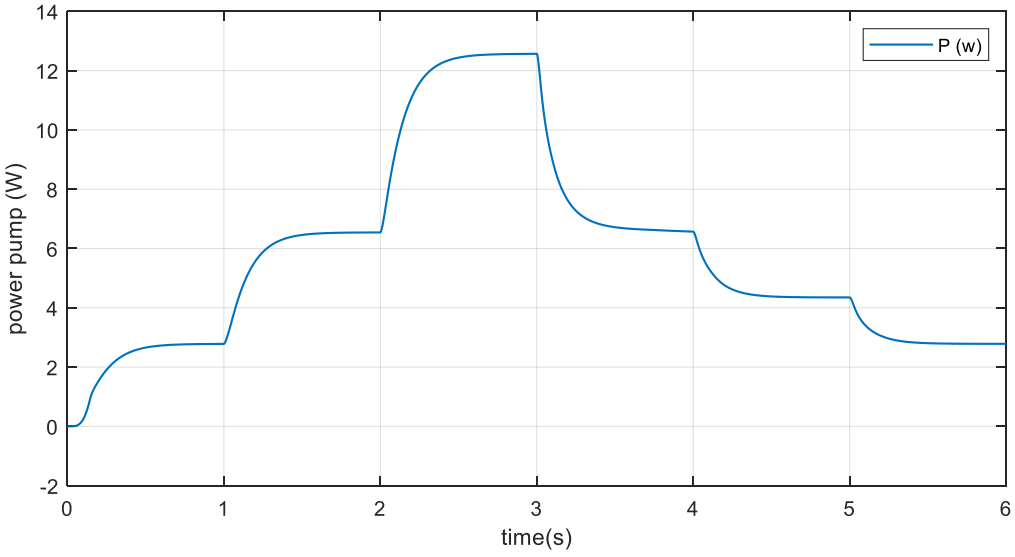


Figure IV.18 Pump Power.

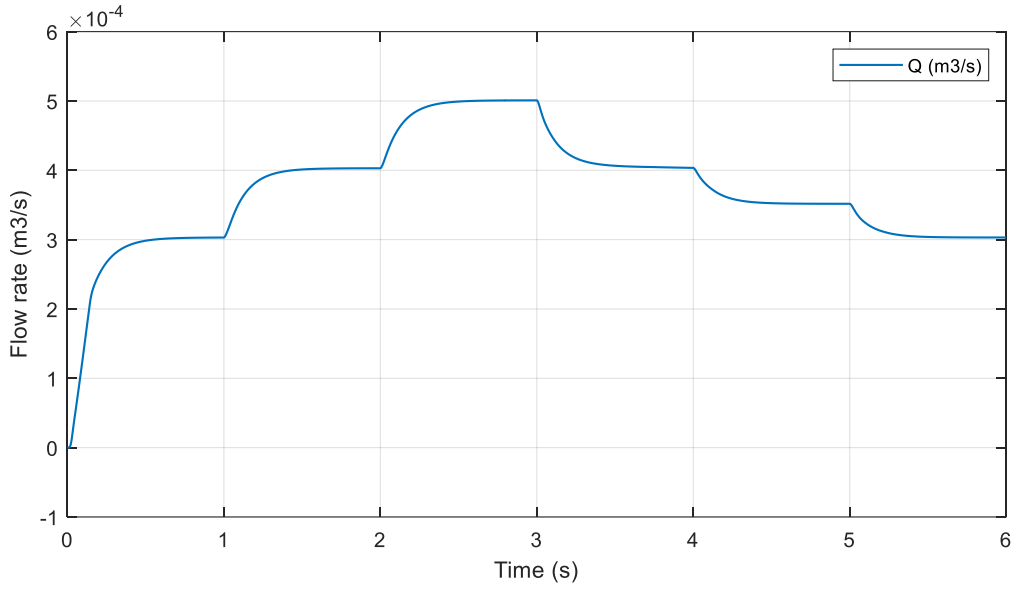


Figure IV.19 Pump flow rate Characteristics.

It is observed that the pump parameters vary according to changes in the machine's speed and, consequently, the solar irradiance. An increase in the machine's speed produces a proportional increase in both the pump's starting torque and power output.

IV.10.4. Simulation Results Comparison

This phase involves a comparative analysis of the global system's simulation results to validate our proposed system. The comparisonincludes:

- Speed parameters: Actual vs. estimated machine speed
- Power metrics: Solar panel output power
- Torque components:
    - Machine electromagnetic torque
    - Pumpload torque
    - Machine opposing torque

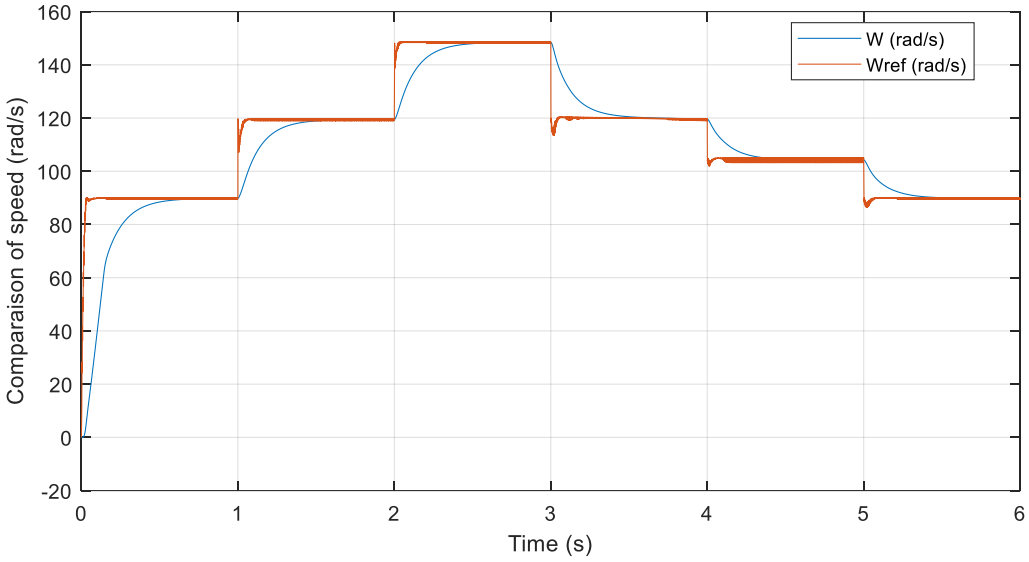


Figure IV.20 Speed Comparison.

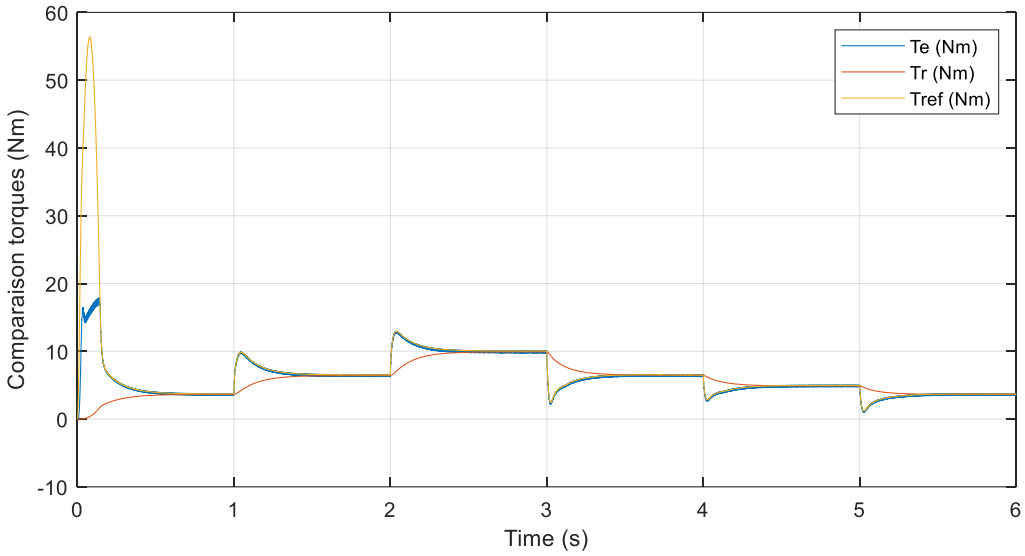


Figure IV.21 Torque Comparison.

Based on the obtained results, a clear overlap can be observed between:

- The machine's actual speed and the reference speed
- All torque components

These results demonstrate that the Direct Torque Control (DTC) technique used in the solar pumping system delivers excellent performance.

IV.11. Conclusion

In this chapter, we presented a modeling and simulation study of a solar pumping system powered by a DTC-controlled induction motor (asynchronous machine). The simulation results demonstrate strong performance, encouraging us to pursue further work and practical implementations of photovoltaic-based pumping systems.

General Conclusion

General Conclusion

This capstone project integrated elements of electric machine modeling, power electronics, renewable energy generation, and contemporary control methods to present a thorough performance analysis of a photovoltaic solar water pumping system. Evaluating such systems operational behavior, dependability, and efficiency under varied load and solar conditions was the goal.

The study was organized into four interconnected chapters:

A thorough review of photovoltaic water pumping systems was given in Chapter 1, along with an explanation of their main parts, working principles, and benefits. It underlined how important they are becoming to advancing sustainable development, particularly in isolated and off-grid areas.

The modeling and simulation of the photovoltaic generator were the main topics of Chapter 2. It was investigated how environmental factors, including temperature and solar irradiance, affected the system's functionality. Additionally, to guarantee the best possible energy extraction from the solar panels, a Maximum Power Point Tracking (MPPT) algorithm was put into place. [76]

The modeling and simulation of an induction machine driven by a voltage source inverter were covered in Chapter 3. This section examined the motor's dynamic behavior when powered by the PV system, emphasizing how its simplicity and robustness make it suitable for pumping applications.

We presented Direct Torque Control (DTC) as a high-performance induction motor control method in Chapter 4. According to simulation results, DTC is a promising strategy for solar pumping applications because it offers quick torque response, fewer ripples, and increased overall system efficiency.

The technical viability and energy efficiency of photovoltaic solar water pumping systems were validated by this study's simulations and performance assessments. The system's ability to adjust to changing water demands and solar conditions is greatly enhanced by the application of MPPT and DTC techniques.

In rural and agricultural settings, where access to clean water and sustainable energy can have a profound effect on communities and local economies, this work lays a strong foundation for future research and practical application.

Bibliography

Bibliography

[1] International Renewable Energy Agency (IRENA). (2021). Renewable Power Generation Costs in 2020.

[2] **Campana, P. E**., et al. (2019). Solar Energy for Sustainable Water Pumping. Springer.

[3] **Messenger, R. A**., &Ventre, J. (2010). Photovoltaic Systems Engineering (3rd ed.). CRC Press.

[4] **Bose, B. K**. (2002). Modern Power Electronics and AC Drives. Prentice Hall.

[5] **Takahashi, I**., &**Noguchi, T**. (1986). "A New Quick-Response and High-Efficiency Control Strategy of an Induction Motor". IEEE Transactions on Industry Applications, IA-22(5), 820-827.

[6] **Boyle G**, « Renewable Energy: Power for a Sustainable Future », 3rded, Oxford: Oxford University Press and Open University, 2012.

[7] https://nso.edu/blog/earth-day-2022/

[8] **Duffie, J.A** &**Beckman, W.A**. «Solar Engineering of Thermal Processes, photovoltaics and Wind» (5thed).Wiley.2020

[9]**CADI Mohammed**, **BenazzaHicham**,**Merselab**, **BoumediniM.Amine**, **Trifa** Mohamed «Energy transition and Sustainable Development Practices in Algeria: Challenges and Opportunities ». EuropeanEconomicLetters (EEL) ; vol.15,2025.

[10] **A.Ferrai,** « Dimensionnement des Infrastructures utilisant Diverses sources énergétiques Renouvelables Potentielles pour l'alimentation Electrique d'un village »; Mémoire de magister ; Ecole nationale polytechnique, Alger ,2008.

[11] **OuahibaBendaikha** et **Salah Larbi** « Hydrogen Production System analysis using Direct Photo-Electrolysis Process in Algeria » Revue International Conference on Renewable Energy Research and Applications , P.6 ,2013.

[12]**Chapman**, **Stephen J**. « Electric Machinery Fundamentals »,5th edition, McGraw-Hill Education, New York, USA,2011.

[13] **Wiles**, « Photovoltaic Power Systems », McGraw-Hill, USA, 2nd ed , 2015.

[14] https://energyeducation.ca.enclopedia/Photovoltaic_effect .

[15] https://www.greenmatch.co.uk/blog/2015/09/types-of-solar-panels

[16] https://Solaredition.com/Solar_cell_technologies_can be _broken _down into _6/three generations.

[17] **I.BchsaisetA.Sebbagh** A, « Optimisation d'un système de pompage photovoltaïque pour l'irrigation d'un hectare de palmier dattier en utilisant les méthodes Métaheuristiques » ; Mémoire de master, Université M'hamedBougara-Boumerdes, 2017.

[18] https://www.Alternative energy tutorials.com/photovoltaics.

[19] **M.Degla** et **B.Ben Ahmed** «Dimensionnement d'un système de pompage photovoltaïque » Mémoire de master univK.M.Ouergla 2017.

[20] **N.Debili**, « Etude et optimisation en environnement MATLAB/SIMULINK d'un système de pompage Photovoltaïque » ; Mémoire de magister, Université de Constantine, 2015.

[21]https://www.researchgate.net/figure/An-exploded-diagram-of-a-conventional-c-Si-PV-module_fig3_341701780

[22] **S.Makhloufi** : « Contribution à l'optimisation des installations photovoltaïques par des commandes intelligentes » ; Thèse de doctorat, Université de Batna, 2013.

[23]**F.Bendioudi** et **F.Lakhdari,** « Etude et Simulation d'un Système de Pompage Photovoltaïque avec batteries » ; Mémoire de master, Université Abderrahmane Mira, Bejaïa, 2014.

[24] **S.Aoufi,** « Modélisation et commande d'un système de pompage photovoltaïque » ; Mémoire de master, Université Ferhat Abbas— Setif-1 2014.

[25]https://www.csiro.au/en/news/All/News/2016/September/New-hybrid-energy-centre-transforming-low-emission-technologies

[26] https://www.researchgate.net/figure/Grid-connected-PV-system_fig10_316258436

[27] https://www.phaetondrive.com/news/what-is-solar-pump-system.html

[28] **A. BELHOCINE** et **S.ZAIDI**, « Etude et dimensionnement d'un système de pompage photovoltaïque autonome » ; Mémoire de master , Université de Bejaïa, 2012.

[29] **GevorkovL**,**Dominguez-Garcia** and **Romero L T**« Review on Solar Photovoltaic-Powered Pumping Systems », Energies ,vol.16,p.03,2023

[30] **M.Benaissa** «Contribution à l'étude du transfert d'énergie dans les systèmes photovoltaïques » ; Thèse doctorat, Université DjillaliLiabes De Sidi-Bel-Abbes, 2018.

[31] **Durin B**, **Lajqi S**, **Plantak L** and **KranjcicN** , « Using Solar Photovoltaic Energy for Irrigation: A Review of the Application» , advances in Environmental studies , vol.04,p.03,2020.

[32] **JamesP.Dunlop** « Photovoltaic Systemes » 3rd edition ,2012.

[33] **Foster**, **Majid Ghassemi**, **Alma Cota**, « Solar energy: Renewable energy and the Environment », 2010.

[34]**Foster**,**Majid Ghassemi, Alma Cota**, « Solar energy: Renewable energy and the Environment », 2010.

[35]https://otogeorgia.ge/shop/accumulators/varta/accumlator-varta-sil-74%E1%83%90%E1%83%A1-l

[36] https://www.rpc.com.an/Solar_Systemes/Solar_pump_systems/floating_pumps_html

[37] **DJERIOU Salim**, « Performance Improvement of photovoltaic pumping system, PhD Dissertation », University M'Hamed BOUGARA – Boumerdes 2018, Page 27.

[38] **Pr.A. Meroufel,** « Commande découplée d'une machine asynchrone sans capteur mécanique », Thèse de doctorat, Université DjillaliLiabes De Sidi-Bel-Abbès, 2004.

[39] **M.NEFSI**, «Commande directe du couple d'une machine asynchrone sans capteur mécanique», Mémoire de magister, Université Djilali Liabes De Sidi-Bel-Abbès, 2008.

[40] **A.melilie**, « Modélisation et simulation d'un système photovoltaïque par la commande MPPT (P&O) » ; Mémoire master, Université Djilali Liabes, 2016.

[41] **E.Karatepe**, **M.Boztepe** and **M.Colak** ,Neural Network Based Solar-Cell Model ,Energy.Conversion and Management, Vol. 47, N°9-10, pp. 1159-1178, 2006.

[42] **W.DeSoto**, **S.A. Klein**, **W.A. Beckman**, Improvement and validation of a model for photovoltaic array performance, Solar Energy 80, pp. 78-88, 2006.

[43] **A. DJALAB**, **A. REZAOUI**, **M. MAZOUZ**, **L.TETA, A. SABRI**, **N.ROBUST** / Method for Diagnosis and Detection of Faults in Photovoltaic Systems Using Artificial Neural Networks./ PeriodicaPolytechnica Electrical Engineering and Computer Science / 2020.

[44] **D. SERA** /Real-time modeling, diagnostics and optimized MPPT for residential PV systems / Doctoral Thesis / Institute of energy technology-Alborg university, Denmark / 2009.

[45] **V.TAMRAKAR,S.GUPTA**, **Y.SAWLE**/Single-diode and two-diode PV cell modeling using Matlab for studying characteristics of solar cell under varying conditions / Electrical & Computer Engineering: An International Journal.

[46] **A. KHENFER** / Etude et conception d'une architecture en vue de la détection de défauts dans une installation photovoltaïque / Mémoire de Magister / Université Ferhat Abbas Sétif 1– Sétif / 2015.

[47] **H.ABBES**, **H.ABID**, **K.LOUKIL**, **A.TOUMI**, **M.Abid** / Etude comparative de cinq algorithmes de commande MPPT pour un système photovoltaïque / Revue des Energies renouvelables, Vol 17, pp. 435- 445 / 2014.

[48] **V.SALAS**, **E.OLIAS**, **A.BARRADO**, **A.LAZARO** / Review of the maximum power point tracking algorithms for stand-alone photovoltaic systems /Solar energy materials solar cells, Vol 90 /2006 /

[49]**Esram,T**., &**Chapman, P. L**. (2007). "Comparison of Photovoltaic Array Maximum Power Point Tracking Techniques". IEEE Transactions on Energy Conversion, 22(2), 439-449.

[50] **J.H. Lee**, **H.Bae**, and **B.H.Cho**,"Advanced incremental conductance mppt algorithm with a variable step size," in 2006 12th International Power Electronics and Motion Control Conference, pp. 603–607, IEEE, 2006.

[51] **M.Al-Dhaifallah**, **A.M.Nassef**, **H.Rezk**, and **K.S.Nisar**, "Optimal parameter design of fractional order control based inc-mppt for pv system," Solar Energy, vol. 159, pp. 650–664, 2018.

[52]https://www.pvxchange.com/Solar-Modules/Sunpower/SPR-305-WHT-D_12108250 /20/04/2022.

[53] **Abdelhamid ZEKKOUR**, "Direct Torque Control of the Induction Motor without Speed Sensor Associated with an Adaptive Observer," Magister thesis, University of Batna, 07/11/2010.

[54] **Sihem DAMKHI**, "Speed Sensorless Control of an Asynchronous Motor Using Signal Flow Graphs (SFG)," Magister thesis, University of Batna, 2007.

[55] **Riad TOUFOUTI,** "Contribution to the Direct Torque Control of the Asynchronous Machine," PhD thesis, Mentouri University of Constantine, 02/06/2008.

[56] **Abdelhamid ZEKKOUR**, "Direct Torque Control of the Induction Motor without Speed Sensor Associated with an Adaptive Observer," Magister thesis, University of Batna, 07/11/2010.

[57] **Arezki SEDDIKI** "Contribution to the Direct Torque Control (DTC) of a Squirrel-Cage Asynchronous Machine Powered by a Multi-Level Inverter," Magister thesis, University of Boumerdès, 2009.

[58] **K.Laroussi,**"Développement dun SuperviseurFlou appliqué à la Commande d'un Moteur à Induction, "Development of a Fuzzy Supervisor Applied to the Control of an Induction Motor," PhD thesis, University Mohamed Bougara, Faculty of Hydrocarbons and Chemistry, Boumerdès, 2013.

[59] **Contribution**"Control of the Asynchronous Machine via DTC and Fuzzy Logic," Magister thesis, Mentouri University, Faculty of Engineering Sciences, Constantine 07/19/2006. "

[60] **The Dung Nguyen**, "Study of Modulation Strategies for Three-Phase Inverters Aimed at Reducing DC Bus Disturbances in Embedded Environments," PhD thesis, University of Technology of Compiègne, November 2011.

[61] **Maurice Fadel**, "Control of Synchronous Machines in Their Environment," "Modeling and Advanced Control of Static Converters," "Adaptive and Predictive Control," Course at ENSEEIHT, 2013.

[62] **Christophe Conilh,** "Control of an Asynchronous Machine Dedicated to telectric handling trolleys", INPT thesis, Order No. 2449, February 2007.

[63] **Aissa AMEUR**, "Commande sans capteur de vitesse par DTC d'un moteur synchrone a aimants permanents en utilisant des techniques de l' intelligence artificielle " Thèse de doctorat de L'université de Batna, 23/05/2012.

[64] **Souad CHAOUCH**, " Commande vectorielle robuste d'une machine a induction sans capteur de vitesse " Thèse de doctorat de L'université de Batna, 03/12/2005.

[65] **A. Elbacha**, **M.T.Lamchichi**, **M.Cherkaoui**, " Contrôle Direct de Couple d'une Machine Asynchrone Système de Régulation de Vitesse avec Anti Emballement ", Physical and chemical News ISSN 1114-3800 pp. 128-134, 2006.

[66] **Arezki SEDDIKI** , " Contribution au contrôle directe du couple (DTC) d'une machine asynchrone à cage alimentée par un onduleur multi-niveaux " mémoire de Magister, université de Boumerdès,2009.

[67] **M'hamedBIRAME ,** " commande sans capteur de vitesse d'un moteur a reluctance variable par l'utilisation des techniques de l'intelligence artificielle " Thèse de doctorat, université de Batna,22/10/2015.

[68] **Rabah ZAIMEDDINE**, " Contrôle directe du couple d'une machine asynchrone alimentée par des onduleur multi-niveaux " Thèse de doctorat, Ecole Nationale Polytechnique, Alger, 03/07/2007.

[69] **R.Zaimeddine**, **E.M.Berkouk**, " Enhanced Direct Torque control Using a Three-Level Voltage Source Inverter ", Proceedings of the 9th WSEAS International Conference on Systems, Athens,Greece Article No. 63 Year of Publication: 2005 ISBN:960-8457-29-7.

[70] **A.Ghoneim**, "Design optimization of photovoltaic powered water pumping systems," Energy Conversion and Management, vol. 47, no. 11, pp. 1449-1463, Oct 2006.

[71] **A.Mokeddem** and **A.Midoun,** "Performance of a directly-coupled PV water pumping system," Energy Conversion and Management, vol. 52, no. 10, pp. 3089-3095, April 2011.

[72] **J.Appelbaum**, "Starting and steady-state characteristics of dc motors powered by solar cell generators," IEEE Transactions on Energy Conversion, vol. EC-1, no. 1, pp. 17-25, March 1986.

[73] **P.Packiam** and N. K. Jain, "Steady and transient characteristics of a single stage PV water pumping system," Energy Systems, vol. 6, no. 2, pp. 173-199, December 2014.

[74] **H.Bouzeria**, **C.Fetha** and **T.Bahi**, "Fuzzy logic space vector direct torque control of PMSM for photovoltaic water pumping system," Energy Procedia, vol. 74, pp. 760-771, April 2015.

[75] **A.Betka** and **A.Attali**, "Optimization of a photovoltaic pumping system based on the optimal control theory," Solar Energy, vol. 84, no. 7, pp.1273-1283, April 2010.

[76] **Al-Mohammed**, **A. H**., & **Sharkh**, **S. M**. (2020). "Performance Analysis of Photovoltaic Water Pumping Systems Using MPPT and DTC Techniques." RenewableEnergy Journal, 15(3), 45-60.